DELINEATING THE MECHANISMS UNDERLYING RARE DISORDERS OF ECTOPIC CALCIFICATION TO REVEAL NOVEL THERAPEUTIC STRATEGIES

by

Shira G. Ziegler

A dissertation submitted to Johns Hopkins University in conformity with the requirements for the degree of Doctor of Philosophy

Baltimore, Maryland

May, 2017

ABSTRACT

Biallelic mutations in *ABCC6* cause pseudoxanthoma elasticum (PXE), a disease characterized by calcification in the skin, eyes, and blood vessels. While the function of ABCC6 and pathogenesis of PXE remains unclear, the mechanisms of related ectopic calcification disorders are better understood. Generalized arterial calcification of infancy (GACI) is caused by biallelic mutations in *ENPP1*, which encodes an enzyme that converts ATP to AMP and pyrophosphate (PPi), a major inhibitor of tissue calcification. AMP is further degraded to adenosine and inorganic phosphate by CD73, encoded by *NT5E*. We recently discovered that biallelic mutations in *NT5E* cause calcification of joints and arteries. We reasoned that a test for genetic interaction in mouse models of ectopic calcification might inform the pathogenesis of PXE. *Enpp1*$^{-/-}$ and *Abcc6*$^{-/-}$ mice showed fibrous capsule calcification of the vibrissae (an early marker of ectopic calcification) at 15 weeks of age, while *Nt5e*$^{-/-}$ mice calcified after one year. *Abcc6*$^{-/-}$ mice with one mutated *Enpp1* or two defective *Nt5e* alleles showed accentuated calcification with strong statistical evidence for synergy. Additionally, ABCC6, ENPP1, and CD73 exhibited regulatory interactions; human fibroblasts with biallelic *ABCC6* mutations had increased ENPP1 and decreased CD73 activity. Taken together, these data suggest that ABCC6 participates with ENPP1 and CD73 in ATP metabolism. Under osteogenic culture conditions, *ABCC6* mutant cells calcified, suggesting a provoked cell-autonomous defect. Using a conditional *Abcc6* knockout mouse model, we excluded the prevailing hypothesis that singularly invokes failure of hepatic secretion of an endocrine inhibitor of calcification. Instead, deficiency of *Abcc6* in both local and distant cells was necessary to achieve the early onset and penetrant ectopic calcification observed upon

constitutive gene targeting. Given their ability to recapitulate pathogenic events, PXE patient fibroblasts emerged as a viable model for investigating therapies. *ABCC6* mutant cells additionally had increased expression and activity of tissue non-specific alkaline phosphatase (TNAP), an enzyme that degrades PPi, a major inhibitor of calcification. A novel, selective, and orally bioavailable TNAP inhibitor prevented calcification in *ABCC6* mutant cells in vitro and attenuated both the development and progression of calcification in *Abcc6*$^{-/-}$ mice in vivo, without the deleterious effects on bone associated with other proposed treatment strategies. In summary, our studies provide evidence that ectopic calcification in PXE integrates both local and systemic perturbations of extracellular ATP metabolism, which can be attenuated in patient cells or *Abcc6* knockout mice with a TNAP inhibitor.

Advisor: Harry C. Dietz, M.D.

Reader: Daniel Warren, Ph.D.

PREFACE

I am indebted to many individuals for their contribution to my thesis. Mainly, Hal Dietz for allowing me to pursue a project peripheral to his TGFβ-focused research program. Hal has given me the autonomy and latitude to explore new hypotheses and navigate through my PhD independently while always being supportive and engaged in my research efforts. He has taught me how to think independently, ask meaningful questions, and communicate effectively.

I also wanted to thank my thesis committee members, William A. Gahl, William Guggino, Susan Michaelis, Jeremy Nathans, and in particular Dan Warren, for their insightful and thoughtful advice. Members of the Dietz laboratory, both past and present, created a fun and intellectually stimulating work environment, especially: Rustam Bagirzadeh, James Beckett, Russ Gould, Benjamin Kang, Elena Gallo MacFarlane, Sarah Parker, Koen Raedschelders, Graham Rykiel, Manny Seman Senderos, Robert Wardlow, and Nicole Wilson. Nothing could be accomplished without Debbie Churchill or Sara Cooke, who has also instilled a special sense of family in the Dietz Lab.

I am indebted to Bob Siliciano, Andrea Cox, and Sharon Welling for the opportunity to train in the MD/PhD program and Dave Valle and Sandy Muscelli for their guidance through the Human Genetics training program.

I wanted to also thank my mother, Regina Ziegler, and twin brother, Micah Ziegler, for their unwavering support.

TABLE OF CONTENTS

LIST OF TABLES

LIST OF FIGURES

CHAPTER 1

DISORDERS AND MECHANISMS OF ECTOPIC CALCIFICATION

I. INTRODUCTION

Once considered passive precipitation of calcium and phosphate (Pi), ectopic calcification is now seen as a complex process actively regulated by several circulating and local factors. These factors maintain vessel and tissue homeostasis, which normally involves trophic inhibition of calcification and is disrupted in pathological disorders. Several rare Mendelian diseases, as well as some common disorders, present with strikingly similar histological findings but vastly different clinical manifestations and pathologic sequelae. Here, we describe the clinical presentations, diagnostics, molecular genetics, and treatment of the known disorders of ectopic calcification, in addition to reviewing experimental models and disease mechanisms.

II. DISORDERS OF ECTOPIC CALCIFICATION

Generalized Arterial Calcification of Infancy (GACI)

Clinical Presentation and Diagnostic Aspects

Infantile calcification of the arteries was first described by Durante in 1899[1], and the first report in the English medical literature dates back to 1901[2]. Since then, it has been known by various different names, including idiopathic obliterative arteriopathy, infantile calcifying arteriopathy, occlusive infantile arteriopathy, medial coronary sclerosis of infancy, diffuse arterial calcifying elastopathy of infancy, arteriopathia calcificans infantum, and perhaps more commonly as Idiopathic Infantile Arterial Calcification (IIAC)[3]. Since the identification of the molecular etiology in 2003[4], the preferred

nomenclature has been GACI. The incidence of GACI, calculated from the carrier frequency noted in a cohort of over 60,000 exomes from unrelated adults, should be approximately 1 in 200,000 live births, although it is likely that only a fraction of affected infants receive that diagnosis. GACI shows a bimodal age of onset, with about half of all patients presenting in utero or during the first week of life, and the other half presenting later in life, with a median age of onset of three months[5]. Common signs of the disease in utero include fetal distress, polyhydramnios, and effusions or hydrops, while a common presentation postnatally includes respiratory distress, cyanosis, and heart failure[5].

GACI is characterized by diffuse calcification of large- and medium-sized arteries (Fig. 1A). Extravascular calcifications can occur around the joints (Fig. 1B) in 29% of cases[6], as well as in the ear lobes[7–9], myocardium[10–12], pancreas, liver, and kidneys[8,13]. Skin and retinal findings typical of pseudoxanthoma elasticum (PXE; see below) can also present later in life in individuals who survive infancy[8,13–16]. Elevated inflammatory markers such as white blood cell count and C-reactive protein commonly occur, leading to the erroneous diagnosis of sepsis. Despite the best medical care, the mortality rate remains 55% within the first seven months of life[6].

GACI is diagnosed through imaging studies, including ultrasonography, and echocardiography that detect vessel echobrightness, as well as computed tomography (CT), which remains the preferred technique to evaluate vascular calcification. In the past, the diagnosis was made by histologic means, either through the biopsy of a medium-sized artery, or at autopsy. The characteristic pathology involves fragmentation and

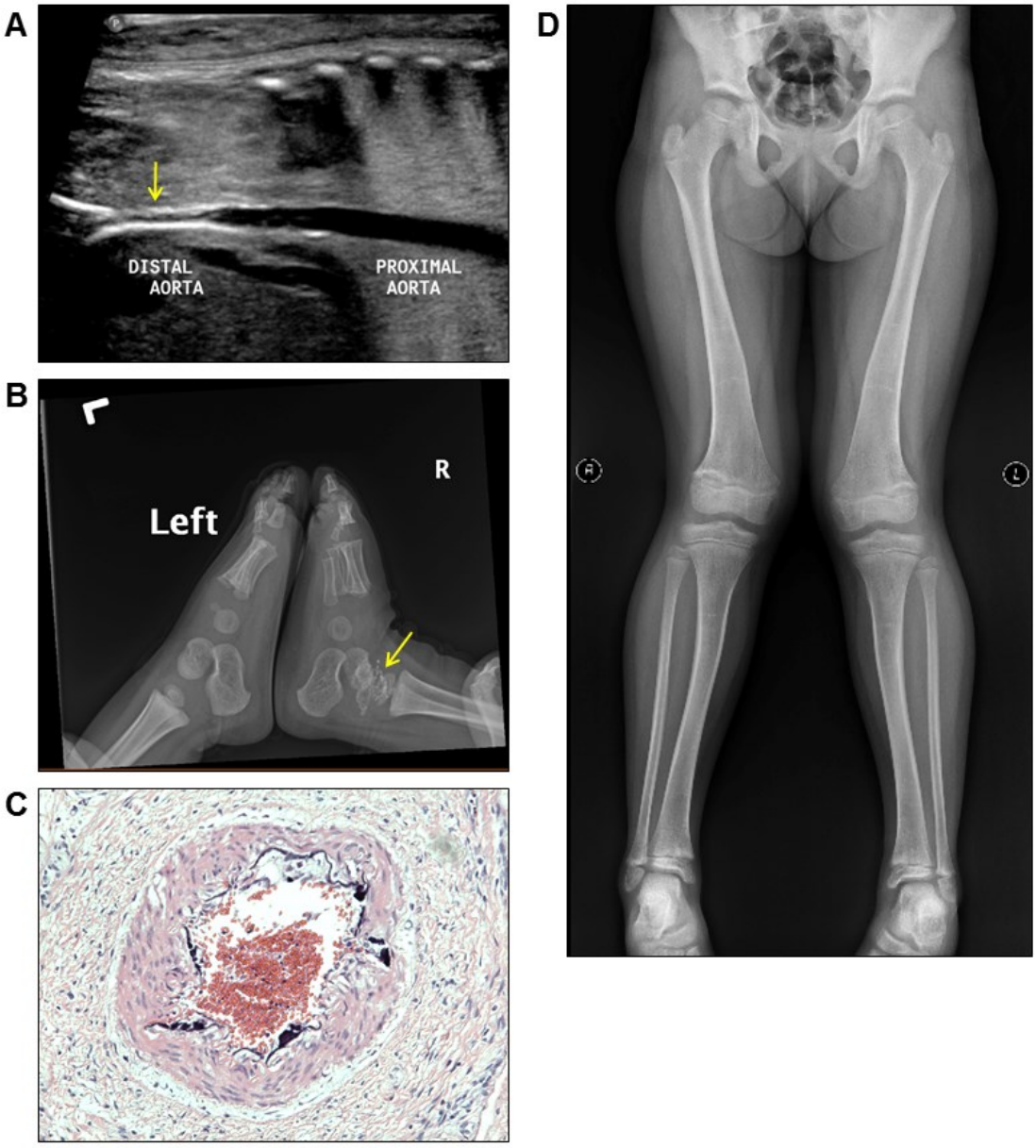

Fig. 1. Common clinical and histological features of GACI. (**A)** Ultrasound imaging showing luminal narrowing and echobrightness (arrow) of the distal aorta in a child. (**B)** Calcification noted in the right ankle joint (arrow). (**C**) Medium-sized vessel within connective tissue showing calcification of the internal elastic lamina (hematoxylin and eosin stain). (**D**) Bilateral genu valga in a child with untreated hypophosphatemic rickets due to *ENPP1*-associated GACI.

calcification of the internal elastic lamina of large- and medium-sized arteries (Fig. 1C); fibrointimal hyperplasia frequently contributes to luminal narrowing and can occur in the absence of calcification. The authors know of one child with biallelic *ENPP1* mutations (see Molecular Genetics below) with no arterial calcifications on CT imaging, but with diffuse arterial narrowing, initially diagnosed as fibromuscular dysplasia.

Molecular Genetics

GACI generally results from biallelic mutations in *ENPP1,* which encodes an extracellular ectonucleotide pyrophosphatase that converts ATP into AMP and pyrophosphate (PPi)[4]. While mutations in *ENPP1* account for 67% of all cases of GACI, biallelic mutations in *ABCC6* account for 9% of cases[8], and over 20% of all patients have no known molecular etiology. In general, the different molecular bases of GACI are clinically indistinguishable. However, hypophosphatemic rickets develops in the majority, if not all, survivors of GACI carrying *ENPP1* mutations[6] (Fig. 1D), while it is not a complication of GACI due to *ABCC6* mutations (see below). Hearing loss, either conductive, sensorineural, or mixed, can also complicate *ENPP1*-GACI at any point in a patient's lifetime, including the neonatal period[9]. No genotype-phenotype correlation is known for patients with *ENPP1*-GACI, other than all patients homozygous for the p.Pro305Thr died in infancy[6].

Treatment

Because of the lack of understanding of the disease pathogenesis, treatment options for disorders of ectopic calcification have been limited. One possible therapy consists of

bisphosphonates, which have a pyrophosphate (PPi) backbone that inhibits mineral formation, and a side chain that inhibits mineral resorption. Although the main reason for using bisphosphonates in other conditions, such as osteoporosis, stems from their antiresorbtive effect, the rationale for their use in GACI is related to their antimineralization effect. First-generation bisphosphonates, specifically etidronate, have been proposed as treatment for vascular calcification disorders[17], and are currently being used to treat GACI. Because of the limited number of GACI patients, the therapeutic efficacy has not been well-established, though a retrospective study has shown that etidronate treatment was associated with better clinical outcomes and prolonged survival[6]. The optimal duration of treatment remains to be established, but prolonged bisphosphonate therapy can lead to severe skeletal toxicity[18]. Treatment of subsequent rickets, when performed judiciously, does not lead to worsening of vascular calcification[19], although overtreatment can result in hypercalciuria and iatrogenic calcification[13].

Arterial Calcification due to Deficiency of CD73 (ACDC)

Clinical Presentation and Diagnostic Aspects

In 2011, mutations in *NT5E* were identified in members of three families with symptomatic arterial and joint calcification[20]. Today, a total of 13 patients are followed at the National Institutes of Health, and more patients have been identified around the world[21–23]. Patients typically present in their late teenage years or early adulthood with joint pain, mostly in the hands and feet, but a rheumatology evaluation fails to provide a specific diagnosis despite radiographs showing periarticular calcification[21,24]. Patients

later develop claudication, and plain radiographs show massive calcification of the arteries of the lower extremities (Fig. 2). Patients lack classical risk factors for cardiovascular disease, such as diabetes or renal insufficiency, but are treated empirically for peripheral vascular disease, either medically or surgically. Isolated patients with ACDC have had calcification of upper extremity vessels[22], splenic artery, coronary arteries, soft tissue in the neck, and a calcified brain meningioma.

Molecular Genetics

ACDC results from biallelic mutations in *NT5E*, which encodes CD73, an ecto-5'-nucleotidase that degrades AMP to adenosine and inorganic phosphate (Pi)[20]. Mutations identified in the original three families caused reduced endoplasmic reticulum retention and reduced trafficking of the defective protein to the plasma membrane[25]. No genotype-phenotype correlation is known.

Treatment

A phase 1 clinical trial to evaluate the effectiveness of etidronate is currently underway (ClinicalTrials.gov identifier: NCT01585402).

Pseudoxanthoma elasticum (PXE)

Clinical Presentation and Diagnostic Aspects

PXE is characterized by fragmentation and mineralization of elastic fibers, mainly affecting the skin, retina, and cardiovascular system. In 1881[26], Rigal first described the

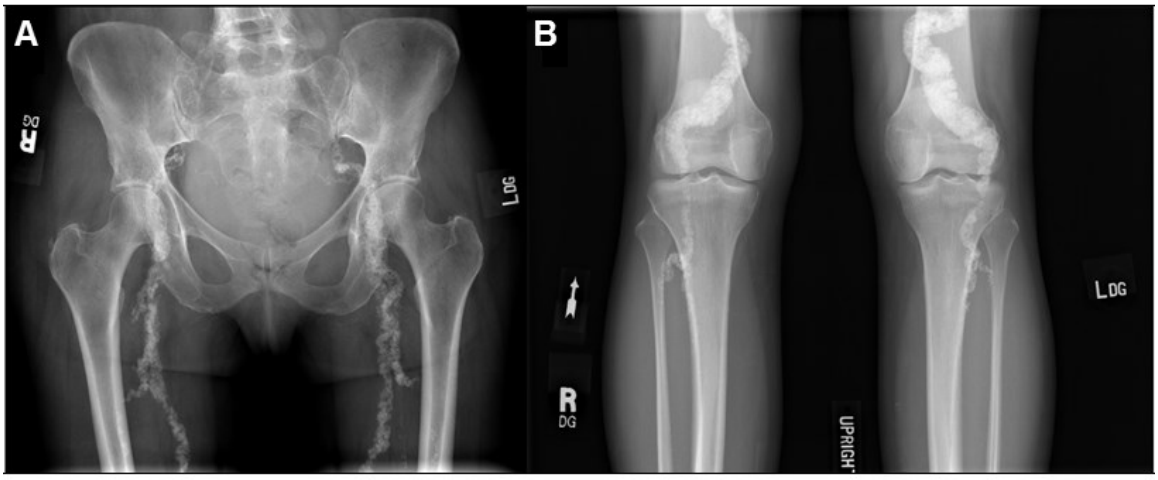

Fig. 2. Calcification of the popliteal and posterior tibial arteries in a patient with ACDC.

skin findings and attributed them to a form of diffuse xanthelasma. Later, Ferdinand-Jean Darier realized that the skin lesions were not xanthomatous, but rather caused by calcification of the elastic fibers; thus, he coined the term pseudoxanthoma elasticum[27]. In 1929, the association of the typical skin findings with retinal angioid streaks was independently reported by two Swedish doctors, Ester Grönblad[28] and James Strandberg[29]; the disorder is still sometimes known as Grönblad-Strandberg syndrome.

Although it was initially thought to be an exceedingly rare disease, with older literature mentioning a prevalence of 1 in 1,000,000, a prevalence as high as 1 in 25,000 has been proposed[30]. Based on the allele frequency for the most common *ABCC6* mutation, R1114*, a prevalence as high as 1 in 4,450 has been calculated in the Dutch population[30,31]. A founder effect has been reported in the Afrikaner population of South Africa[32]. The female-to-male ratio is approximately 2 to 1[33].

From a series of 100 patients, the mean age at onset of symptoms was 13.5 years, with mean age at diagnosis of 22.9 years[33]. The first symptoms are almost always cutaneous[33], in the form of small, asymptomatic, yellow papules that coalesce over time into larger plaques. The appearance of the skin has been described as that of "plucked chicken", "Moroccan leather", "cobblestone", "crépe-like", or "pseudoxanthomatous"[34]. In more advanced stages, the papules can become obscured by folds of redundant skin[34]. The first site of involvement in 96% of cases is the lateral neck, but the axillae, antecubital fossae, inguinal fossae, and groins can be involved, typically following a cephalad to caudal order of progression[33]. Other affected areas include the inner aspect

of the lower lip (33% of cases), rectal mucosae, supraumbilical area, flexor surface of the wrist, medial thighs, dorsum of the ankles, penis, and genital labia.[33] In cases with facial involvement, the skin redundancy leads to a "hound dog" appearance.

The typical retinal findings of PXE include angioid streaks, mottled hyperpigmentation (peau d'orange), atypical drusen, and retinal hemorrhages (Fig. 3). Angioid streaks are irregular lines that radiate from the optic disc, and are the manifestation of ruptures in Bruch's membrane; they are seen in 83% of cases and start appearing during the second decade of life[33]. Peau d'orange represents a mottled pigmentation of the retinal pigment epithelium best seen in the periphery of the retina; this finding is present in 96% of patients, making it the most common retinal sign of PXE[33]. Other findings include atypical drusen (52% of cases) and hyperpigmented spots on both sides of an angioid streak ("owl's eyes")[33]. All these findings are asymptomatic until neovascularization occurs, leading to hemorrhages and the consequent visual loss.

Regarding cardiovascular complications, intermittent claudication is present in 30% of cases, angina pectoris in 13%, gastrointestinal bleeding in 8%, mitral valve prolapse in 4%, myocardial infarction in 1%, and cerebrovascular accidents in 1%[33].

Testicular microlithiasis affects the majority of male patients with PXE[35], sometimes very early in life[36]. Calcification of the placenta has been described in pregnant women[37].

Fig. 3. Fundus photograph of a patient with PXE. Oval indicates peau d'orange in the peripheral retina, arrow indicates macular hemorrhage, and arrowheads point to angioid streaks (Courtesy of Dr. Emily Chew, National Eye Institute, NIH).

The minimal criteria for establishing a clinical diagnosis of PXE requires the presence of angioid streaks in the retina in addition to typical skin findings with characteristic histopathologic changes of mineralization and fragmentation of elastic fibers (elastorrhexis)[38]. The first finding is that of mineralization of the central core of the elastic fiber, followed by formation of central holes, and then fragmentation of the fibers[39]. Special stains used in light microscopy include Verhoeff-van Gieson (staining elastic fibers black) and calcium stains such as von Kossa and alizarin red (staining calcium brown black and reddish orange, respectively).

There are several conditions that can cause PXE-like phenotypes. The reported incidence of angioid streaks in patients with sickle cell disease has varied from 1-2%[40] to 22%[41], the latter in patients over 40 years old. Angioid streaks have been found in 20% of patients with β-thalassemia[42] (showing a positive correlation with age) and in 10% of patients with sickle-thalassemia[43]. Of 40 patients with β-thalassemia, 55% had calcification of the posterior tibial arteries, 20% had skin lesions typical of PXE, and 52% had angioid streaks, with 85% having at least one of the three[44]. The pathology of the skin lesions, based on light microscopy, electron microscopy, and immunohistochemistry, is identical to that seen in PXE[45]. Exposure to potassium nitrate (saltpeter) is also associated with skin lesions that are clinically and histopathologically identical to those of PXE[46,47]. Penicillamine use can induce similar skin changes, described as pseudo-pseudoxanthoma elasticum[48–50]; there is a case of familial pseudo-PXE in relatives who were taking penicillamine for the treatment of cystinuria[51]. PXE has also been described in three liver transplant recipients, although liver specimens from

donors did not reveal mutations in *ABCC6*[52]. Patients with juvenile Paget disease can also have PXE-like skin lesions[53–56] and retinal findings[57–59]. Finally, an unknown disorder with manifestations of pseudoxanthoma elasticum, hyperphosphatemia, hypercalcemia, and non-suppressed 1,25-dihydroxyvitamin D has been described[60].

Molecular Genetics

PXE is most commonly caused by mutations in *ABCC6*, but it can also be caused by mutations in *ENPP1*[8,61]. No genotype-phenotype correlation is known[62], other than patients with *ENPP1*-associated PXE are likely to have experienced rickets during childhood or adolescence. PXE is inherited in an autosomal recessive manner; although historically there have been many reports of autosomal dominant inheritance, cases with unambiguous PXE in two different generations have been proven to represent instances of pseudodominance[63,64]. Polymorphisms in the xylosyltransferase genes have been described as modifiers of PXE phenotype severity[65]. PXE-like disorder with multiple coagulation factor deficiency (OMIM 610842) is an autosomal recessive condition due to mutations in the *GGCX* gene. Similarities to PXE include yellowish papules, retinal angioid streaks and peau d'orange, and dermal elastorrhexis[66]. Differences from PXE include more diffuse skin involvement with cutis laxa over time, no decrease in visual acuity, the presence of coagulation abnormalities, and the finding of mineralization of the periphery–as opposed to the core–of the elastic fiber on electron microscopy[66].

Treatment

No specific treatment exists. Therapeutic options for choroidal neovascularization include laser photocoagulation, transpupillary thermotherapy, photodynamic therapy, and anti-angiogenic agents. Plastic surgery has been performed for cosmetic improvement of skin lesions[67].

Familial chondrocalcinosis type 2

Clinical Presentation and Diagnostic Aspects

Familial chondrocalcinosis was first described by Zitnan and Sitaj in 1957[68], during the Ninth International Congress on Rheumatic Diseases in Toronto. It is characterized by early-onset deposition of calcium pyrophosphate dihydrate (CPPD) in cartilage, mainly affecting the knees and wrists (hyaline cartilage), and the menisci, pubic symphysis, and intervertebral disks (fibrocartilage)[69]. This crystal deposition is evidenced radiographically, and leads to arthropathy. The clinical patterns described include pseudogout alone (with acute or subacute attacks, 19%), pseudogout with osteoarthritis (chronic osteoarthritis with superimposed attacks, 44%), pseudo-osteoarthritis alone (similar to osteoarthritis but with a different pattern of joint involvement affecting the metacarpophalangeal joints, wrists, elbows, and shoulders in a symmetric fashion, 22%) and pseudo-rheumatoid arthritis (chronic inflammatory arthritis, 15%)[69]. Pseudogout attacks typically start between the late third and early fourth decades[70]. There is radiographic evidence of chondrocalcinosis affecting the knees (93%), pubis symphisis (67%), wrists (59%), and hips (52%)[69]. Occasionally, affected individuals can show radiographic evidence of chondrocalcinosis and still remain asymptomatic, while others can have destructive arthropathy necessitating joint replacement[69]. Laboratory studies do

not disclose blood abnormalities of mineral metabolism[69]. CPPD crystals can be identified in synovial fluid by their positive birefringency on compensated polarized light microscopy.

Other genetic disorders that have been associated with CPPD deposition include hemochromatosis[71], disorders causing hypomagnesemia such as Gitelman syndrome[72], hypophosphatasia[73–75], Wilson disease[76], and alkaptonuria[77–79].

Molecular Genetics

Familial chondrocalcinosis type 2 results from mutations in *ANKH*[80], which also causes a rare skeletal dysplasia known as craniometaphyseal dysplasia and characterized by hyperostosis, sclerosis of craniofacial bones, and abnormal modeling of the metaphyses of long bones[81]. Both conditions are inherited in an autosomal dominant manner, with chondrocalcinosis likely being caused by gain-of-function mutations, and craniometaphyseal dysplasia by dominant negative mutations[82]. Mutations that lead to craniometaphyseal dysplasia cluster in the C-terminus of *ANKH*, whereas mutations in the N-terminus result in chondrocalcinosis[83]. Craniometaphyseal dysplasia has been reported to cosegregrate with chondrocalcinosis in females from an Australian family[84]. An autosomal recessive disorder caused by homozygous mutations in *ANKH* was reported in one family, whose affected members presented with painful periarticular calcification of small joints, progressive spondyloarthropathy leading to ankylosis, osteopenia, mixed hearing loss, intellectual disability, and mild hypophosphatemia[85].

Treatment

There is no specific therapy for the condition. Treatment is symptomatic, including the use of nonsteroidal anti-inflammatory drugs and intra-articular or systemic glucocorticoids for the management of pain or inflammation.

Familial Tumoral Calcinosis (FTC)

Clinical Presentation and Diagnostic Aspects

FTC is characterized by the development of calcified masses around one or more large joints (Fig. 4). It was first described by Giard and Duret in 1898 and 1899, respectively[86,87]. Teutschlaender called the disease lipocalcinogranulomatosis and studied it since the 1930s in Europe[88], where the condition came to be called Teutschlaender disease. Inclan was the first to report the disease in the American literature, and he coined the term tumoral calcinosis[89], which subsequently became widely adopted. FTC can be either hyperphosphatemic or normophosphatemic.

A condition known as hyperostosis-hyperphosphatemia syndrome is characterized by cortical hyperostosis, periosteal reaction, and hyperphosphatemia, and is now known to belong to the spectrum of hyperphosphatemic FTC[90,91]. A review of 56 patients with molecularly-confirmed hyperphosphatemic FTC found hyperphosphatemic FTC alone in 54% of cases, hyperostosis-hyperphosphatemia alone in 11%, and combined hyperphosphatemic FTC with hyperostosis in 36% of patients[92]. Males and females are equally affected, but hyperostosis occurs more commonly in females[92]. Age at presentation was 2 to 13 years in 78% of cases[92]. Dental involvement was seen in 39% of

cases[92], and included short bulbous teeth with blunted roots, thistle-shaped dental pulps, obliteration of the pulp chamber and root canal, and pulp stones[93]. Vascular calcification was present in 18%, and eye involvement in 16% of patients[92], including calcification of the eyelids or conjunctiva, band keratophy, retinal angioid streaks, or optic nerve head drusen[92,94,95]. Testicular microlithiasis has been described[96].

The laboratory findings of hyperphosphatemic FTC include increased tubular resorption of Pi for the degree of hyperphosphatemia, elevated or inappropriately normal 1,25-dihydroxyvitamin D, low intact FGF23 with markedly increased C-terminal FGF23–indicative of increased FGF23 cleavage–with normal calcium and parathyroid hormone. Some patients present with systemic inflammation and increased C-reactive protein[97].

Normophosphatemic FTC is characterized by the appearance of an erythematous papular eruption during the first year of life (earlier than the typical age of onset of hyperphosphatemic FTC), followed by the appearance of calcified masses in the extremities; patients also show severe conjunctivitis and gingivitis.[98]

Molecular Genetics

Patients and families with hyperphosphatemic FTC have mutations of either the fibroblast growth factor 23 (*FGF23*), polypeptide N-acetylgalactosaminyltransferase 3 (*GALNT3*), or Klotho (*KL*) genes, all of which encode proteins involved in Pi regulation. FGF23 is a secreted osteocyte protein, whose post-translation processing requires GALNT3-mediated mucin type O-glycosylation. FGF23 acts on the renal tubule via a

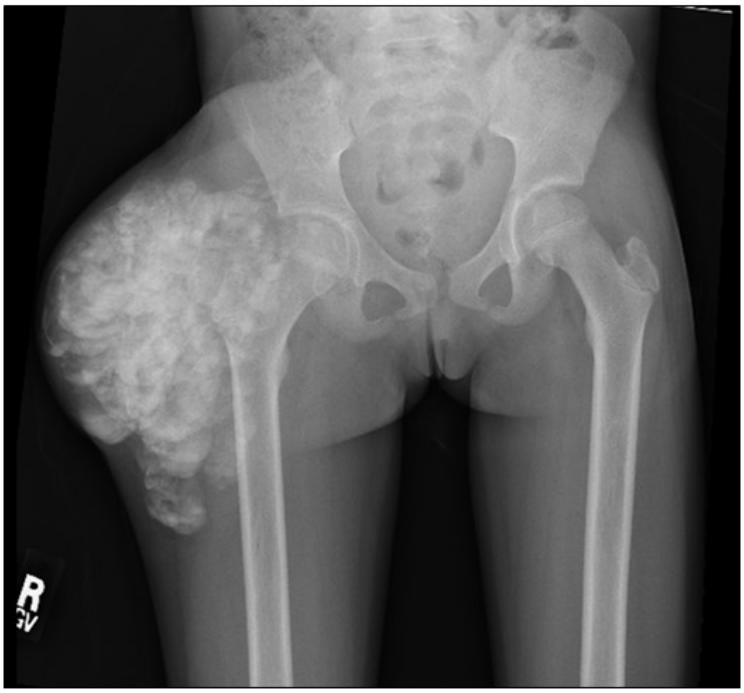

Fig. 4. Patient with familial tumoral calcinosis. Evidence of an amorphous, multilobulated calcific mass around the right hip joint (Courtesy of Drs. Rachel I. Gafni, Michael T. Collins, and Mary S. Ramnitz, National Institute of Dental and Craniofacial Research, NIH).

membrane protein complex comprising the FGF receptor and co-receptor, Klotho, to promote renal Pi excretion by downregulating type 2 sodium-phosphate co-transporters.

FGF23 also decreases intestinal Pi absorption by inhibiting the renal via D-1alpha-hydroxylase mediated synthesis of 1,24-dihydroxyvitamin D. Mutations in *GALNT3* account for 75% of FTC cases, while mutations in *FGF23* and *KL* account for 23% and 2%, respectively. Vascular calcification is more common in patients carrying *FGF23* mutations, while dental involvement is more common in those with *GALNT3* mutations[92].

Normophosphatemic FTC is caused by biallelic loss-of-function mutations in *SAMD9*, while the newly-described MIRAGE syndrome (Myelodysplasia, Infection, Restriction of growth, Adrenal hypoplasia, Genital phenotypes, and Enteropathy) is caused by de novo heterozygous gain-of-function mutations in *SAMD9*[99].

Regardless of the gene involved, all forms of FTC show autosomal recessive inheritance.

Treatment

Treatment is targeted at decreasing enteral absorption of Pi or increasing the renal excretion of Pi. Decreased intestinal absorption can be achieved by dietary phosphate restriction (with a goal of 400 to 900 mg/day) and use of Pi binders, such as aluminum hydroxide or sevelamer. Increased renal excretion can be achieved by the use of acetazolamide or probenecid[93,97,100]. The response to treatment is quite variable, with some patients showing complete resolution of lesions, and others showing no

improvement. In patients with systemic inflammation, the use of interleukin-1 antagonists can be beneficial[97]. Surgical debulking can be performed in case of pain, deformity or restriction of joint mobility, but lesions tend to recur.

Idiopathic Basal Ganglia Calcification (IBGC)

Clinical Presentation and Diagnostic Aspects

Vascular calcification of the basal ganglia was first described by Delacour in 1850[101], in a 56-year-old man with weakness and spasticity of the lower extremities, as well as tremor[102]. Eighty years later, Karl Theodor Fahr reported the case of an 81-year-old man with a long history of dementia; that was a sporadic rather than a familial case. The patient may have had hypoparathyroidism, and the calcification was primarily located in the white matter vasculature, not in the basal ganglia. This, added to the fact that over time the term Fahr disease came to be used for any form of bilateral basal ganglia calcification regardless of etiology, has led to a recommendation against the use of that eponym[103].

In IBGC, calcifications are found not only in the basal ganglia (Fig. 5), but also in the thalamus, dentate nucleus, and centrum semiovale[104]. In a review of 99 cases, 67 were symptomatic at the time of evaluation[104]. The most common symptoms were movement disorders (55%), cognitive defects (39%), speech disorder (36%), cerebellar signs (36%), psychiatric manifestations (31%), pyramidal signs (22%), sensory symptoms (16%), genitourinary symptoms (13%), gastrointestinal symptoms (12%) and seizures (9%). Of

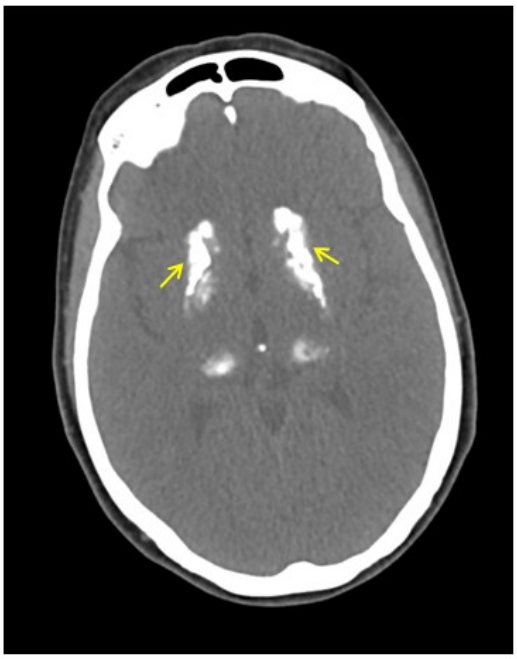

Fig 5. Brain computed tomography of a patient with IBGC showing bilateral calcification (arrows) of the basal ganglia.

the movement disorders, the most common were parkinsonism (57%), followed by chorea (19%), tremor (8%), dystonia (8%), athetosis (5%), and orofacial dyskinesia (3%)[104]. The mean age of onset of symptoms is 39 ± 20 years[105]; 25% have onset before 18 years of age, presenting predominantly with isolated psychiatric or cognitive signs, and 25% have onset after 53 years of age, presenting mainly with movement disorders[106]. Migraine is found in approximately one in four patients[106].

Other genetic conditions commonly associated with basal ganglia calcifications include Down syndrome[107], Cockayne syndrome[108], mitochondrial disorders[109], dihydropteridine reductase deficiency[110], Fried syndrome[111], Coat's plus syndrome[112], Raine syndrome[113], Aicardi-Goutieres syndrome[114], pseudohypoparathyroidism[115], Krabbe disease[116], carbonic anhydrase II deficiency[117], ISG15 deficiency[118], CANDLE syndrome[119], Kenny-Caffey syndrome[120] and Nasu-Hakola syndrome[121]. Lipoid proteinosis is typically associated with calcification of the amygdalae, but sometimes the calcium deposits can extend to the basal ganglia[122].

Molecular Genetics

There are currently four genes that are known to account for the IBGC phenotype: *SLC20A2*, *PDGFB*, *PDGFRB*, and *XPR1*, all exhibiting autosomal dominant inheritance. Approximately 41-50% of familial cases were initially reported to be caused by heterozygous mutations in *SLC20A2*[123,124], with 4.3% of sporadic cases caused by mutations in that gene[123]. However, a recent French series described *SLC20A2* mutations in 20% of familial IBGC and 17.2% of sporadic cases, *PDGFB* mutations in 10% of

familial and 13.8% of sporadic cases, and *PDGFRB* mutations in 5% of familial and 6.9% of sporadic cases[125]. Mutations in *XPR1* account for less than 8% of patients who are negative for those three genes[126]. Calcification tends to be more severe in patients carrying mutations in *SLC20A2* than in those with *PDGFRB* mutations[105,106].

Treatment

No specific treatment exists for IBGC. Treatment is targeted to the symptoms, including medications for movement disorders, psychiatric symptoms, seizures and migraines. Etidronate use was attempted in one patient, leading to improved speech and gait, but there was no improvement in spasticity, dystonia, or ataxia, and no reduction in intracranial calcification[127]. Alendronate was recently used in seven patients, with good tolerance and either stability or subjective improvement of symptoms, particularly in younger patients[128]. The benefits of bisphosphonates in this condition, if any, are still equivocal.

Keutel syndrome

Clinical Presentation and Diagnostic Aspects

Keutel et al. first described this condition in 1972 in a brother and sister born from a consanguineous union[129]. The disease is characterized by diffuse cartilage calcification, including the nose, pinna, larynx, trachea, bronchi, and costochondral junctions[129], which can lead to persistent respiratory symptoms (68%), recurrent sinusitis and otitis media (67%), and tracheobronchial stenosis (50%)[130]. Patients also have stippled epiphyses of long bones, peripheral pulmonary stenosis (72%) and cardiac murmur (69%), and hearing

loss (91%)[130], the latter typically mixed. Midface hypoplasia with a flat nasal bridge confers a classic facial appearance known as Binder phenotype[131]. Brachytelephalangy, with shortening and broadening of the first through fourth distal phalanges and sparing of the fifth finger, is considered highly specific for Keutel syndrome, and is present in 75% of patients[132]. Autopsy of the original brother described by Keutel revealed calcification of the internal elastic lamina of the pulmonary, coronary, hepatic, renal, meningeal, and cerebral arteries[133]. Long term follow up of patients into adulthood identified multiple erythematous macular skin lesions located in the trunk, neck, dorsum of hands and elbows, typically appearing after the age of 30 years old[134]. Adult patients can also develop massive bullous emphysema, severe systemic hypertension, and short-term amnesia[134].

The main differential diagnosis is that of brachytelephalangic chondrodysplasia punctata (CDPX1) due to arylsulfatase E deficiency, as this condition can also be accompanied by the Binder phenotype, epiphyseal stippling, tracheal calcification and brachytelephalangy[135]; although the latter tends to affect all digits[132], sparing of the fifth distal phalanx has also been described in CDPX1[135]. Another close differential diagnosis is pseudo-warfarin embryopathy due to vitamin K epoxide reductase deficiency, since patients with this syndrome also have digital hypoplasia, nasal hypoplasia, and stippled epiphyses; those patients, however, also have coagulation abnormalities[136]. Other genetic conditions associated with auricular calcification include Primrose syndrome[137] and juvenile Paget disease[138].

Molecular Genetics

Keutel syndrome is an autosomal recessive condition caused by mutations in matrix Gla protein, encoded by *MGP*[139]. The glutamate residues of matrix Gla protein are converted to γ-carboxyglutamate by the action of GGCX, with vitamin K as a cofactor for the reaction. Decreased levels of carboxylated matrix Gla protein have been reported in a patient[140]. No genotype-phenotype correlation is known to date.

Treatment

No specific treatment is available. In particular, vitamin K supplements failed to increase circulating levels of carboxylated matrix Gla protein[140].

Singleton-Merten syndrome (SMS)

Clinical Presentation and Diagnostic Aspects

In 1973, Edward Singleton and David Merten first described the condition that now carries their name. This disorder is characterized by aortic and valvular calcification (10/11, 91%; Fig. 6A), cardiac arrhythmia (6/11, 55%; Figure 6A), subungual calcification (3/8, 38%), acro-osteolysis (6/9, 67%; Fig. 6B), short stature (6/9, 67%), osteopenia (9/10, 90%; Fig. 6A), scoliosis (3/10, 30%), wide medullary cavities of the phalanges (9/10, 90%), spontaneous tendon rupture (6/11, 55%), joint subluxation (8/9, 89%), glaucoma (5/10, 50%), psoariasiform rash (8/9, 89%), and early loss of secondary dentition (10/11, 91%)[141].

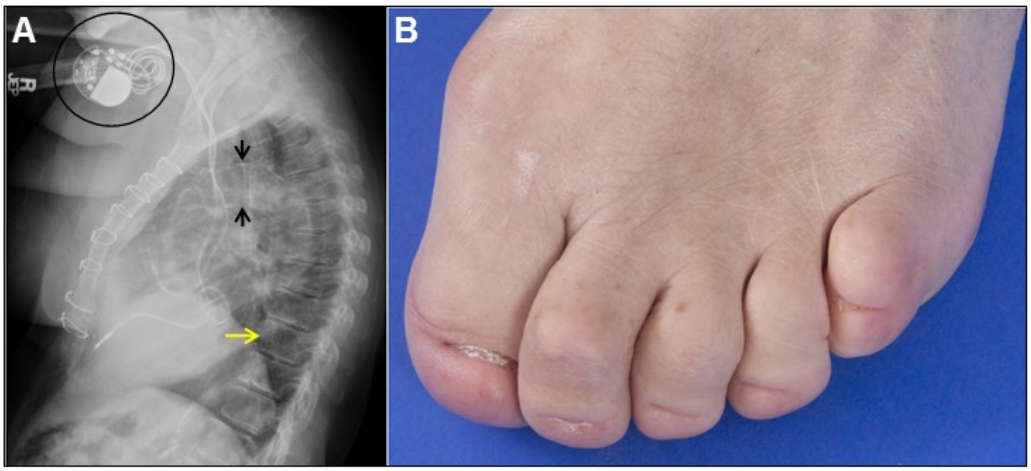

Fig. 6. Typical clinical manifestations associated with Singleton-Merten syndrome. (**A**) A pacemaker generator is noted (oval), implanted due to the presence of bradyarrhythmia; the aorta is markedly calcified ("porcelain aorta", arrowheads); the vertebral bodies show evidence of low bone mineral density (arrow). In addition, sternotomy wires can be seen, reflecting prior open heart surgery for mitral valve replacement. (**B**) Hypoplastic (first toe) and aplastic (toes 2-5) nails.

Molecular Genetics

Currently, only heterozygous mutations in *IFIH1*[142] or *DDX58*[143] account for this autosomal dominant condition. Mutations in either gene lead to interferon signature upregulation. Both genes encode components of the RIG-I-like Receptor (RLR) pathway, involved in antiviral innate immunity. A third component of this pathway is encoded by *DHX58*, not yet associated with a human disease. The authors have evaluated a family with Singleton-Merten syndrome without mutations in the two known genes, so mutations in other genes, particularly those participating in the RLR pathway, could lead to SMS. Regarding genotype-phenotype correlation, dental involvement has not been described in those carrying *DDX58* mutations[143].

Treatment

No specific treatment is known, but medications that modulate interferon pathway activation might be beneficial.

Mönckeberg medical calcific sclerosis

Mönckeberg medial calcific sclerosis is characterized by calcific deposits in the small and medium-sized muscular arteries that occurs independently of inflammation or atherosclerosis. Since the intima is not involved, luminal narrowing does not occur. It was originally described by Johann Georg Mönckeberg in 1903. This type of calcification is typically associated with chronic kidney disease, diabetes, aging, osteoporosis, and vitamin D toxicity. Although historically considered an incidental finding without clinical repercussions, it has more recently been described as a risk factor

for cardiovascular disease. Upon histopathological review of cases of Mönckeberg sclerosis, all had calcification of the internal elastic lamina, while calcification of the media was frequent but not universal. Thus, among the different causes of acquired vascular calcification, Mönckeberg's sclerosis most closely mimics the pattern of involvement seen in hereditary causes of vascular calcification.

III. ANIMAL MODELS

Animal models of ectopic calcification can produce critical insights into disease mechanism, uncover novel therapeutic targets, and provide evidence for preclinical drug efficacy. Here, we describe the rodent models that have been generated to recapitulate human diseases of pathological ectopic calcification.

GACI, PXE, and ACDC

The first sign of calcification in GACI, PXE, and ACDC mouse models occurs in the fibrous capsule surrounding their vibrissae (whiskers) on their snout. While there is no human equivalent for this fibrous structure, it has been well-established as an early biomarker for ectopic calcification. Mice harboring biallelic loss-of-function mutations in *Enpp1* manifest robust vibrissae capsule calcification by one month of age and variable aortic and kidney calcification by five months of age. *Enpp1* mutant mice also develop debilitating extraarticular joint capsule calcification and ankylosis in their forelimbs and vertebral column, leading to progressively limited mobility and death, typically within six to eight months. The architecture and mineralization of the long bones are disrupted in *Enpp1* mutant mice, emphasizing the importance of ENPP1 in both bone and vessel

homeostasis. Specifically, *Enpp1* mutant mice have reduced trabecular mass and cortical bone thickness with hypomineralization in the femur and tibia. The bone phenotype in *Enpp1* mutant mice has been attributed to increased plasma FGF23 levels, and consequently decreased circulating calcium and Pi[144], though the mechanism by which *Enpp1* mutations lead to excessive FGF23 production remains unknown.

Like *Enpp1* mutant mice, *Abcc6* knockout mice develop ectopic fibrous capsule vibrissae calcification, but with a milder and more delayed presentation. When aged beyond one year, *Abcc6* knockout mice develop focal and sporadic calcification in the skin, eyes, vessels, and other solid organs, recapitulating the common adult-onset and often indolent course of human PXE[145]. *Nt5e* knockout mice develop minor vibrissae capsule calcification at approximately one year of age without evidence of other ectopic calcification.

Though the phenotype of fibrous capsule vibrissae calcification has variable onset and severity, the observation that it is shared among *Enpp1*, *Abcc6*, and *Nt5e* mutant mice indicates the potential for a unifying disease mechanism. Nevertheless, genotypic heterogeneity cannot be excluded. While it is already established that ENPP1 and CD73 work in the same metabolic pathway, ENPP1 breaking down ATP to AMP, the substrate for CD73, the role of ABCC6 remains unknown. These data suggest that ABCC6 is also integral to the extracellular ATP metabolism pathway.

Use of an acceleration diet composed of high Pi and low magnesium or warfarin and vitamin K1 stimulates the *Enpp1* and *Abcc6* mutant mouse models to develop multi-organ pathological calcification within one to six months[146,147]. Whereas wildtype mice do not typically calcify when placed on an acceleration diet, mice harboring biallelic *Enpp1* or *Abcc6* mutations exhibit robust aberrant vascular and solid organ calcification[146–148]. *Nt5e* knockout mice develop extraarticular joint capsule calcification at approximately one year of age when provoked with an acceleration diet[149].

Since diet modification exacerbates disease presentation in the mice, manipulation of the dietary mineral content has also been attempted to attenuate disease progression, specifically in *Abcc6* knockout mice. While variation in dietary calcium or Pi does not affect calcification in this mouse model, increasing magnesium reduces vessel calcification in the heart and kidney at one year of age[150] and prevents new, but does not reverse existing, calcium Pi deposition[151,152]. The mechanism by which high magnesium modulates the calcification process in vivo remains unclear, although it has been shown that magnesium can physically disrupt the crystal lattice, slowing hydroxyapatite formation[153]. Importantly, magnesium and other serum minerals including Pi, sodium, calcium, and chloride, are normal in *Abcc6* mutant mice[154] indicating that magnesium is likely modifying disease presentation through a parallel pathway instead of correcting a basic defect in the disease.

In addition to high dose magnesium, nonhydrolyzable analogs of PPi, such as bisphosphonates, are also known to directly disrupt calcium and Pi precipitation and

deposition[155]. First-generation bisphosphonates, specifically etidronate, have been proposed as treatments for vascular calcification disorders[17]. A recent study reported that treating *Enpp1* mutant mice with etidronate (100 μg/kg intraperitoneally) twice a week did not resolve the calcification phenotype[156]. However, high-dose oral etidronate (240 mg/kg/day) was effective at attenuating fibrous capsule vibrissae calcification in *Abcc6* mutant mice[157]. The etidronate dose used in the latter mouse trial was 12 times higher than the corresponding dose used to treat osteoporosis in humans, and it resulted in significant changes to bone microarchitecture[157].

While treatment strategies have focused on disrupting calcium Pi precipitation, correction of the basic defect has also been pursued. An enzyme replacement strategy with recombinant ENPP1-Fc fusion protein restored circulating serum PPi levels and prevented mortality and vascular calcification in the aorta, heart, and coronary arteries in *Enpp1* mutant mice fed an acceleration diet[158]. When ENPP1-Fc treatment was discontinued, pathologic vascular calcification slowly reemerged but did not lead to death, suggesting that early intervention during a critical interval can extend survival. The efficacy of ENPP1-Fc enzyme replacement in other disorders with defects in extracellular ATP metabolism or more common disorders with established deficiencies in PPi remains to be determined.

Overexpressing *Alpl*, the gene that encodes tissue non-specific alkaline phosphatase (TNAP), in vascular smooth muscle cells has also been used as a model to recapitulate the GACI phenotype and provide insight into a novel therapeutic target. Among other

things, TNAP degrades PPi, the main negative regulator of calcification, and is increased in cell lines derived from GACI, PXE, and ACDC patients[20,45]. TNAP-overexpressing mice have extensive aortic calcification, high blood pressure, cardiac hypertrophy, and increased mortality[160]. This mouse model has been treated with the pharmacological small molecule TNAP inhibitor SBI-425 to suppress the genetically induced, high TNAP levels and successfully prevent the pathologic calcification[160]. Genetic manipulation to knockout TNAP in *Enpp1* mutant mice also ameliorates the calcification phenotype, specifically the intervertebral mineral deposits[161], further establishing TNAP as a drugable target in an endogenous disease model. Use of TNAP inhibitors in other mouse models in which elevated TNAP has been noted in patients' cells are currently underway.

Chondrocalcinosis and craniometaphyseal dysplasia

As in humans, mice with mutations in *Ank*, which encodes a transmembrane PPi transporter, manifest variable phenotypes with the unifying trait of ectopic calcification. Mice with complete *Ank* deficiency develop extraarticular joint capsule calcification and progressive ankylosis of the vertebral column, leading to progressive joint immobility and complete rigidity and death by six months of age[162–164]. Mice with joint-specific knockout of *Ank* have a delayed onset, but eventually develop the same characteristic phenotype as the complete *Ank* knockout mice demonstrating that, although *Ank* is expressed in many tissues, local *Ank* deficiency is sufficient to mimic the disease state[164].

While the ectopic calcification in *Ank*-deficient mice is composed of hydroxyapatite crystals, the crystals found in humans with chondrocalcinosis consist of CPPD. This

fundamental difference in pathology is a consequence of the underlying genetic mutations; while *Ank* deficiency in mice results in loss of function of the transporter and decreased extracellular PPi, human chondrocalcinosis mutations are likely gain-of-function and lead to an accumulation of extracellular PPi[164]. These conclusions are supported by data showing that human disease-causing chondrocalcinosis mutations retain normal transport activity of PPi in *Xenopus* oocytes and can partially rescue the joint calcification phenotype in *Ank* knockout mice[82].

In recent studies, closer examination revealed that *Ank* complete knockout mice exhibit some characteristic features of craniometaphyseal dysplasia patients, including increased skull bone thickness, foramen magnum narrowing, middle ear bone fusion, and decreased trabeculation of femur metaphyses, but do not fully recapitulate other main features of the human disease[82]. A new mouse model with a homozygous in-frame deletion in exon 9 of *Ank* more thoroughly resembles craniometaphyseal dysplasia; these mutant mice develop craniofacial and mandibular hyperostosis, obliteration of nasal sinuses, and flared metaphyses[165]. Of note, craniometaphyseal dysplasia patients have heterozygous, not homozygous, mutations in *ANKH*[81]. Mice harboring this knock-in mutation in the heterozygous state developed a mild skeletal phenotype by one year of age, but no other significant phenotypic differences. Taken together, these findings suggest that *ANKH* mutations causing craniometaphyseal dysplasia are not merely loss of function and might in fact be dominant negative[82]. Indeed, there is evidence to suggest that such mutations cause defects in osteoclastogenesis and bone resorption in addition to dysregulated PPi transport[166].

Daily injections of phosphocitrate, a structural PPi analogue that potently inhibits hydroxyapatite formation[167], block ectopic calcification and mitigate joint immobility in *Ank* complete knockout mice[168]. Phosphocitrate prevented new calcification, but did not reverse already established calcification; importantly, there were no adverse effects on bone mineralization[168].

Ank knockout mice have a phenotype remarkably similar to that of *Enpp1* knockout mice, although *Enpp1* mutant mice have a more extensive hypermineralization phenotype, specifically in the phalanges, and develop pathology in other soft tissue areas, such as the Achilles tendon[169]. *Enpp1* and *Ank* deficient mice also have identical expansion of the acellular cementum[170], the mineralized tissue that surrounds the tooth and anchors it to the periodontal ligament. Since acellular cementum is highly sensitive to local PPi levels, these findings suggest that both ENPP1 and ANK act in resident cells to maintain tissue homeostasis[170,171].

Mice deficient for both *Ank* and *Enpp1* qualitatively show more extensive vertebral column calcification than the single mutants alone[169], suggesting that ANK and ENPP1 have independent effects on extracellular PPi concentrations. There is evidence that ENPP1 can function both extracellularly and intracellularly[172–174], indicating that intracellular ENPP1 might be generating PPi for export by ANK. Further studies with double *Ank* and *Enpp1* deficient mice are currently underway to probe if ENPP1 and ANK work in series, in parallel, or both (personal communication with Drs. Brian L.

Foster and Emily Chu, College of Dentistry, The Ohio State University and National Institute of Arthritis and Musculoskeletal and Skin Diseases, NIH, respectively).

Interestingly, mice with inactivating mutations in *Ent1*, which encodes a facilitative diffusion carrier responsible for the movement of hydrophilic nucleosides such as adenosine across the plasma membrane, also develop ectopic mineralization of the paraspinal ligament that extends into the intervertebral discs[175]. While there is no known human equivalent, *Ent1* mutant mice develop a strikingly similar phenotype to *Enpp1*- and *Ank*-deficient mice, though six months delayed[175]. *Ent1* mutant mice have increased circulating adenosine and PPi levels and decreased *Alpl, Enpp1*, and *Ank* expression in the local tissue that calcifies. Adenosine decreases the expression of *Alpl* [20], the gene encoding TNAP, and this could explain the increased circulating PPi; however, it is unclear if the decreased expression of *Enpp1* and *Ank* is primary or compensatory. In any event, these overlapping mouse phenotypes illustrate the complex and poorly delineated intersection of PPi production and intracellular adenosine signaling.

Tumoral calcinosis

Tumoral calcinosis is caused by biallelic inactivating mutations in *Galnt3*, *Fgf23*, or *Klotho*; mouse models have been generated to disrupt these genes to define their function and probe the interaction of Pi-regulating factors in vivo. Mutant mouse models develop hyperphosphatemia secondary to increased renal tubular Pi reabsorption with associated ectopic subcutaneous soft tissue and vascular calcification, in addition to increased or inappropriately normal 1,25-dihydroxyvitamin D levels[176–178]. *Galnt3* and *Fgf23* mutant

mice have decreased serum concentrations of intact (functional) Fgf23 since their basic defect is in Fgf23 processing whereas *Klotho* deficient mice have elevated Fgf23 levels, reflecting compensation for defective signaling at the FGF receptor[178,179].

By 12 weeks of age, the ENU-mutated *Galnt3* mouse presents with widespread calcification in the cutaneous striated muscle, heart, kidney, tongue submucosa, and in the vasculature localized to the aorta and testis, and closely recapitulates the clinical features of tumoral calcinosis[177]. The *Galnt3* knockout mouse model, however, only develops ectopic calcification when provoked with a high Pi diet[180]. Nicotinamide, which is hypothesized to lower serum Pi by decreasing activity of sodium-dependent Pi reuptake co-transporters in the gut[181] and kidney[182], was used to treat *Galnt3* knockout mice initially fed a high Pi diet. Although the nicotinamide modestly prevented new calcification, it did not reverse existing calcium deposits and in fact increased calcium content in the heart. It was shown that nicotinamide further decreased circulating levels of intact Fgf23, likely as a compensatory mechanism to increase Pi reabsorption in the kidney in response to the drug[183]. These findings emphasize the tight regulation of this pathway.

In addition to the common features of tumoral calcinosis, mice deficient in *Fgf23* or *Klotho* also present with extensive occlusive aortic calcifications, vascular and parenchymal renal calcification, thickening and calcification of the auditory ossicles, pulmonary calcification with emphysematous changes, skin atrophy, osteopenia, hypercalcemia, hypoglycemia, and early death[176,178,184,185]. The additional phenotypic

features and premature death of *Fgf23* and *Klotho* deficient mice represent a more severe phenotype than that of patients with tumoral calcinosis, and suggest that rodent models, compared with humans, are more sensitive to disruptions in this pathway and less likely to compensate for deficiencies in Pi -regulating factors.

However, these mouse models still provide valuable insights into disease mechanism and potential therapeutic interventions. *Fgf23* knockout mice fed a low Pi diet had decreased serum Pi and 50% of mutants survived longer, although they still demonstrated growth retardation, hypoglycemia and elevated 1,25-dihydroxyvitamin D levels; ectopic calcifications were not evaluated in this study[176]. In a trial with more severe dietary restrictions of Pi, Pi deficiency corrected the hyperphosphatemia, prevented vascular calcification, and rescued the lethality in *Fgf23* knockout mice[186].

Modulating vitamin D activity and levels has also been attempted as therapy for tumoral calcinosis mouse models. Genetically ablating vitamin D activity by knocking out the gene encoding an activator of vitamin D synthesis, 1α-hydroxylase, or inactivating the vitamin D receptor in *Fgf23* knockout mice eliminates the soft tissue and vascular calcification and ameliorates other aspects of the phenotype including body weight, skin atrophy, and premature death[187–189]. These genetic models corrected both the hyperphosphatemia and high vitamin D levels in the *Fgf23* mutant mice and therefore did not assess the independent contributions of excessive serum Pi and vitamin D on vascular calcification. Restricting only vitamin D in mouse models of tumoral calcinosis has had variable effects. Lowering vitamin D by dietary restriction failed to correct the

hyperphosphatemia or the vascular calcification, although it did extend survival in *Fgf23* null mice[186] while also preventing ectopic kidney calcification and restoring normal body weight in *Klotho* mutant mice[190]. Taken together, these data implicate both Pi and vitamin D as predominant mediators of the tumoral calcinosis phenotype. Although the therapeutic efficacy of lowering vitamin D levels remains unclear, these studies imply that decreasing Pi reduces ectopic calcification.

In other studies, the mineralocorticoid receptor antagonist spironolactone reduced vascular and soft tissue calcification and slightly increased the lifespan of *Klotho* deficient mice, without significantly affecting circulating Pi, vitamin D, FGF23, or calcium concentrations[191]. It has been suggested that spironolactone acts locally to decrease expression of genes involved in procalcific reprogramming and differentiation in the vessel wall[191]. These data indicate that ectopic calcification is not controlled only by circulating Pi and calcium, but that cell-intrinsic factors also mediate pathologic calcification. Recently, independent supplementation of sodium chloride, ammonium chloride, or bicarbonate also mildly attenuated tissue calcification and extended the lifespan of *Klotho* deficient mice[192–194], suggesting that dysregulation of extracellular volume and pH can influence the disease phenotype.

There is no mouse model for normophosphatemic familial tumoral calcinosis, since the *SAMD9* ortholog was lost in mice due to a genomic rearrengement[195].

Idiopathic basal ganglia calcification

Four genes, *SLC20A2* (*PIT2*), *XPR1, PDGFRB*, and *PDGFB,* have been implicated in idiopathic basal ganglia calcification. Homozygous *Slc20a2* knockout mice present with brain calcification localized to arterioles, specifically in the thalamus, basal ganglia, and cortex, by 19 weeks of age[196]. *Slc20a2* knockout mice also developed microphthalmia, calcified cataracts and optic nerve tissue, and moderate to severe hydrocephalus, phenotypes not typically seen in idiopathic basal ganglia calcification patients[197]. *Slc20a2* mice that are heterozygous for the knockout allele more closely recapitulate the human phenotype and develop brain vessel calcification later and without the additional manifestations of homozygous *Slc20a2* knockout mice[197].

While serum Pi and calcium concentrations did not differ among wildtype, heterozygous, and homozygous *Slc20a2* mice, cerebrospinal fluid Pi levels were trending high and were significantly increased in heterozygous and homozygous *Slc20a2* mutant mice, respectively[197]. Decreased phosphate import was also observed in vascular smooth muscle cells with experimentally knocked down *Slc20a2*, suggesting that the calcification phenotype is caused by a combination of high circulating Pi in the cerebrospinal fluid and defects in the local cell population[197]. *Slc20a2* mutant mice have not been subjected to behavioral or neuropsychiatric testing to see if calcification in brain arterioles leads to functional consequences. *Xpr1* mutant mice are commercially available but have not yet been evaluated for pathologic calcification or a corresponding phenotype.

While mutations in *Slc20a2* suggest that idiopathic basal ganglia calcification is caused by a combination of circulating and local disruptions in Pi homeostasis, mice completely

null for *Pdgfrb* and *Pdgfb* exhibit an inability of pericyte recruitment to developing microvessels; this leads to vascular dysfunction and perinatal death, and implicates a role for the blood-brain barrier maintenance in disease pathogenesis[198]. Central and peripheral nervous system-specific *Pdgfrb* knockout mice have reduced social behavior and increased locomotor activity, reminiscent of some atypical neurological findings seen in idiopathic basal ganglia calcification patients; however, brain calcification was not reported[199]. A mouse model with a hypomorphic allele of *Pdgfb* presented with calcific foci in the midbrain and thalamus at four months that expanded with age. Although blood-brain barrier integrity was not directly tested, these hypomorphic *Pdgfb* mice were rescued by overexpression of PDGF-B in the endothelium[200]. Supporting the role of blood-brain barrier defects in disease pathogenesis, fibrinogen depositions at autopsy have been associated with areas of calcification of one idiopathic basal ganglia calcification patient, indicating increased permeability of the blood-brain barrier. However, it is uncertain if this blood-brain barrier deficit is a cause or a consequence of the underlying pathology[201].

Also to note, knocking out *Occludin*, an integral tight junction component of the blood-brain barrier, in mice results in cerebellar and basal ganglia calcification, similar to that seen in the mouse models of idiopathic basal ganglia calcification[202]. Taken together, these findings strongly implicate Pi homeostasis[203] and the PDGFB-PDGFRB signaling pathway[204] in ectopic brain calcification. Though the intersection of these pathways remains unclear, it has been reported that PDGFB increases the expression of *Slc20a2* in culture[205].

Keutel syndrome

Homozygous ablation of *Mgp*, the gene encoding the vitamin K-dependent gamma carboxylated matrix Gla protein, results in extensive arterial and cartilaginous calcification in mice, recapitulating the Keutel syndrome phenotype[206]. Calcification develops at approximately two to three weeks of age and is limited to elastic and muscular arteries and cartilaginous structures; the phenotype rapidly progresses and results in aortic rupture and death within two months[206]. There is evidence of both elastic fiber calcification and cartilaginous metaplasia that can lead to ossification of affected vessels[206].

In addition to genetic ablation of the gene, matrix Gla protein has also been experimentally decreased by administration of exogenous warfarin, a vitamin K reductase inhibitor[207]. Rats treated with warfarin and concurrent vitamin K1 had decreased extrahepatic vitamin K but normal vitamin K-dependent blood clotting factors and coagulation[207,208]. Warfarin treatment resulted in extensive arterial calcification that did not regress when warfarin was removed[207], but that did regress when the rats were repleted with vitamin K[209]. Mice with deficiency of osteoblast-specific *Ggcx*, the gene necessary for gamma-glutamyl carboxylase that, along with vitamin K, modifies and activates matrix Gla protein, also presented with aberrant calcification[210]. Indeed, phenotypic similarities between the effects of genetic and environmental mediators of matrix Gla protein illustrate the importance of this factor in suppressing pathologic calcification.

Singleton-Merten syndrome

An ENU-mutated mouse model with a heterozygous gain-of-function mutation in *Ifih1*, which encodes the intracellular viral sensor MDA5 that has recently been associated with Singleton-Merten syndrome, predominantly develops lupus-like nephritis and systemic autoimmune symptoms without a viral insult[211]. Although these mice do not closely recapitulate the Singleton-Merten phenotype, *Ifih1* mutant mice develop spontaneous multiorgan inflammation and liver calcification[211]. These mice have not been evaluated for a more extensive calcification phenotype.

Chronic kidney disease, diabetes, and aging

Common disorders of vascular calcification, including chronic kidney disease, diabetes, and aging, have also been studied in rodents. Chronic kidney disease has been modeled by subjecting rodents to diets composed of high adenine, warfarin, or by partial or complete ablation of the kidneys, while calcification in chronic kidney disease models has been induced through diets high on vitamin D or Pi[212–214]. These dietary and surgical provocations typically result in increased plasma concentrations of urea, Pi, and FGF23 and cause extensive, though variable, medial vascular calcification, closely mimicking the reduced penetrance of vascular calcification-associated chronic kidney disease.

Decreasing circulating Pi levels, attempted in a tumoral calcinosis mouse model, was also investigated in rodent models of chronic kidney disease. Nicotinamide prevents the development of hyperphosphatemia by suppressing intestinal sodium-dependent Pi

transport in rats with adenine-induced renal failure[215]; however its effect on ectopic calcification was not evaluated. Studies have shown that administering exogenous PPi via subcutaneous injection or continuous intraperitoneal infusion inhibits medial arterial calcification in vitamin D-toxic rats without affecting bone formation or mineralization[216–218].

Bisphosphonates have also been shown to prevent aortic calcification in uremic rats[17]. However, as in other vascular calcification disorders such as GACI and PXE, attempts to treat chronic kidney disease-induced vascular calcification with bisphosphonates required doses that disrupted bone mineralization and architecture[17]. Additionally, the bone toxicity coupled with the fact that bisphosphonates require renal clearance has discouraged their use in chronic kidney disease[17].

Low-density lipoprotein receptor-null mice fed a high fat and cholesterol diet develop characteristics of metabolic syndrome including hypertension, obesity, dyslipidemia, and insulin resistance, in addition to robust vascular calcification with some evidence of cartilaginous metaplasia[219,220].

Mouse models recapitulating disorders of early aging also present with calcification. Knock-in *Lmna* mice recapitulate some of the clinical manifestations of Hutchinson-Gilford progeria syndrome, an accelerated aging disorder that leads to premature death[221]. *Lmna* mutant mice show excessive aortic calcification. Vascular smooth muscle cells derived from these animals have increased TNAP expression and activity and

subsequently reduced PPi levels and therefore a reduced capacity to inhibit in vitro calcification[221]. Treatment of these mice with intraperitoneal injections of PPi inhibited vascular calcification[221]. It has been questioned, however, if the rapid hydrolysis of PPi in vivo prevents translation of this therapy to patients[222].

IV. DISEASE MECHANISMS

Regulators of Calcification: Phosphate, Pyrophosphate, and Matrix Gla protein

Mineralization of cartilage, bone, and tooth extracellular matrix is a physiological process whereas ectopic calcification is a pathological one. Nevertheless, evidence suggests that ectopic calcification, like bone formation, is a highly regulated process involving both inductive and inhibitory processes. These determinants include extracellular levels of calcium, the presence of a scaffolding extracellular matrix for mineral deposition, and the relative amounts of mineralization activators (e.g., Pi) and inhibitors (e.g., PPi and matrix Gla protein) present within the extracellular matrix environment. Fetuin, osteopontin, and osteoprotegerin are also negative regulators of calcification, although data suggest that they are more actively involved in atherosclerosis and bone mineralization rather than ectopic calcification, and will not be discussed further[223]. These factors are tightly balanced both in the circulation and in local microenvironments to maintain homeostasis and prevent pathologic calcification.

Phosphate

Pi is a major component and promoter of calcification. In the presence of calcium, various calcium Pi salts are formed to neutralize the negative Pi ions; these amorphous

calcium Pi precipitates eventually form hydroxyapatite[224,225]. In culture systems, high phosphate can induce osteochondrogenesis (see Osteochondrogenic Differentiation below). In more common disorders of vascular calcification, serum phosphate is elevated, especially in patients with chronic kidney disease[226].

The role of Pi in pathologic calcification is most readily appreciated in patients with tumoral calcinosis, whose hyperphosphatemia leads to precipitation of Pi and calcium in ectopic tissue. GALNT3, KLOTHO, and FGF23 are part of a tightly regulated Pi reabsorptive pathway (Fig. 7). In the bone, GALNT3 O-glycosylates FGF23, preventing the proteolytic processing of FGF23, and therefore allowing the secretion of intact FGF23 into the circulation. At the kidney, FGF23 binds to the FGFR1 receptor along with the co-receptor KLOTHO. FGF23 signaling inhibits expression of renal 1α-hydroxylase, thereby decreasing serum concentrations of 1,25-dihydroxyvitamin D and reducing intestinal inorganic Pi absorption. In addition, FGF23 signaling downregulates the renal type 2 sodium-phosphate co-transporters (NaPi-2a and NaPi-2c), thereby decreasing renal tubular reabsorption of Pi[100]. When this pathway is defective, there is increased Pi reabsorption from both the gut and the kidneys.

The regulation of Pi is also seen in idiopathic basal ganglia calcification. SLC20A2 is a sodium-dependent Pi importer, while XPR1 is a phosphate exporter[227,228] (Fig. 8). Inactivating mutations in both genes cause idiopathic basal ganglia calcification emphasizing the tight regulation of Pi homeostasis. *XPR1* mutation-mediated calcium Pi precipitation has been suggested to occur intracellularly, whereas mutations in *SLC20A2*

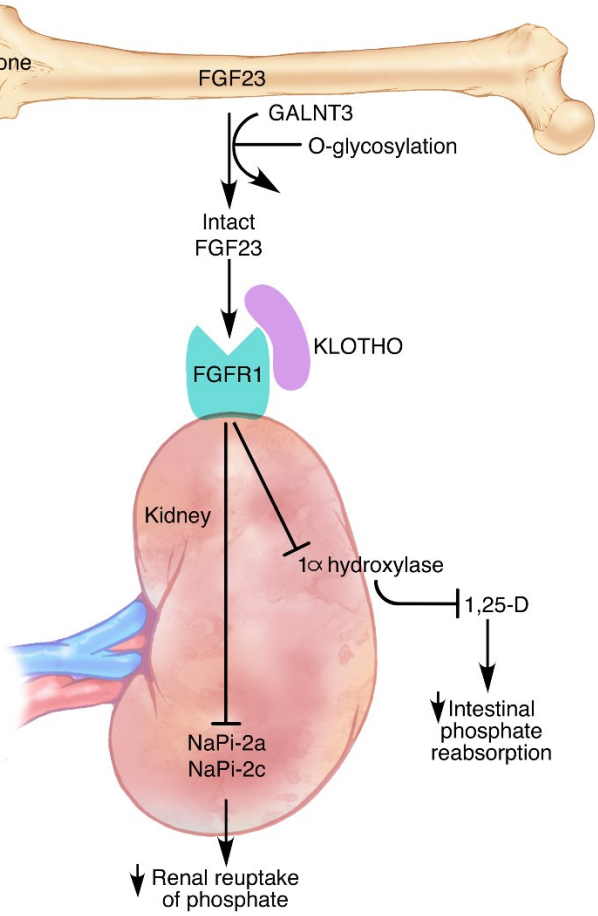

Fig. 7. The roles of GALNT3, FGF23, and KLOTHO in Pi homeostasis. In the bone, GALNT3 glycosylates FGF23, preventing the proteolytic processing of FGF23, and therefore allowing the secretion of intact (active) FGF23 into the circulation. At the renal tubular cell membrane, FGF23 binds to the FGFR1 receptor along with co-receptor KLOTHO. FGF23 signaling inhibits expression of renal 1α-hydroxylase, thereby decreasing concentrations of 1,25-dihydroxyvitamin D in the circulation; this reduces intestinal Pi absorption. FGF23 signaling also downregulates the renal type 2 sodium- Pi co-transporters (NaPi-2a and NaPi-2c) thereby decreasing renal tubular reabsorption of Pi. When the FGF23 pathway is defective, there is increased Pi reabsorption from both the gut and the kidneys.

are thought to lead to deposition of calcium Pi in the extracellular matrix. However, this paradigm has yet to be established in vivo[228].

Pyrophosphate

PPi acts as a potent inhibitor of calcification; it antagonizes the ability of Pi to crystallize with calcium to form hydroxyapatite, presumably by occupying some of the inorganic Pi sites on the surface of nascent growing hydroxyapatite crystals; the irregularities created slow or terminate crystal growth[229]. Three molecules (ENPP1, ANK, and TNAP) have been identified as central regulators of PPi levels (Fig. 9).

ENPP1 is the primary source of extracellular PPi and hydrolyzes extracellular ATP into AMP and PPi[230]. ENPP1 is a cell surface glycoprotein enzyme that functions in synergy with the multiple-pass transmembrane protein ANK which mediates intracellular to extracellular channeling of PPi[169]. While ENPP1 is known to work extracellularly, it has been recently shown that soluble ENPP1 functions intracellularly and might also be the source of PPi for transport by ANK[172–174].

The extracellular concentration of PPi is further influenced by TNAP, another cell surface enzyme located on the membrane of cells and matrix vesicles. TNAP exerts its effects by hydrolyzing PPi, reducing the concentration of this mineralization inhibitor and establishing an Pi /PPi ratio permissive for the formation of hydroxyapatite crystals.

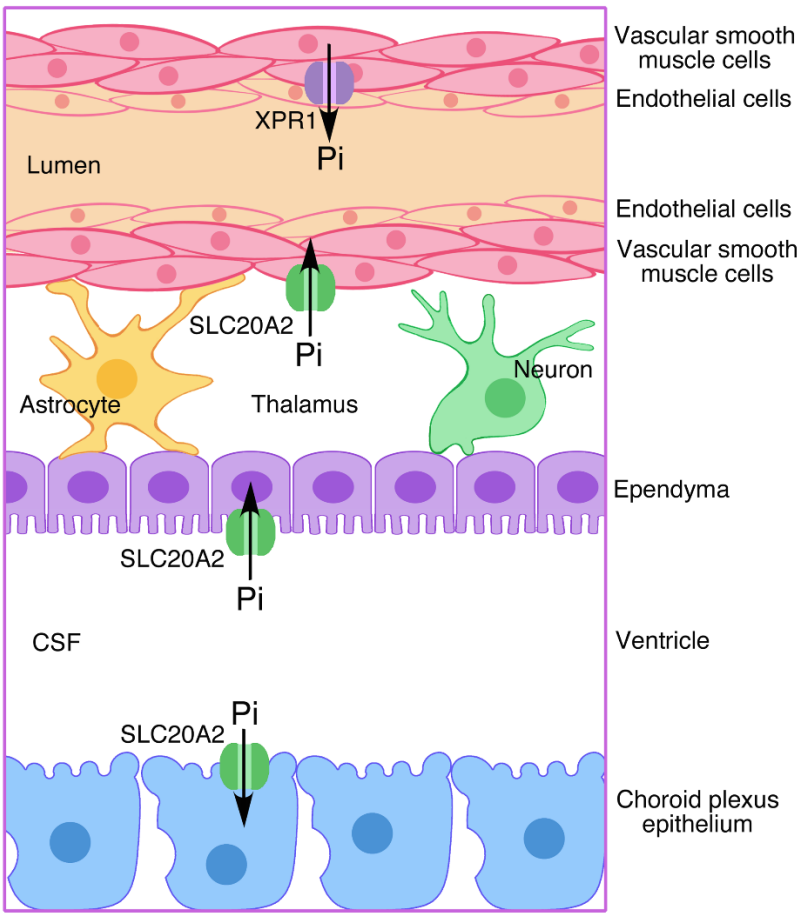

Fig. 8. The regulation of Pi in idiopathic basal ganglia calcification. SLC20A2, a sodium-dependent Pi importer, is predominantly expressed on cerebrospinal fluid-producing cells surrounding the ventricle and on vascular smooth muscle cells encompassing vessels in the brain. XPR1, a Pi exporter, is also expressed on vascular smooth muscle cells. Inactivating mutations in *SLC20A2* and *XPR1* result in basal ganglia calcification emphasizing the tight regulation of Pi homeostasis. While mutations in *SLC20A2* lead to increased cerebrospinal fluid phosphate levels and dysfunction of local vascular smooth muscle cells which likely cause ectopic calcification in the extracellular matrix, *XPR1* mutation-mediated calcium Pi precipitation has been suggested to occur intracellularly.

Decreases in PPi cause pathologic calcification, as seen in GACI patients who reportedly have low plasma[231] and urinary[232] PPi levels. While calcification in GACI appears directly related to PPi deficiency, the vascular mineralization in ACDC patients involves a downstream metabolite, namely adenosine. Adenosine signaling trophically inhibits *ALPL* expression[20,175]. Impaired intracellular signaling mediated by adenosine receptors is considered responsible for the increased levels of TNAP in ACDC patient-cultured fibroblasts[20]. Increased TNAP activity degrades extracellular PPi, promoting pathologic calcification.

Levels of PPi are reduced in hemodialysis patients[233] and correlate inversely with the amount of vascular calcification in patients with advanced chronic kidney disease[234]. Circulating PPi levels are primarily reduced, most likely because of increased alkaline phosphatase activity in the vessel wall. Consistent with these findings, intact aortas and aortic homogenates from uremic rats showed a substantial increase in TNAP enzyme activity[235].

PPi is considered a potent inhibitor of calcium Pi crystal formation, but when present at high levels, PPi itself can precipitate with calcium ions to form an alternative type of crystal called CPPD. Indeed, gain-of-function mutations in *ANKH* cause chondrocalcinosis, and lead to higher steady-state concentration of PPi in the joint space[82].

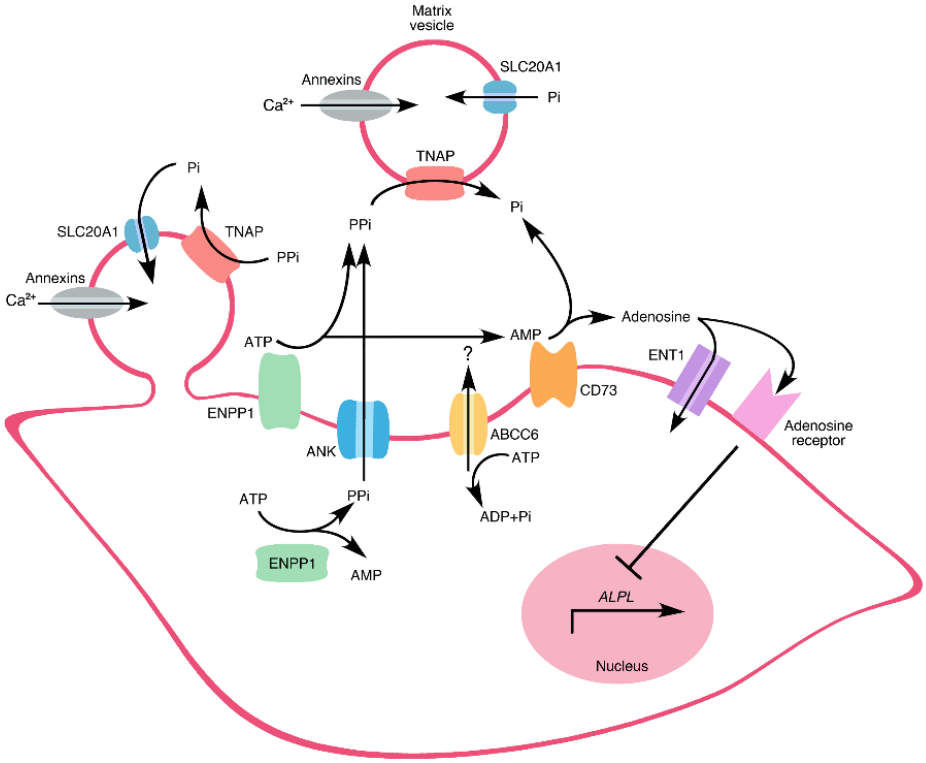

Fig. 9. Schematic representation of the predominant enzymatic reactions and transported substrates in local cells involved in ectopic calcification. ENPP1 breaks down ATP into AMP and PPi. ANK transports PPi out of the cell, also contributing to extracellular PPi levels. CD73 further degrades AMP into adenosine and Pi. ABCC6 is integral to the extracellular ATP metabolism pathway, though its substrate and function remain elusive. Adenosine can be transported into the cell by ENT1 or bind to a cell surface adenosine receptor to promote a number of diverse downstream actions, including repression of *ALPL*, the gene encoding TNAP. TNAP degrades PPi into Pi and is a primary distal regulator of Pi and PPi homeostasis. Matrix vesicles bud off of local cells and accumulate Pi through SLC20A1 and calcium though annexins. Calcium and Pi precipitate as a nidus of calcification inside the matrix vesicles. Continued calcium- Pi accumulation eventually leads to matrix vesicle breakage and propagation of hydroxyapatite in the extracellular space.

Matrix Gla protein

Matrix Gla protein is recognized as a potent local inhibitor of vascular calcification[140,236]. To be fully functional, matrix Gla protein requires posttranslational modification by a gamma-carboxylase, a vitamin K-dependent protein that is inhibited by warfarin. Interestingly, only when matrix Gla protein is overexpressed in vascular smooth muscles cells–instead of the liver–does it inhibit calcification in vivo, strongly suggesting that matrix Gla protein acts locally to prevent ectopic calcification[237].

Matrix Gla protein binds to calcium and is secreted by chondrocytes and vascular smooth muscle cells[206]. It directly inhibits calcification, co-localizing with elastin in the arterial elastic lamina and physically disrupting calcium-phosphate deposition[238]. Matrix Gla protein also sequesters bone morphogenic protein (BMP), specifically BMP2, in vitro and subsequently inhibits vascular BMP signaling and osteogenic differentiation[239]; it is unclear if this process is relevant in vivo.

Local versus Circulating Hypotheses

Pi, PPi, and matrix Gla protein have been widely accepted as regulators of ectopic calcification, largely because they also function in the physiologic mineralization of skeletal hard tissues. There is considerable controversy, however, concerning the relative contribution of these factors from the local microenvironment versus the circulation. Determining the biologically relevant tissues and/or cell types producing these factors has been most extensively explored in the context of disease states, specifically PXE and IBGC.

The protein defective in PXE, ABCC6, is a member of the multidrug resistant protein family, with known transporter activity[240], but its endogenous substrate remains elusive. The ABCC6 protein has very low expression in the peripheral cells directly affected in PXE, i.e., dermal fibroblasts and vascular smooth muscle cells[241], but strong expression in the liver[242] and, to a lesser extent, kidney. This has led to the prevailing hypothesis that ABCC6 exports an endocrine inhibitor of calcification that acts at distant target sites[243], but only circumstantial evidence exists for this "metabolic" theory (Fig. 10). Specifically, a wildtype muzzle transplanted onto the back of an *Abcc6* mutant mouse developed ectopic calcification in the fibrous capsule surrounding the vibrissae[244]. It is unclear if the observed calcification completely recapitulates the PXE mouse model phenotype since the extent of calcification of an *Abcc6* mutant muzzle transplanted onto an *Abcc6* knockout mouse was not investigated. In another study, parabiosis between *Abcc6* mutant and wildtype mice in which the two circulations were connected showed attenuation of the calcification phenotype in the mutant mouse compared to that seen in the parabiosis of two *Abcc6* mutant mice[245]. If PXE is solely driven by a circulating factor, however, it would be expected that both the mutant mouse and wildtype mouse would have the same degree of calcification since they were paired before the onset of the phenotype; however, there was no calcification observed in the wildtype mouse when the *Abcc6* mutant and control mice were paired. Taken together, these data suggest that a defect in a circulating factor is sufficient to induce ectopic calcification and repletion of this factor diminishes the phenotype. However, since the *Abcc6* mutant mouse in the *Abcc6* mutant-wildtype mouse parabiosis pairing showed calcification whereas its paired

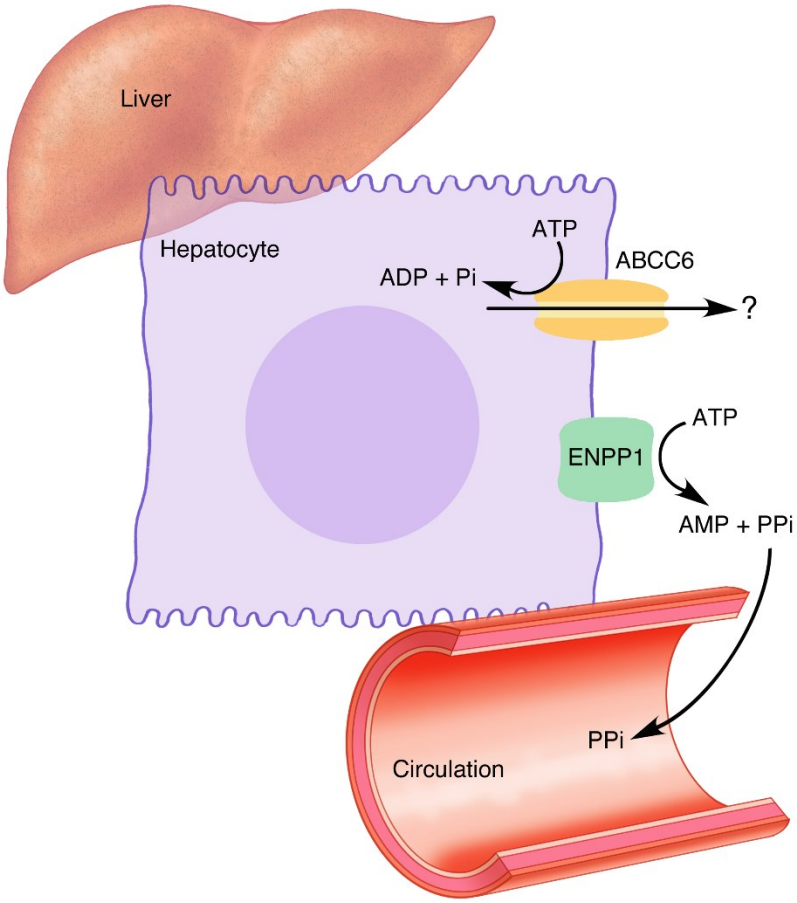

Fig. 10. The contribution of circulating factors in PXE pathogenesis. The lack of knowledge pertaining to the substrate transported by ABCC6 complicates our understanding of PXE. The strong expression of ABCC6 in the liver has led to the prevailing hypothesis that hepatocellular ABCC6 exports an endocrine inhibitor of calcification that acts at distant target sites. However, recent evidence (discussed in Chapter 4) suggests that local cells might be involved in PXE pathogenesis. It has been shown that PXE patients and mice have decreased circulating PPi levels. Low PPi could be indirectly mediated by the actions of ENPP1 in the liver, or as a consequence of high TNAP activity in local cells. A unifying hypothesis would propose that mutations in *ABCC6* make local cells vulnerable to decreased circulating PPi.

wildtype mouse did not, this indicates that another factor, perhaps a local cell, might also be involved in PXE-related calcification.

Dermal fibroblast cell lines derived from PXE patients are morphologically and biochemically distinct from controls; they have higher proliferation rates, decreased cell-cell and cell-matrix adhesion properties, and altered synthesis of connective tissue components, including elastin, collagen, and proteoglycans, in addition to different integrin subunit expression[246,247]. *ABCC6* mutant cells also produce 30% less matrix Gla protein compared to controls[248]. Finally, *ABCC6* mutant cells have a tendency for matrix mineralization and an altered metabolic profile, including higher gene expression of the PPi metabolizing enzymes, TNAP[249].

Some scientists contend that these cultured fibroblast-specific changes are due to persistence of a circulating factor that impairs the function of the fibroblasts in vitro[250]; however, it is also possible that there are inherent, cell-autonomous defects in PXE patient-derived cells. Indeed *Abcc6* mutant zebrafish showed signs of excessive pathologic calcification and *Abcc6* gene expression was localized to sites of ectopic calcification, specifically in osteoblasts, instead of the liver[251].

The lack of knowledge pertaining to the substrate transported by ABCC6 complicates our understanding of PXE pathogenesis. It has recently been proposed that ABCC6 indirectly mediates ATP transport from the liver, which is then immediately broken down into AMP and PPi[252], implicating PPi as the circulating metabolic factor missing in PXE

(Fig. 10). In support of this hypothesis, it has been established that there are decreased levels of circulating PPi in PXE mice and humans. However, low levels of PPi could also be a result of high TNAP activity, which has been observed in *ABCC6*-deficient cells.

A unifying hypothesis would propose that mutations in *ABCC6* make local cells (such as vascular smooth muscle cells or fibroblasts; Fig. 9) vulnerable to decreased circulating PPi, which is mediated by transport from the liver (Fig. 10). This hypothesis would reconcile the published results showing that there is low circulating PPi with the data demonstrating a cell-autonomous phenotype.

The dispute between circulating and local factors is also apparent in the disease pathogenesis underlying idiopathic basal ganglia calcification. *Slc20a2* knockout mice have high Pi levels in the cerebrospinal fluid compared to control mice[197] because of decreased Pi reuptake in cerebrospinal fluid-generating tissues, including the choroid plexus and ependyma (Fig. 8). It has also been shown that *Slc20a2* is expressed locally in vascular smooth muscle cells, but not in pericytes or endothelial cells. When *Slc20a2*-deficient vascular smooth muscle cells are exposed to osteogenic media in vitro, they have an increased susceptibility to calcification. Thus, basal ganglia calcification may be caused by the combination of abnormal cerebrospinal fluid Pi homeostasis and increased susceptibility of vascular smooth muscle cells[197].

These examples illustrate that both circulatory and local factors are necessary to maintain tissue homeostasis. In PXE, there is a circulatory deficit of blood PPi whereas in idiopathic basal ganglia calcification there is excess Pi in the cerebrospinal fluid. In both diseases, local cells are sensitized by their basic genetic defects to the circulating imbalances, resulting in pathologic calcification.

Osteochondrogenic Differentiation

While dysregulation of PPi and Pi may directly lead to precipitation of calcium Pi and eventual hydroxyapatite formation, local changes in PPi and Pi homeostasis might also trigger cell-mediated mineralization, acceleration of the calcification process, and potential for ossification and/or chondrification. Transdifferentiation of vascular smooth muscle cells into osteochondrocyte-like cells has been reported in the media of calcified vessels of rare diseases (e.g., Keutel syndrome[139,206]) and common disorders, such as chronic kidney disease, type 2 diabetes, and patients on dialysis[220,253–256]. These cells express bone and/or cartilage-specific proteins, such as TNAP, which often co-localize with calcium-Pi minerals in the vessel wall[253]. Matrix vesicles, which accumulate calcium and Pi and eventually become the nidus for calcification, have also been identified in situ in these sites of calcification[257].

In vitro, cells derived from the arterial media, mainly vascular smooth muscle cells, undergo osteochondrogenic differentiation in response to elevated Pi levels by increasing expression of bone regulatory proteins while simultaneously downregulating markers of smooth muscle lineage[258,259]. Specifically, when stimulated with inorganic phosphate,

these cells express the sodium-dependent phosphate transporter (*SLC20A1*) which induces the early osteogenic/chondrogenic transcription factor RUNX2[254,260]. In addition to Pi dysregulation, a number of other signaling pathways have been implicated in directly promoting osteochondrogenic differentiation, including BMP2[261] and PDGF-BB signaling through PDGFRB[262]. These osteochondrocyte-like cells elaborate matrix vesicles[263] and eventually mineralize their extracellular matrix, much like the physiological conditions driving bone formation[264].

There is conflicting evidence pertaining to the onset of lineage reprogramming in the context of pathologic calcification. Some evidence suggests that osteochondrogenic differentiation occurs before calcium deposition, such as in matrix Gla protein-null mice where calcified cartilaginous lesions originate from phenotypically transformed vascular smooth muscle cells[264]. However, other reports indicate that while cells with osteochondrocyte-like morphology are resident in the calcified aorta, osteochondrogenic markers are not upregulated in the arteries prior to the initiation of calcification[265].

To probe the relative contributions of osteochondrogenic transdifferentiation versus calcium Pi deposition, the *Mgp*-null mouse was independently bred to transglutaminase 2 and Elastin knockout mice. Knocking out transglutaminase 2, a promoter of BMP signaling, in matrix Gla protein-null mice decreased calcification presumably by inhibiting the phenotypic transdifferentiation of vascular smooth muscle cells into osteochondrocyte-like cells[266]. Elastin haploinsufficiency in matrix Gla protein -null mice also significantly reduced arterial calcification[265]. Indeed, both genetic crosses

reduced calcification, indicating that these processes are co-existent and likely both necessary to promote ectopic calcification.

Despite the controversy over whether osteochondrogenic differentiation is an inciting event or a consequence of ectopic calcification, complete ossification or chondrification only occurs in a minority of diseased arteries. While bone and cartilage have been observed in vessels from mice with *Mgp* deficiency[206], long-standing diabetes, and renal failure[267,268], bone or cartilage metaplasia has not been seen in any other disorders of ectopic calcification. This is possibly because of slower angiogenic invasion or the greater abundance of elastin, which maintains the smooth muscle cell phenotype[269]. Additionally, this cellular differentiation process might be attenuated in this disease context, maintaining only partial capacity for bone or cartilage formation.

Viral Mechanisms

There is also evidence that implicates the disruption of the viral maintenance machinery in ectopic calcification. MDA5, encoded by *IFIH1*, is a member of the RIG-1-like receptor family and functions as a cytoplasmic pattern-recognition receptor recognizing viruses, double-stranded RNA, and secreted bacterial nucleic acids[270]. How these pathways intersect with the known pathways of ectopic calcification remains to be elucidated.

V. CONCLUSIONS

The balance between Pi and PPi, in addition to other factors, is strictly controlled by a complex interplay of genes and plays an undisputed role in ectopic calcification. Understanding this homeostasis and the pathways involved will help us better identify new treatment targets and design therapeutic strategies. Insights into rare diseases should also inform more common presentations.

CHAPTER 2

NT5E MUTATIONS AND ARTERIAL CALCIFICATIONS

I. ABSTRACT

Background

Arterial calcifications are associated with increased cardiovascular risk, but the genetic basis of this association is unclear.

Methods

We performed clinical, radiographic, and genetic studies in three families with symptomatic arterial calcifications. Single-nucleotide-polymorphism analysis, targeted gene sequencing, quantitative polymerase-chain-reaction assays, Western blotting, enzyme measurements, transduction rescue experiments, and in vitro calcification assays were performed.

Results

We identified nine persons with calcifications of the lower-extremity arteries and hand and foot joint capsules: all five siblings in one family, three siblings in another, and one patient in a third family. Serum calcium, Pi, and vitamin D levels were normal. Affected members of Family 1 shared a single 22.4-Mb region of homozygosity on chromosome 6 and had a homozygous nonsense mutation (c.662C→A, p.S221X) in *NT5E*, encoding CD73, which converts AMP to adenosine. Affected members of Family 2 had a homozygous missense mutation (c.1073G→A, p.C358Y) in *NT5E*. The proband of Family 3 was a compound heterozygote for c.662C→A and c.1609dupA (p.V537fsX7). All mutations found in the three families result in nonfunctional CD73. Cultured

fibroblasts from affected members of Family 1 showed markedly reduced expression of *NT5E* messenger RNA, CD73 protein, and enzyme activity, as well as increased alkaline phosphatase levels and accumulated calcium Pi crystals. Genetic rescue experiments normalized the CD73 and alkaline phosphatase activity in patients' cells, and adenosine treatment reduced the levels of alkaline phosphatase and calcification.

Conclusions

We identified mutations in *NT5E* in members of three families with symptomatic arterial and joint calcifications. This gene encodes CD73, which converts AMP to adenosine, supporting a role for this metabolic pathway in inhibiting ectopic tissue calcification.

II. INTRODUCTION

Vascular calcification, arising either in the intima or media of vessels, is associated with an excess risk of cardiovascular events[271,272]. This was initially considered a passive response to degenerative events, but mounting evidence suggests it is the result of a process that mimics active bone remodeling[273,274]. Extracellular calcification is increasingly viewed as arising from a default biochemical default pathway and requiring the constant stimulation of inhibitory systems to prevent its occurrence.

Only a single Mendelian disorder of isolated vascular calcification – idiopathic infantile arterial calcification, now also referred to as generalized arterial calcification of infancy (GACI) – has been described[4]. This autosomal recessive disease, due to mutations in the ectonucleotide pyrophosphatase phosphodiesterase 1 gene (*ENPP1*), often results in death during childhood, apparently owing to disruption of the trophic influences that

inhibit vascular-cell calcification. We conducted a study to evaluate an adult-onset disorder in three families whose affected members had extensive calcifications of the lower-extremity arteries and small joint capsules and to investigate a possible genetic basis of the symptoms.

III. RESULTS

Case reports

Family 1 was of English descent. The proband (Fig. 11A), Patient VI.1, was a 54-year-old woman with a 20-year history of intermittent claudication of the calves, thighs, and buttocks and chronic ischemic pain in the feet at rest. Her parents were third cousins. On evaluation at the NIH, her ankle–brachial blood-pressure index values were markedly reduced, but the levels of serum calcium, Pi, vitamin D, alkaline phosphatase, creatinine, and cholesterol, and other chemical values were normal (Table 1). Contrast-enhanced magnetic-resonance angiography revealed extensive occlusion of the iliac, femoropopliteal, and tibial arteries, with extensive collateralization. Plain radiography of the lower extremities revealed heavy calcification with areas of arteriomegaly (Fig. 11B and 11C); chest radiography revealed no vascular calcifications above the diaphragm. Radiography also revealed juxta-articular joint-capsule calcifications of the fingers (Fig. 11D), wrists, ankles, and feet.

All four siblings of Patient VI.1 had disabling intermittent claudication (ability to walk only 1 to 6 blocks) and hemodynamically significant lower-extremity obstructive peripheral artery disease, with resting ankle–brachial blood-pressure index values

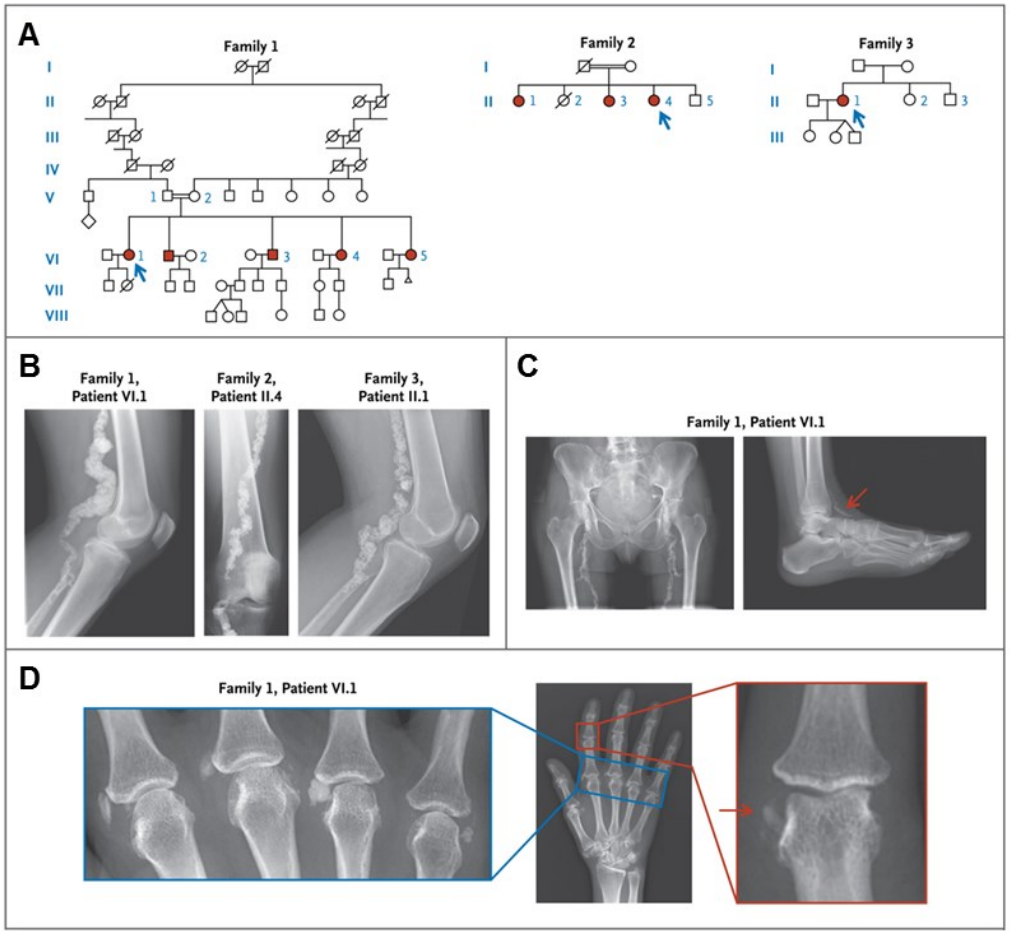

Fig. 11. Pedigrees of the study patients and radiographic findings. (**A**) The pedigrees of the three study families. Open symbols indicate unaffected family members, and solid red symbols affected members. Arrows indicate the probands. Squares indicate male family members, circles female members, slashes deceased members, and double horizontal lines consanguinity. The diamond indicates offspring of unknown number, and the triangle a lost pregnancy. (**B**) Plain radiographs of popliteal arteries of the three probands. (**C**) Plain radiographs of the pelvis and femurs (left) and ankle (right) of Patient VI.1 of Family 1, revealing calcified arteries (arrow). (**D**) Radiographs of metacarpal phalangeal and interphalangeal joint calcification (arrow) in Patient VI.1 of Family 1.

between 0.3 and 0.8 (normal range, 1.0 to 1.3). All had extensive femoropopliteal occlusion evident on magnetic-resonance arteriography, with diffuse, mild aneurysmal remodeling in a pattern of arteriomegaly. Computed tomographic (CT) angiography in three of the siblings showed that the obstructive lesions were diffusely and heavily calcified. Whole-body CT scanning for calcium, performed in one sister (Patient VI.5), showed prominent circumferential vascular calcifications in the lower extremities; CT angiography revealed extensive vascular obstruction with diffuse calcification (see the video, available at NEJM.org).

The proband of Family 2 (Fig. 11A), Patient II.4, was a 68-year-old northern Italian woman whose mother's surname was the same as that of some of her father's relatives four generations ago. She reported having intense joint pain in her hands that was unresponsive to glucocorticoids administered from 14 to 27 years of age. Radiographs of the lower limbs revealed calcifications (Fig. 11B), initially diagnosed as chondrocalcinosis. Serum electrolyte, calcium, and cholesterol levels were normal. Two sisters, 73 and 70 years of age (Fig. 11A), also had lower-extremity pain and had vascular calcifications that were similar to those of the proband.

The proband of Family 3 (Fig. 11A), Patient II.1, was a 44-year-old woman with an English father and a French mother. At 42 years of age, mild paresthesias in the lower legs prompted an evaluation that revealed extensive calcifications of the distal arteries (Fig. 11B), with sparing of the carotid arteries, aorta, and coronary arteries. Extensive rheumatologic evaluations were negative. Concern about impending ischemia in the right

Characteristic	Patient VI.1	Patient VI.2	Patient VI.3	Patient VI.4	Patient VI.5	Unaffected Persons
Age (yr)	54	53	51	49	44	
Sex	F	M	M	F	F	
Calcification						
Coronary arteries	Normal	Moderate	Normal	Normal	Normal	Normal
Aorta	Normal	Normal	Normal	Normal	Normal	Normal
Iliac arteries	Calcified, occluded	Mildly calcified	Tortuous, mildly calcified	Minimally calcified	Calcified but not obstructed	Normal
Femoral arteries	Calcified, occluded; popliteal arteriomegaly	Calcified, occluded; femoropopliteal arteriomegaly	Calcified, occluded	Calcified, occluded; femoropopliteal arteriomegaly	Calcified, occluded; popliteal arteriomegaly	Normal
Tibial arteries	Calcified, occluded	Calcified	Normal	Calcified, occluded	Calcified, proximal occlusion	Normal
Diabetes mellitus	No	No	No	No	No	No
White cells (per mm^3)	3570	5200	7390	4150	3560	3980–10,040
Hemoglobin (g/dl)	13.5	15.7	13.9	12.4	12.3	11.2–15.7
Calcium (mmol/liter)	2.31	2.30	2.42	2.29	2.29	2.05–2.50
Phosphate (mg/dl)	3.8	3.2	3.7	3.8	3.4	2.5–4.8
Alkaline phosphatase (U/liter)	70	69	62	62	65	37–116
Parathyroid hormone (pg/ml)	102	59.4	18.6	39.7	24.9	16.0–87.0
Vitamin D (pg/ml)	72	55	37	53	58	18–78
Creatinine (mg/dl)	0.70	0.82	0.73	0.40	0.54	0.70–1.30
Cholesterol (mg/dl)	182	109	143	204	153	<200
Ankle–brachial blood-pressure index						
Right	0.4	0.8	0.7	0.3	0.7	1.0–1.3
Left	0.4	0.5	0.7	0.3	0.8	1.0–1.3

Table 1. Clinical characteristics of affected members of Family 1.

leg prompted a femoral–popliteal bypass at 43 years of age. Serum C-reactive protein, cholesterol, lipid, calcium, Pi, and vitamin D levels were within the normal range.

None of the nine affected patients and none of their parents or children had abnormal bone morphologic characteristics, type 2 diabetes mellitus, or decreased kidney function. The parents of the five siblings in Family 1 had no clinically significant calcifications in their lower extremities or joint capsules.

SNPs, mutation analyses, and expression studies

We identified biallelic nonsense, missense, and single-nucleotide insertion–frameshift mutations in the ecto-5′-nucleotidase gene *NT5E*, encoding the CD73 enzyme, which generates extracellular adenosine, directly downstream of ENPP1 in the extracellular ATP–degradation pathway.

The consanguineous pedigree of Family 1, with disease confined to one generation (Fig. 11A), suggested autosomal recessive inheritance. Therefore, we searched for a region of the genome in which all five affected siblings were homozygous and identical by means of descent but in which both parents were heterozygous. There was only one such region in the entire genome: a 22.4-Mb region (Fig. 12A) on chromosome 6q14 (86,157,551 to 108,573,717 bp), containing 7977 genotyped SNPs and 92 genes. The lod score for the region in this family, calculated with the use of parametric multipoint linkage analysis, was 4.81.

Of the 92 genes in this region, three were evaluated: *ATG5* and *CASP8AP2* because they are involved in degenerative cellular processes that could lead to calcification, and *NT5E* because its enzyme substrate is the product of ENPP1, mutations in which cause arterial calcifications in infants[4]. Direct sequencing identified a homozygous nonsense mutation (c.662C→A, resulting in p.S221X) in exon 3 of the *NT5E* gene in all five siblings of Family 1 and the same nonsense mutation in the heterozygous state in both parents (Fig. 12B). Quantitative PCR analysis documented decreased expression of NT5E messenger RNA in the fibroblasts of Patients VI.1 and VI.4 in Family 1 (Fig. 12C). Affected members of Family 2 were homozygous for a missense mutation, c.1073G→A (p.C358Y), in exon 5 of *NT5E*; the mother was heterozygous for this variant of the amino acid, which is conserved across 16 species. The affected member of Family 3 was a compound heterozygote for the c.662C→A nonsense mutation found in Family 1 and a c.1609dupA (V537fsX7) mutation leading to a premature stop codon in exon 9 of *NT5E*. None of these mutations was present in 400 alleles in ethnically matched controls.

Protein and enzyme activity

NT5E encodes CD73, a membrane-bound ecto-5′-nucleotidase (specifically, 5′–ribonucleotide phosphohydrolase; EC 3.1.3.5) involved in extracellular ATP metabolism. The enzyme preferentially binds AMP and converts it to adenosine and Pi[275]. Protein analysis involving Western blotting of fibroblast extracts from Patients VI.1 and VI.4 of Family 1 revealed markedly reduced expression of CD73 protein, as compared with normal controls. An enzymatic assay of CD73 in fibroblasts from our patients revealed nearly absent activity (Fig. 12D); values for fibroblasts from the patients' parents were

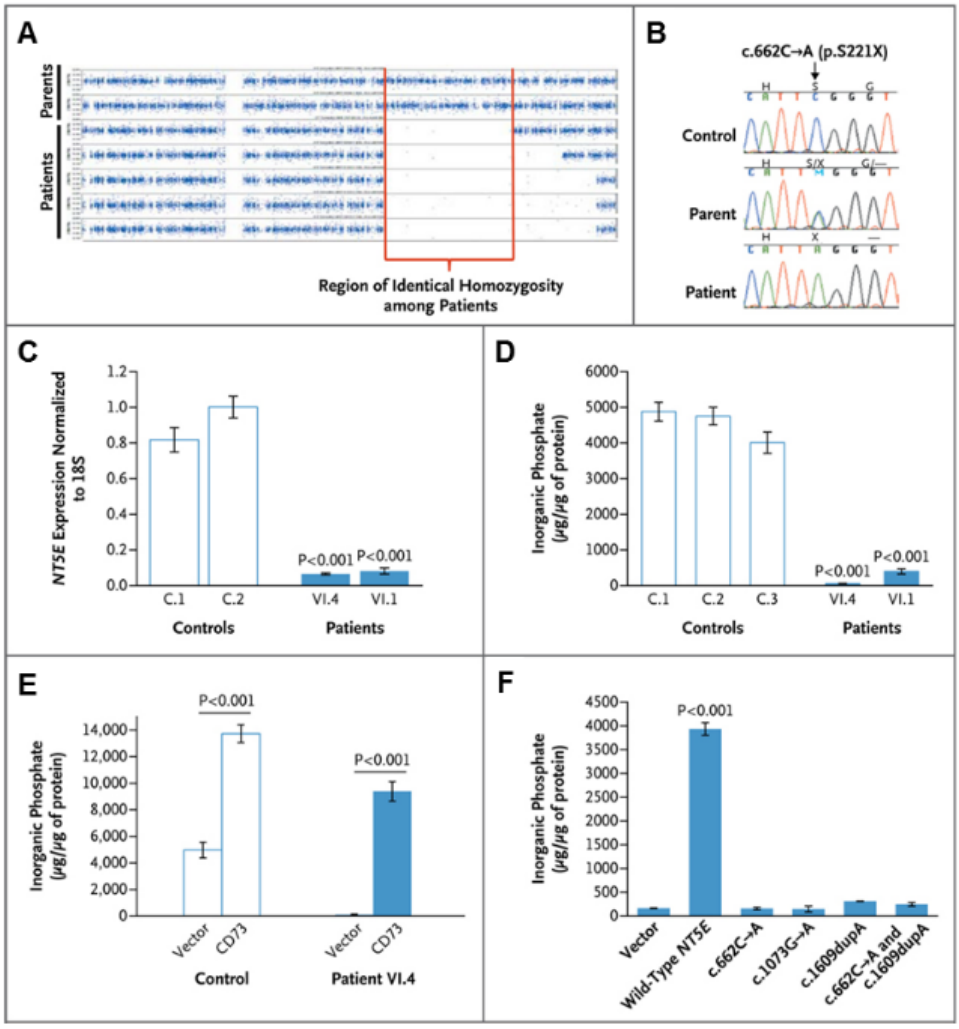

Fig. 12. Results of genetic and enzyme studies in Family 1. (**A**) SNP–array homozygosity plots for the five affected siblings in Family 1 and their parents. (**B**) Sequence chromatograms for a control, a parent of an affected member of Family 1, and an affected member. (**C**) *NT5E* messenger RNA expression in Patients VI.4 and VI.1 as compared with controls. (**D**) Deficiency in CD73 enzyme activity in cultured fibroblasts from Patient VI.4 and Patient VI.1 of Family 1. (**E**) CD73 enzyme activity in fibroblasts from controls and from Patient VI.4 after the fibroblasts were transduced with either an empty vector or a CD73-containing vector. (**F**) CD73 activity in HEK293 cells transfected with an empty vector or a vector containing wildtype *NT5E* or mutant *NT5E*.

approximately 72% of the control level. Genetic rescue with a CD73-encoding lentiviral vector reestablished normal AMP-dependent Pi production (Fig. 12E). The enzymatic activities of normal and mutant CD73 constructs were tested in HEK293 cells, which have low endogenous CD73 activity. Transfection with normal *NT5E* cDNA resulted in abundant CD73 activity, whereas transfection with the c.662C→A *NT5E*, c.1073G→A NT5E, or c.1609dupA *NT5E* yielded negligible production of AMP-dependent Pi (Fig. 12F).

Cellular studies

A key enzyme in tissue calcification in vitro and in vivo is tissue-nonspecific alkaline phosphatase (TNAP)[161]. After 3 days of calcific stimulation, fibroblasts from Patient VI.4 of Family 1 stained abundantly for TNAP, as compared with control cells; treatment with adenosine substantially reduced the amount of TNAP staining (Fig. 13A). TNAP activity was also assayed in the lysates of fibroblasts grown in calcifying medium. As compared with control cells, cells from Patient VI.4 showed high levels of TNAP that were significantly reduced after transduction with CD73-encoded lentiviral vector or by adenosine treatment (Fig. 13B). Three weeks of calcific stimulation resulted in abundant calcium Pi crystal formation in mutant fibroblasts (from Patient VI.4) but no formation in normal fibroblasts (Fig. 13C). Calcium Pi crystal formation was prevented in cells transduced with a CD73-encoding lentiviral vector but not control vector expressing β-galactosidase. Adenosine treatment largely abrogated the calcification process, and the noncompetitive alkaline phosphatase inhibitor levamisole completely prevented calcification in the mutant cells (Fig. 13C).

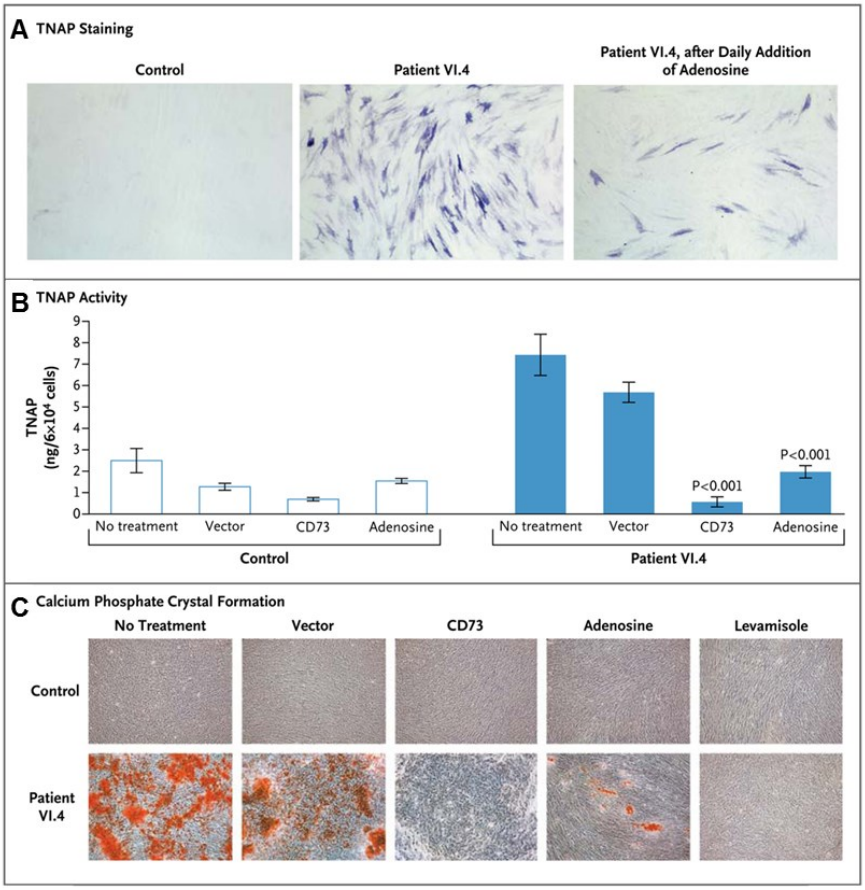

Fig. 13. **Studies of fibroblasts obtained from Patient VI.4 of Family 1.** (**A**) Staining for TNAP in fibroblasts from a control and from Patient VI.4. The increased staining in the patient's cells was reduced by adding 30 μM adenosine. **(B)** TNAP activity in fibroblasts from a control and from Patient VI.4. Transduction with a control vector expressing β-galactosidase had little effect on alkaline phosphatase activity, whereas transduction with a CD73-encoding vector reduced alkaline phosphatase activity significantly; incubation in 30 μM adenosine produced TNAP levels similar to those seen in control cells. (**C**) The effects of interventions on calcium Pi crystal formation in fibroblasts from a control and from Patient VI.4. Calcium staining was prevented by transduction with a CD73-encoding lentiviral vector and by treatment with 1 mM levamisole; treatment with 30 μM adenosine partially abrogated the calcification process.

IV. DISCUSSION

Medial arterial calcification of the lower extremities with periarticular calcification was described first by Magnus-Levy[276] in 1914 and again by Levitin[277] in 1945. The familial nature of this condition was first suggested in a report on two affected siblings by Sharp[278] in 1954, leading to a subsequent record in the Online Mendelian Inheritance in Man database (OMIM number, 211800). Other, single cases were described by Nosaka and colleagues and Mori and coworkers[279], yielding a total of seven cases published to date. Here, we describe the molecular and enzymatic basis of this disorder in nine patients with three different mutations in *NT5E*.

Considerable evidence supports the association of these families' vascular disease with mutations in the *NT5E* gene. The results of segregation analysis were consistent among our families, and the nonsense mutation (p.S221X) and single-nucleotide insertion (p.V537fsX7) predict truncated CD73 proteins. The missense mutation (p.C358Y), which was not found in 200 unaffected persons, predicts a pathologic change in an amino acid conserved through evolution and is located in the critical nucleotidase domain of CD73. Furthermore, the nonsense mutation resulted in markedly reduced levels of CD73 mRNA and protein in cultured cells. Enzyme activity was virtually absent in fibroblasts from affected members of Family 1 and was rescued by transduction of a lentiviral vector expressing NT5E. Each of the three different mutations in the three families produced essentially nonfunctional CD73.

CD73 participates in the extracellular pathway that converts ATP to adenosine on the

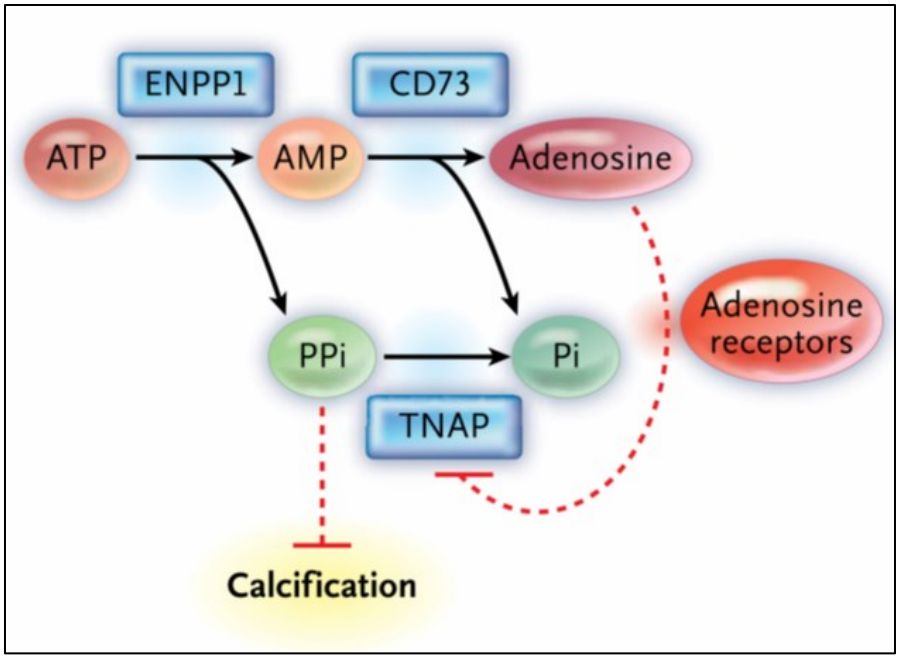

Fig. 14. **Proposed mechanism of mineralization due to CD73 deficiency from an *NT5E* mutation.** On the surface of vascular cells, ENPP1 (the protein encoded by the ectonucleotide pyrophosphatase–phosphodiesterase 1 gene) converts ATP to AMP and PPi, and CD73 converts AMP to adenosine and inorganic phosphate (Pi). PPi inhibits calcification, TNAP degrades PPi, and adenosine inhibits TNAP. Deficiency of CD73 results in decreased adenosine levels, eliminating the inhibition of TNAP from the pathway either directly or by way of adenosine receptor signaling. Increased TNAP from the pathway activity results in decreased PPi and increased cell calcification.

surface of various types of cells, as follows. First, ENPP1 produces AMP and PPi from ATP; then CD73 produces adenosine and Pi from AMP (Fig. 14). Cellular calcification depends critically on levels of pyrophosphate, a strong inhibitor of calcification, and TNAP, which degrades PPi[161]. In patients with hypophosphatasia due to TNAP deficiency, increased levels of PPi result in defective bone mineralization[280]. In patients with generalized arterial calcification of infancy, ENPP1 deficiency leads directly to decreased PPi levels[169], causing early-onset vascular calcification, myocardial infarction, and often death in infancy[4]. In our adult patients, CD73 deficiency may not lead directly to decreased PPi levels, but the consequent reduction in extracellular adenosine levels apparently enhances TNAP activity; adenosine supplementation reversed the increase in TNAP activity in CD73-deficient cells. We hypothesize that increased TNAP activity reduces PPi levels, leading to calcification; indeed, levamisole, an inhibitor of TNAP, prevented calcium crystal formation by CD73-deficient fibroblasts. The selective involvement of lower-extremity arteries may be related to the particular distribution of adenosine receptors in these tissues[281].

Knowledge of the basic defect in our patients allows for consideration of therapeutic interventions. Bisphosphonates, which are PPi analogues and potent inhibitors of tissue calcification, have been successfully used to treat ENPP1 deficiency and might prove beneficial in patients with CD73 deficiency[6,282]. Dipyridamole, an antithrombotic drug used successfully in patients with aneurysmal vascular remodeling, could provide adenosine rescue, since it inhibits cellular reuptake of adenosine (and subsequent degradation by adenosine deaminase) both in vitro and in vivo[283]. Other therapeutic

possibilities include the use of adenosine-receptor agonists or a direct inhibitor of TNAP such as lansoprazole[284,285]. The potential efficacy of such interventions can be investigated in cultured cells, which exhibit both TNAP and calcification phenotypes that are abrogated by transduction with a CD73-encoded lentiviral vector. Mice with CD73 deficiency can also be studied, if a calcification phenotype can be discerned[286,287], to elucidate the role of adenosine in regulating vascular calcification, influencing bone mineralization, and modulating ectopic calcium deposition.

In summary, we identified mutations in *NT5E* in members of three families with symptomatic arterial and joint calcifications. This gene encodes CD73, a nucleotidase that converts AMP to adenosine. Thus, our results support a role for this metabolic pathway in inhibiting ectopic tissue calcification.

V. METHODS

Patients

Three families were studied. Members of Family 1 and Family 3 were admitted to the National Institutes of Health (NIH) Undiagnosed Diseases Program and enrolled in clinical studies whose protocols had been approved by the institutional review board of the National Human Genome Research Institute. The genetic studies for Family 2 were approved by the institutional review board of Azienda Ospedaliera Universitaria San Giovanni Battista. All subjects provided written informed consent.

Fibroblast cell cultures

Fibroblast cultures were prepared from a 4-mm punch-biopsy skin specimen obtained from each patient and grown in Dulbecco's modified Eagle's medium containing 10% fetal-calf serum and 1% penicillin–streptomycin, as previously described[288]. Cells were fed every other day and split 1:2 at confluence.

SNP array analysis

Genomic DNA in Family 1 was isolated from peripheral leukocytes and genotyped on a genotyping array (Human 1M Duo, Illumina). Homozygosity-allele plots were generated with the use of GenomeStudio software. Anomalous regions of homozygosity were identified visually and confirmed by means of haplotype imputation (ENT program). A lod score was established with the use of parametric multipoint linkage analysis, as previously described[289].

Mutation analysis of CD73

Coding exons and intron–exon junctions of *NT5E* were amplified with the use of a touchdown polymerase-chain-reaction (PCR) assay of 50 ng of genomic DNA, 3 μM of sense and antisense oligonucleotides, and 5 μl of HotStart Master Mix (Qiagen) in a final volume of 10 μl. PCR products were sequenced in both directions with the use of the Big Dye terminator kit (version 1.1, Applied Biosystems) and an automated capillary sequencer (ABI PRISM 3130xl Genetic Analyzer, Applied Biosystems). We compared electrophoretogram-derived sequences with reference sequences for *NT5E* (Ensembl gene number ENSG00000135318) by using Sequencher software (version 4.8). Screening of 200 DNA samples from controls of white race (panel HD200CAU, Coriell Cell

Repositories) was performed by means of the 5′–nuclease allelic discrimination (TaqMan) assay, as previously described[290]. Details of the PCR amplification, primer sequences, and allelic discrimination assay are available in the Supplementary Appendix, available with the full text of this article at NEJM.org.

Expression studies

RNA was isolated from cultured fibroblasts with the use of the RNeasy kit (Qiagen), and complementary DNA (cDNA) was generated from 1-μg RNA samples with the use of the SuperScript II Reverse Transcriptase kit (Invitrogen). Expression of NT5E was measured by means of a quantitative real-time PCR assay involving SYBR Green technology on a Chromo4 Real Time PCR Detection System (Bio-Rad). Expression levels were calculated on the basis of the $2^{-\Delta Ct}$ method, in which the cycling threshold (Ct) of the candidate gene is compared with the Ct of 18S ribosomal RNA and expressed as a power of two (2(Ct of *NT5E* −Ct of *18S*)).

Western blotting for CD73

Cells were grown to confluency, trypsinized, pelleted, and lysed by addition of 50 mM Tris-HCl pH7.4, 150 mM NaCl, 2 mM EDTA, 1% NP-40 and 0.1% SDS (RIPA buffer) supplemented with 0.5% Triton-x 100 and 1x Complete Mini Protease Inhibitor Cocktail (Roche). After 10 min on ice, the lysate was vortexed at 4°C for 5 min and centrifuged at 15,000 x g and supernatant protein quantified using the bicinchoninic acid assay (Pierce). Thirty mg of protein was mixed with SDS protein gel loading solution (Quality Biologicals), loaded on a 4-20% polyacrylamide gel (Bio-Rad), and electrophoresed at

120V for 1.5 h. After protein transfer, antibodies against CD73 (Abcam) and actin (Sigma-Aldrich) were used at dilutions of 1:1000 and 1:50,000, respectively.

CD73 enzyme assay

Fibroblasts were washed with a solution of 2 mM magnesium chloride, 120 mM sodium chloride, 5 mM potassium chloride, 10 mM glucose, and 20 mM HEPES. Incubation buffer, consisting of the wash solution supplemented with 2 mM AMP, was added, and cells were incubated at 37 °C for 10 minutes[291]. The supernatant was removed, and Pi was measured with the SensoLyte MG Phosphate Assay Kit (AnaSpec) according to the manufacturer's instructions. Pi measurements were normalized to micrograms of protein.

Cloning of mutations and production of lentivirus

The plasmid pCMV-Sport6 containing human CD73 cDNA was purchased from Open Biosystems. Mutations were introduced by means of the QuikChange XL Site-Directed Mutagenesis Kit (Stratagene). Primer sequences used for site-directed mutagenesis for each family are provided in the Supplementary Appendix.

Construct sequences were confirmed by sequencing in both directions. Since the pCMV-Sport6 vector contains Gateway cloning (Invitrogen) recombination sites, we used this cloning strategy to insert normal and mutated CD73 cDNA into the vector pLenti6.3/V5-DEST; lentivirus was generated with the use of the ViraPower HiPerform Lentiviral Gateway Expression Kit (Invitrogen). For transduction, viral particles were added to cells in growth medium containing 6 μg of polybrene per milliliter (Sigma). To select for

cells transduced with virus, blasticidin (Invitrogen; 10 μg per milliliter) was added to growth medium 4 days after transduction.

Transfection into HEK293 cells

HEK293 cells (from human embryonic kidneys) were cultured in Dulbecco's modified Eagle's medium supplemented with 10% fetal-calf serum and 1% penicillin–streptomycin. One microgram of pCMV-Sport6 containing green fluorescent protein, wild-type *NT5E* cDNA, or mutated *NT5E* cDNA was transfected into HEK293 cells with the use of FuGENE 6 reagent (Roche) according to the manufacturer's instructions. Three days after transfection, cells were analyzed for CD73 activity, as described above.

In vitro alkaline phosphatase and calcium assays

Staining for alkaline phosphatase was performed by means of the Alkaline Phosphatase Detection Kit (Millipore). Assay of alkaline phosphatase was performed with the use of the Quantitative Alkaline Phosphatase ES Characterization Kit (Millipore) according to the manufacturer's instructions. Briefly, cells were trypsinized and collected in aliquots of 60,000 cells per reaction in p-nitrophenol–phosphate substrate. Alkaline phosphatase was quantified by measuring the amount of p-nitrophenol produced, as gauged by absorption at 405 nm.

A modified protocol for in vitro calcification was used for fibroblasts obtained from patients and controls[292,293]. Cultures were treated with 0.1 μM dexamethasone, 50 μM ascorbic acid-2-phosphate, and 10 mM β-glycerol phosphate in alpha minimal essential

medium supplemented with 10% fetal-calf serum and 1% penicillin–streptomycin for 21 days, with replenishment of the medium every 4 or 5 days. On day 21, cells were washed with phosphate-buffered saline and fixed in 10% formalin for 10 minutes. After washing with water, a solution of 2% alizarin red S, pH 4.2, was used to stain calcium Pi crystals[294].

CHAPTER 3

TREATMENT OF HYPOPHOSPHATEMIC RICKETS IN GENERALIZED ARTERIAL CALCIFICATION OF INFANCY (GACI) WITHOUT WORSENING OF VASCULAR CALCIFICATION

I. ABSTRACT

Patients with GACI develop vascular calcifications early in life. About half of them die within the first six months despite optimal medical care. A subset of those who survive eventually develop hypophosphatemic rickets. Since hypophosphatemia and hyperphosphaturia have been previously associated with increased survival in GACI patients, physicians often avoid Pi repletion as treatment for rickets. As a consequence, GACI patients develop severe rachitic complications such as short stature and skeletal deformities. It appears that the recognition of hypophosphatemia later in life in some GACI patients is a consequence of having survived the first few months of life, and not the cause of their survival per se. Here, we report the long-term follow-up of a GACI patient who was Pi-repleted for his rickets for more than seven years without worsening of vascular calcification.

II. INTRODUCTION

GACI is a disorder characterized by calcifications of large- to medium-sized vessels and/or fibrointimal hyperplasia resulting in cardiovascular morbidity either in utero or soon after birth[3]. Most cases are associated with biallelic loss-of-function mutations in the *ENPP1* gene[4], although biallelic mutations in *ABCC6* have been reported in a

minority of patients[8]. A retrospective study of 55 patients with GACI found that hypophosphatemia and hyperphosphaturia were associated with increased survival[4]. However, the same study found that mortality was largely limited to the so called "critical period" encompassing the first six months of life, with only one death occurring later, at seven months of age. Moreover, hypophosphatemia and hyperphosphaturia did not develop until later in life, so it is unlikely that these Pi abnormalities themselves influenced survival. Later publications found that *ENPP1* mutations are also associated with autosomal recessive hypophosphatemic rickets type 2 (ARHR2)[295,296], so it is not surprising that many patients with *ENPP1*-associated GACI who survive the critical period go on to develop rickets. Thus, the development of hypophosphatemia and hyperphosphaturia represent an acquired — rather than a congenital — biochemical phenotype that does not appear until after the critical period of increased mortality in infancy. We are aware of several GACI patients who developed hypophosphatemic rickets that went untreated for years for fear that calcitriol and phosphorus supplementation would worsen the vascular calcifications, based on the previously reported association of hypophosphatemia with increased survival. These patients went on to develop profound skeletal deformities. In contrast, we now report a patient with GACI and subsequent hypophosphatemic rickets who was treated with calcitriol and phosphorus for more than seven years, without developing new calcium deposits. This demonstrates that hypophosphatemic rickets in the setting of pre-existing GACI can be treated without detrimental effects; in fact, such therapy appears appropriate to prevent rachitic complications such as bone pain, deformities, and short stature.

III. CLINICAL REPORT

Our patient was born at 38 weeks of gestation by spontaneous vaginal delivery after an unremarkable prenatal course. Birth weight was 3.4 kg (25-50th centile) and birth length 48.9 cm (~25th centile); Apgar scores were 9 and 10 at 1 and 5 minutes, respectively. At day 29, he became cyanotic; in the emergency department, he was in severe respiratory distress, with mottled skin and metabolic acidosis. He was placed on a ventilator and on vasopressors, but was breathing room air on his own two days later, and was discharged home on an apnea monitor five days later. On day 48, the infant began crying inconsolably. In the emergency department, he was tachycardic with poor peripheral perfusion, hepatomegaly and splenomegaly. A chest radiograph revealed cardiomegaly and pulmonary edema, and an EKG showed left ventricular hypertrophy. An echocardiogram showed left ventricular enlargement, poor systolic function, and moderate mitral regurgitation. A myocardial biopsy was unremarkable, with no findings of myocarditis. Cardiac catheterization showed severe attenuation of the left coronary artery with subtotal occlusion of the first obtuse marginal branch and occlusion proximal to the circumflex branch. The right coronary artery was occluded proximally. A CT scan revealed calcification of the descending aorta, and the renal, splenic, superior mesenteric, brachial and coronary arteries, consistent with the diagnosis of GACI. Biallelic mutations in *ENPP1* (p.Arg481Gln and p.Tyr471Cys; NM_006208.2) confirmed the diagnosis. During that hospital admission, he was started on etidronate IV for 7 days and then orally at 20 mg/kg/day. During the hospitalization, the echocardiogram improved dramatically, with the left ventricular shortening fraction increasing from 13% on admission to 30% prior to discharge on day 71.

CT at 7 months of age showed reduced calcifications, and by 13 months the calcifications had regressed completely except for mild calcification of the aortic annulus. Etidronate was discontinued at 24 months of age.

At 13 years of age, the patient began complaining of significant, progressive pain in the ankles and knees, accompanied by stiffness of both joints, mainly in the morning. Radiographs revealed significant anterior bowing and thinning of the lower ends of both femora. A skeletal survey at 14 years 5 months showed resorption of the proximal medial metaphyses of both tibias and widening of the growth plates of the distal ulnae bilaterally and, to a lesser extent, the medial margins of the distal radius. Fusion of the posterior arches of C2, C3, C4 and C5 was also found.

At 14 years 5 months, his height was 154.4 cm (7^{th} centile, -1.45 SD) for a mid-parental height of 180.3 cm ± 5 cm (75^{th} centile). He was diagnosed with hypophosphatemic rickets, based on an elevated alkaline phosphatase of 631 U/L (reference: 166-571 U/L), bone specific alkaline phosphatase 241 μg/L (ref: 13-111 μg/L), serum phosphorus 2.5 mg/dL (ref: 3.5-5.3 mg/dL), tubular reabsorption of phosphorus (TRP) 88 % (low for his degree of hypophosphatemia), tubular maximum phosphorus reabsorption per glomerular filtration rate (TmP/GFR, or threshold above which phosphorus is no longer reabsorbed by the tubules) 2.3 mg/dL (ref: 2.8-5.2 mg/dL), intact PTH 39 pg/mL (ref: 15-65 pg/mL), 25-hydroxyvitamin D 35 ng/mL (ref: 30-50 ng/mL) and 1,25-dihydroxyvitamin D 36 pg/mL (ref: 24-86 pg/mL). Phosphorus supplementation was initiated with K-Phos

Neutral at 250 mg every 6 hours (18 mg/kg/d), and calcitriol was begun at 0.5 μg twice a day (18 ng/kg/d) starting at 14 years 8 months of age.

Within a few weeks of starting therapy, the pain in his ankles and knees resolved completely. His deformities remained stable, with no progression or improvement. After his final height was achieved, he underwent two separate osteotomies at age 21 to correct the anterior femoral bowing with tibia vara.

Other pertinent medical findings included progressive hearing loss noted at age 7 years, for which he had PE tubes until the age of 20 years, followed by hearing aids. He also had enamel defects, requiring sealant application.

At the age of 21 years 11 months, the patient was taking calcitriol 0.75 μg every morning and 0.5 μg nightly (13.9 ng/kg/d) and phosphorus 500 mg twice a day (11.1 mg/kg/d). Dose adjustments were made based on blood and urine biochemical findings, although with some medication adherence issues. His ionized calcium was 1.23 mmol/L (ref: 1.1-1.35 mmol/L), serum phosphorus 2.1 mg/dL (ref: 2.5-4.5 mg/dL), alkaline phosphatase 191 U/L (ref: 45-115 U/L), and intact PTH 11 pg/mL (ref: 15-65 pg/mL). Multidetector helical CT from the neck to the legs revealed minimal calcification of the aortic root (Fig. 15A) and inferior portion of the heart, and minimal calcification of the left popliteal artery, with no calcifications elsewhere (including no nephrocalcinosis). Anterior femoral bowing could also be appreciated (Fig. 15B). A dedicated cardiac CT showed no coronary artery calcification, with an Agatston calcium score of zero.

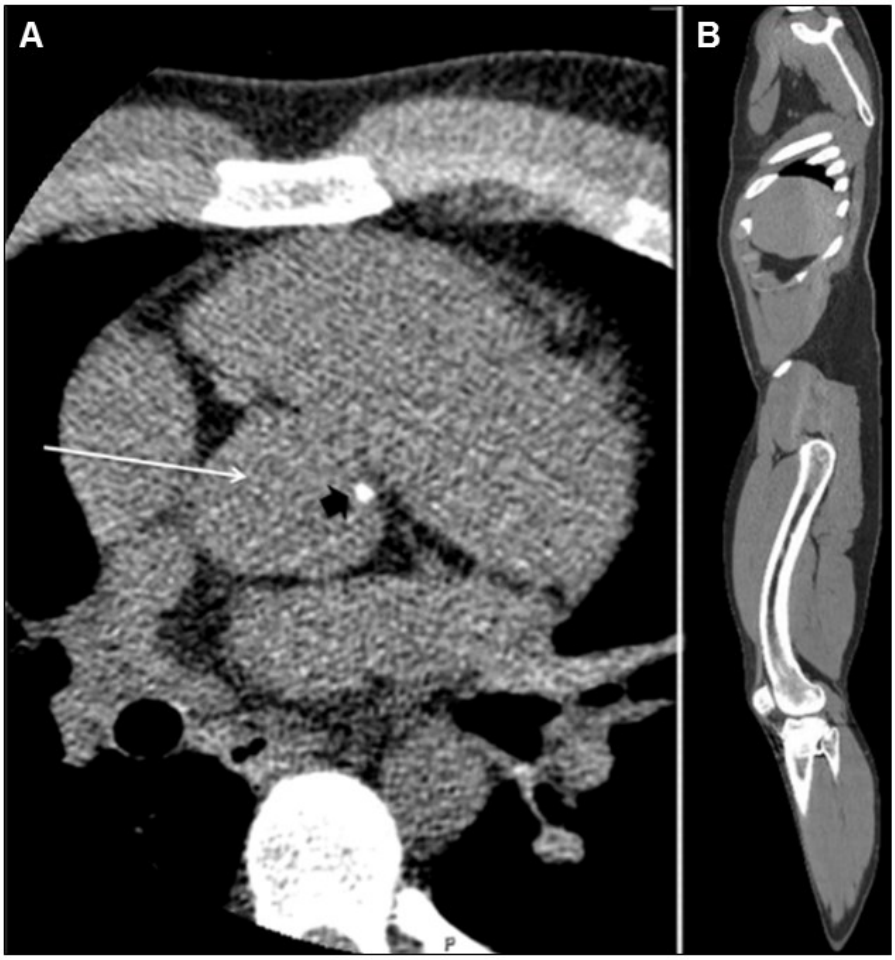

Fig. 15. Imaging of patient with GACI. (**A**) CT revealed minimal calcification in the aortic root. (**B**) Anterior bowing of the legs.

IV. DISCUSSION

In 2008, Rutsch et al. reported the association of hypophosphatemia and hyperphosphaturia with increased survival in patients with GACI[6]. Association, however, does not imply causality, and in fact this association was based upon the finding that GACI patients who survived beyond infancy were hypophosphatemic and hyperphosphaturic. The 2008 report did not address the fact that the GACI patients who died during their first year of life might also have been destined to develop renal Pi wasting and hypophosphatemia later in life. Furthermore, there was no mortality in either patients with or without hypophosphatemia/hyperphosphaturia after 7.5 months of age, meaning that there is no evidence for a causal relationship between survival and hypophosphatemia after early infancy. Thus, the biochemical phenotype of hypophosphatemia and hyperphosphaturia will likely develop over time in many patients with GACI who survive the critical period, but it is not an explanation for survival. Rather, survival itself allows hypophosphatemia to be recognized; hypophosphatemia does not lead to survival.

There are various explanations why a "critical period" in the first six months of life might be followed by a more "refractory period" later. First, in most cases the calcifications regress either spontaneously[297,298] or after treatment with bisphosphonates[299,300]. Second, even though patients with GACI can have vessel narrowing in the presence or absence of calcifications, the authors are aware of several patients who received serial imaging showing that their vessels continued to grow in diameter with age. According to Poiseuille's law, the flow through a vessel is directly proportional to the fourth power of

the radius[301]. Thus, a linear increase in the caliber of a vessel will lead to an exponential increase in blood flow, so that small increases in the radius can lead to dramatic increases in flow.

Based upon the reported association of hypophosphatemia and hyperphosphaturia with increased survival, many physicians avoid treating the rickets that develop in children and young adults with GACI. Yet it is well known that these patients can have *ENPP1*-mediated hyperphosphaturia and hypophosphatemia and go on to develop florid rachitic deformities. Clearly, the decision to start therapy is difficult, since the effects of long-term calcitriol and phosphorus supplementation in GACI patients remain unknown. However, it should be noted that GACI is hypothesized to be caused by a cell-autonomous defect, leading to increased vascular calcification presumably due to lack of PPi synthesis in the local microenvironment of the vessel wall. Indeed, newborn patients with extensive vascular calcifications have normal phosphatemia and calcemia suggesting that vascular calcification does not appear to be related to any abnormalities in circulating levels of Pi or calcium.

Moreover, there is one report of a patient with biallelic *ENPP1* mutations who, after initiation of alfacalcidol, developed new-onset nephrocalcinosis, cardiac, hepatic and pancreatic calcifications as evaluated by ultrasound, and recurrence of previously regressed periarticular calcifications as assessed by radiograph[13]. This, however, was an iatrogenic event, since the patient developed hypercalciuria during treatment, and once the calciuria was maintained at less than 4 mg/kg/day, most of these calcifications —

with the exception of nephrocalcinosis — regressed. In another report, Rutsch et al. found one GACI patient treated with calcitriol and phosphorus supplementation whose arterial stenosis worsened[6]. However, no clinical information was provided regarding the timing of institution of treatment in this patient, the degree of vascular calcification prior to treatment initiation, the dosage of the supplemented medications, or the possibility of iatrogenic adverse effects such as hypercalciuria.

In conclusion, we describe for the first time long-term treatment of hyphosphatemic rickets in the setting of GACI. We show that adequate treatment of rickets can be accomplished without worsening of vascular calcifications, as long as close monitoring is instituted so as to avoid iatrogenic complications.

CHAPTER 4

ECTOPIC CALCIFICATION IN PXE REFLECTS COMPLEX ATP METABOLISM DEFECTS AND RESPONDS TO TNAP INHIBITION

I. ABSTRACT

Biallelic mutations in *ABCC6* cause PXE, a disease characterized by calcification in the skin, eyes, and blood vessels. The function of ABCC6 and the pathogenesis of PXE remain unclear. We used mouse models and patient fibroblasts to demonstrate genetic interaction and shared biochemical and cellular mechanisms underlying ectopic calcification in PXE and related disorders caused by defined perturbations in extracellular ATP catabolism. Under osteogenic culture conditions, *ABCC6* mutant cells calcified, suggesting a provoked cell-autonomous defect. Using a conditional *Abcc6* knockout mouse model, we excluded the prevailing pathogenic hypothesis that singularly invokes failure of hepatic secretion of an endocrine inhibitor of calcification. Instead, deficiency of *Abcc6* in both local and distant cells was necessary to achieve the early onset and penetrant ectopic calcification observed upon constitutive gene targeting. *ABCC6* mutant cells additionally had increased expression and activity of TNAP, an enzyme that degrades PPi, a major inhibitor of calcification. A novel, selective, and orally bioavailable TNAP inhibitor prevented calcification in *ABCC6* mutant cells in vitro and attenuated both the development and progression of calcification in *Abcc6*$^{-/-}$ mice in vivo, without the deleterious effects on bone associated with other proposed treatment strategies.

II. INTRODUCTION

Three human diseases, GACI, CALJA, and PXE, are characterized by debilitating ectopic calcification. The current understanding of the pathogenesis of GACI and CALJA suggests that aberrations in the extracellular ATP catabolic pathway cause ectopic calcification; it is unclear if a similar mechanism also applies to PXE. GACI (OMIM #20800), the most serious of these disorders, often presents by three months of age with myocardial infarction secondary to occlusive coronary artery calcification[4]. Patients also have extensive medial calcification of their medium-sized and large arteries, predisposing to strokes, and heart failure[3]. GACI generally results from biallelic loss-of-function mutations in *ENPP1,* which encodes an extracellular ectonucleotide pyrophosphatase/phosphodiesterase that converts ATP into AMP and PPi^4, a potent inhibitor of calcification in vitro[302] and in vivo[8]. Loss of ENPP1 activity results in decreased levels of PPi both locally and systemically, and GACI patients reportedly have low plasma[231] and urinary[232] PPi levels.

CALJA (OMIM #211800) is an adult-onset disorder of medial arterial and joint calcification. Patients typically present in their third decade of life with lower extremity claudication due to calcification of the femoral, popliteal, and dorsalis pedis arteries, in addition to extra-articular joint calcification. CALJA is caused by biallelic loss-of-function mutations in *NT5E*, which encodes CD73, an ecto-5'-nucleotidase that participates in ATP metabolism by degrading AMP to adenosine and Pi[20]. While calcification in GACI appears directly related to PPi deficiency, dysfunctional CD73 has been linked to increased PPi degradation by TNAP. Increased TNAP activity in CALJA

is believed to be secondary to reduced levels of extracellular adenosine and consequent impairment of intracellular adenosine receptor signaling that inhibits TNAP expression[20]. Thus, in both GACI and CALJA, ectopic calcification appears to be related to reduced extracellular concentration of the calcification inhibitor PPi.

In contrast to our understanding of GACI and CALJA, the mechanism of PXE (OMIM #264800), an autosomal recessive disorder of elastic fiber calcification, remains largely unknown. PXE patients exhibit calcification of elastic fibers in the skin, eyes, and arterial wall, resulting in characteristic papular lesions and skin laxity at flexure regions, fragmentation of Bruch's membrane underlying the retina leading to central vision loss, and medial arterial calcification causing peripheral vascular insufficiency. PXE typically results from mutations in *ABCC6*, which encodes a presumptive ATP-dependent exporter[303,304]. Remarkably, rare patients with biallelic mutations in *ABCC6* develop GACI (OMIM #614473) instead of PXE, without compelling evidence for a genotype-phenotype correlation[8].

The function of ABCC6 remains unclear. ABCC6 is a member of the multidrug resistance protein family with demonstrated transporter activity[240], but its endogenous substrate is unknown. The ABCC6 protein has very low expression in the peripheral cells directly affected in PXE, i.e., dermal fibroblasts and vascular smooth muscle cells[241,242], but strong expression in the liver and, to a lesser extent, kidney. The prevailing mechanistic hypothesis suggests that hepatocellular ABCC6 exports an endocrine inhibitor of calcification that acts at distant target sites[243–245,250] and that failure

of this event is sufficient to cause the systemic manifestations of PXE; only circumstantial evidence exists for this pathogenic model. Lack of understanding of disease pathogenesis has resulted in limited treatment options for PXE. Here, we attempt to unravel the mechanisms underlying PXE to better understand the pathways involved in ectopic calcification and conceive new therapeutic approaches.

III. RESULTS

Crossing *Abcc6* to *Enpp1* and *Nt5e* mutant mice reveals genetic interaction.

Because of the observed locus heterogeneity within the cohort of patients manifesting GACI and the clinical overlap among PXE, GACI, and CALJA, our initial hypothesis was that ABCC6 functions within the extracellular ATP metabolism pathway. To test this, we generated all possible genetic allele combinations by crossing *Abcc6* mutant mice to *Enpp1* or *Nt5e* deficient mice. Micro-computerized tomography (micro-CT) was used to quantify the extent of calcification of the fibrous capsule surrounding the mouse vibrissae (whiskers on the muzzle; Fig. 16), an early marker of ectopic calcification[145]. By 15 weeks of age, $Abcc6^{-/-}$ mice showed only moderate calcification whereas $Abcc6^{-/-}$ mice with one mutated *Enpp1* allele showed worsening of the phenotype (Fig. 17A, B). $Enpp1^{-/-}$ mice showed very aggressive calcification, with no further accentuation upon deleting *Abcc6* alleles. There was significant interaction between *Abcc6* and *Enpp1* (two-way analysis of variance, *Abcc6* effect: $P=2.2\text{x}10^{-16}$, *Enpp1* effect: $P=2.2\text{x}10^{-16}$, interaction effect: $P=2.2\ \text{x}10^{-16}$). The fact that the calcification phenotype is saturated upon full loss of *Enpp1* function, with no added effect of targeting *Abcc6* alleles, is consistent with a model where *Enpp1* functions upstream of *Abcc6.*

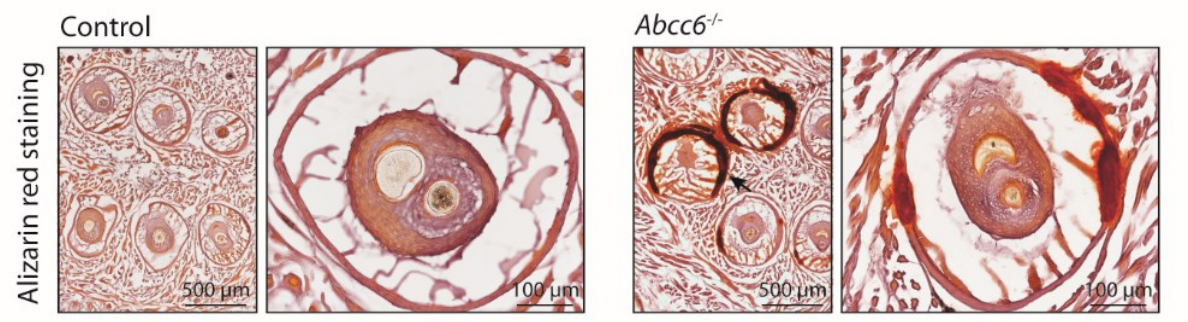

Fig. 16. Location of calcification in the fibrous capsule surrounding the vibrissae.

Arrow indicates calcification, as demonstrated by alizarin red staining.

Crosses between *Abcc6* and *Nt5e* deficient mice also revealed evidence for genetic interaction (Fig. 17C, D). By 15 weeks of age, $Nt5e^{-/-}$ mice with or without one null *Abcc6* allele showed no evidence of calcification and deleting one *Nt5e* allele in $Abcc6^{-/-}$ mice did not exacerbate calcification. However, $Nt5e^{-/-}$ mice with two null *Abcc6* alleles showed calcification that was more severe than that observed in $Abcc6^{-/-}$ mice. This interaction was statistically significant (two-way analysis of variance, *Abcc6* effect: $P=2.2\text{x}10^{-16}$, *Nt5e* effect: $P=1.2\text{x}10^{-4}$, interaction effect: $P=1.1\text{x}10^{-3}$). When aged to one year, $Nt5e^{-/-}$ mice showed mild calcification that was exacerbated by homozygous loss of *Abcc6*, again documenting genetic interaction (Fig. 18A, B; two-way analysis of variance, *Abcc6* effect: $P=2.2\text{x}10^{-16}$, *Nt5e* effect: $P=1.7\text{x}10^{-13}$, interaction effect: $P=5.8\text{x}10^{-7}$). In this set of crosses, the observation that maximal phenotypic severity is only observed upon complete loss of function for both *Abcc6* and *Nt5e* suggests that they work in combination rather than in tandem. Taken together, these findings suggest that PXE is caused by defects in the same pathway as GACI and CALJA; a parsimonious model places ABCC6 acting downstream of ENPP1 and in parallel with CD73, but more complex scenarios cannot be excluded.

Fibroblasts cultured from patients with biallelic *ABCC6* mutations can calcify in vitro and have altered levels of enzymes in the extracellular ATP catabolic pathway. To further probe whether metabolic defects observed in GACI and CALJA might also underlie the calcification phenotype in PXE, we generated primary fibroblast cell lines from patients with confirmed biallelic loss-of-function mutations in *ABCC6* ($ABCC6^{Mut/Mut}$), *ENPP1* ($ENPP1^{Mut/Mut}$), or *NT5E* ($NT5E^{Mut/Mut}$). The disease-causing

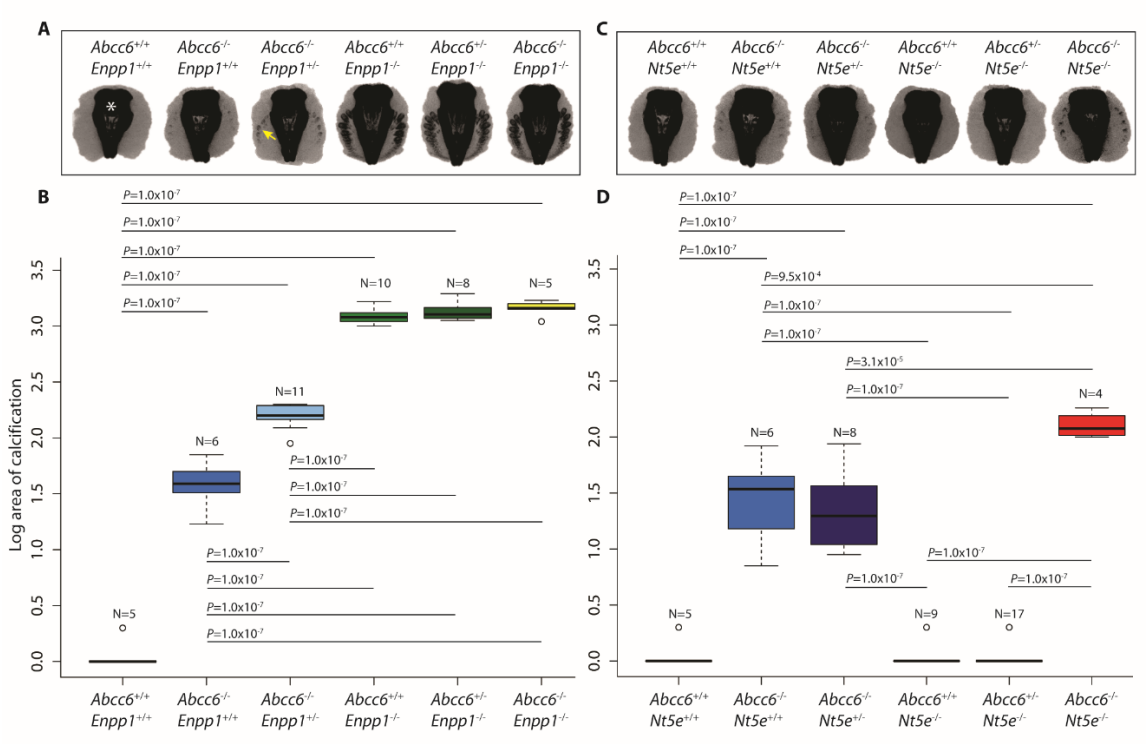

Fig. 17. Crossing *Abcc6* to *Enpp1* or *Nt5e* mutant mice reveals genetic interaction. *Abcc6* mutant mice were crossed to *Enpp1* or *Nt5e* mutant mice to generate all possible genetic allele combinations. (**A, C**) Micro-CT scans of the muzzle to evaluate the extent of vibrissae fibrous capsule calcification were obtained at 15 weeks of age. Representative coronal z-stacked images of the mouse muzzle with the nasal bones and sinuses midline (indicated by white asterisk) and the pathological calcification seen as radiodense lesions (indicated by yellow arrow) in the surrounding soft tissue. (**B, D**) Quantification of ectopic calcification from micro-CT images. A two-way analysis of variance with a Tukey's honest significance difference post-hoc analysis was performed; *P*-values indicated.

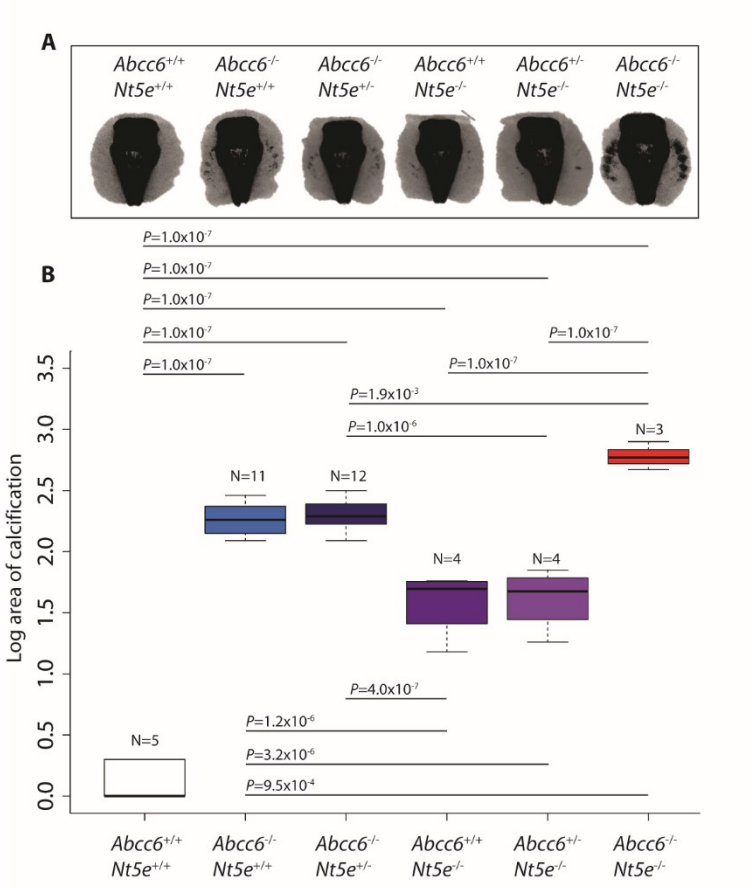

Fig. 18. Demonstration of genetic interaction between *Abcc6* and *Nt5e* mice when aged to one year. (**A**) Micro-CT scans of the muzzle to evaluate the extent of vibrissae fibrous capsule calcification were obtained at one year of age. (**B**) Quantification of ectopic calcification from micro-CT images. A two-way analysis of variance with a Tukey's honest significance difference post-hoc analysis was performed; *P*-values indicated.

mutations were missense, nonsense, frameshift, or deletions (Table 2). In contrast to control fibroblasts *ABCC6*$^{Mut/Mut}$ cell lines, when cultured to confluency and then stimulated with osteogenic media for 21 days, exhibited fully penetrant but variably severe calcification, as assessed by Alizarin red staining (Fig. 19A, B; one-tailed Student's t-test: P=0.045). As previously reported, the same stimulation with osteogenic media is needed to elicit calcification in *ENPP1*$^{Mut/Mut}$ and *NT5E*$^{Mut/Mut}$ fibroblasts[20]. These data demonstrate a cell-autonomous predisposition in *ABCC6*$^{Mut/Mut}$ cells that requires exogenous provocation for phenotypic expression and validate the use of these cells for further biochemical analysis of the functional consequences of *ABCC6* mutations in vitro.

We measured the steady-state enzymatic activity levels of ENPP1 and CD73, and their respective gene expression levels, in confluent cultured *ABCC6*$^{Mut/Mut}$, *ENPP1* $^{Mut/Mut}$, and *NT5E*$^{Mut/Mut}$ fibroblasts. As expected, *ENPP1* $^{Mut/Mut}$ cells had negligible ENPP1 activity. *ABCC6*$^{Mut/Mut}$ and *NT5E*$^{Mut/Mut}$ cells had increased ENPP1 enzymatic activity compared to controls (Fig. 19C; one-way analysis of variance: P=0.001). Additionally, there was a marked increase in *ENPP1* mRNA expression in *ABCC6*$^{Mut/Mut}$ cells compared to controls (Fig. 19D; one-way analysis of variance: P=0.016). *ENPP1* mRNA expression was also elevated in *ENPP1*$^{Mut/Mut}$ cells (all containing at least one missense allele), but the mutated protein lacked function, as predicted. These data are consistent with the ordered biochemical pathway inferred from our genetic interaction data and suggest that mutations in genes encoding for proteins distal to ENPP1 lead to compensatory upregulation of *ENPP1*, with a predicted increase in PPi production. Such compensation

	Allele 1	Allele 2
ABCC6$^{Mut/Mut}$		
Patient I	c.1552C>T (p.Arg518*)	c.951C>A (p.Ser317Arg)
Patient II	c.3940C>T (p.Arg1314Trp)	c.3940C>T (p.Arg1314Trp)
Patient III	c.2861_2866del6 (p.Phe954_Leu955del)	Deletion of exons 2-31
Patient IV	c.3940C>T (p.Arg1314Trp)	c.3940C>T (p.Arg1314Trp)
Patient V	c.3940C>T (p.Arg1314Trp)	c.3940C>T (p.Arg1314Trp)
Patient VI	c.3940C>T (p.Arg1314Trp)	c.3940C>T (p.Arg1314Trp)
Patient VII	c.3421C>T (p.Arg1141*)	c.3490C>T (p.Arg1164*)
Patient VIII	c.999_1403del (deletion of exon 10)	c.2278C>T (p.Arg760Trp)
ENPP1$^{Mut/Mut}$		
Patient I	c.2596G>A (p.Glu866Lys)	c.803A>G (p.Tyr268Cys)
Patient II	c.2713_2717delAAAGA (p.Lys905fs*15)	c.1441C>T (p. Arg481Trp)
Patient III	c.2735T>C (p.Leu91Ser)	delIVS5_IVS6 (3.4kb deletion of exon 6)
Patient IV	c.1438T>C (p.Cys480Arg)	c.2414G>T (p.Gly805Val)
NT5E$^{Mut/Mut}$		
Patient I	c.662C>A (p.S221*)	c.662C>A (p.S221*)
Patient II	c.662C>A (p.S221*)	c.1609dupA (p.V537fs*7)
Patient III	c.1237C>T (p.Arg413*)	c.1237C>T (p.Arg413*)

Table 2. List of patient mutations in *ABCC6* (NM_001171.5), *ENPP1* (NM_006208.2), and *NT5E* (NM_002526.3).

is impossible with biallelic loss-of-function mutations in *ENPP1*, perhaps reconciling the particular severity of the GACI phenotype.

As expected, *NT5E*$^{Mut/Mut}$ fibroblasts had no measurable CD73 enzymatic activity. Both *ABCC6*$^{Mut/Mut}$ and *ENPP1*$^{Mut/Mut}$ cells exhibited decreased CD73 activity compared to controls (Fig. 19E; one-way analysis of variance: P=3.51x10^{-5}). Levels of *NT5E* mRNA in *ABCC6*$^{Mut/Mut}$ and *ENPP1*$^{Mut/Mut}$ cells were similar to those in control cells but decreased in *NT5E*$^{Mut/Mut}$ cell lines, all of which have biallelic mutations creating a premature termination codon expected to elicit nonsense-mediated mRNA decay (Fig. 19F; one-way analysis of variance: P=0.038). These data suggest that reduced production and/or bioavailability of substrate (i.e., AMP) limits CD73 activity, but not expression. This demonstration of metabolic crosstalk among ENPP1, CD73, and ABCC6 further validates the conclusion that ABCC6 contributes to extracellular ATP metabolism.

Liver-specific deletion of *Abcc6* does not fully recapitulate the global *Abcc6*$^{-/-}$ phenotype implicating the role of both local and systemic factors in ectopic calcification.

Prior reports demonstrating high expression of *ABCC6* in the liver and low expression of *ABCC6* in disease-affected tissues[241] have advanced a liver-centric mechanistic hypothesis for PXE[243], i.e., that peripheral tissue calcification reflects failed liver secretion of an endocrine inhibitor of calcification. In contrast, our in vitro findings suggest that a cell-autonomous perturbation of extracellular ATP metabolism in

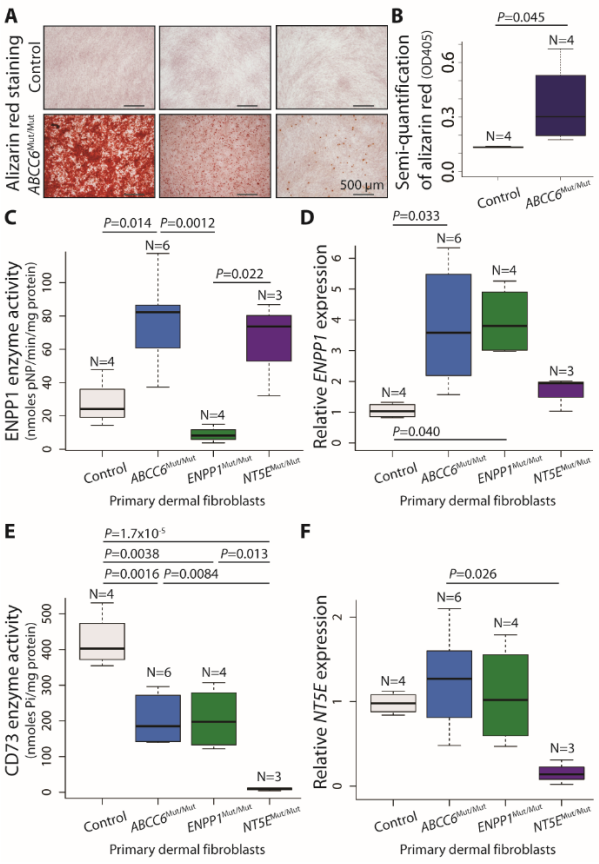

Fig. 19. Evidence for a provoked cell-autonomous defect and alterations in enzymes integral to the extracellular catabolism of ATP in *ABCC6* mutant cells. (**A**) Primary dermal fibroblasts derived from patients with biallelic mutations in *ABCC6* (*ABCC6*$^{Mut/Mut}$) calcify in vitro when stimulated with osteogenic media, as indicated by alizarin red staining. Representative images demonstrating the spectrum of calcification are shown. (**B**) Quantification of the alizarin red staining was determined by colorimetric analysis. A one-tailed Student's t-test was performed; *P*-value indicated. (**C, D, E, F**) Quantification of enzyme activity and gene expression for ENPP1 (*ENPP1*) and CD73 (*NT5E*) in primary dermal fibroblasts derived from patients with biallelic mutations in *ABCC6*, *ENPP1*, or *NT5E*. A one-way analysis of variance with a Tukey's honest significance difference post-hoc analysis was performed; *P*-values indicated.

ABCC6$^{Mut/Mut}$ fibroblasts is sufficient to predispose to calcification, but that an exogenous trigger is required for phenotypic expression. To explore this issue in vivo, we generated a mouse carrying a conditional *Abcc6* allele (*Abcc6*$^{flox/flox}$) that was subsequently crossed to a number of different lines that express *Cre* recombinase in a cell type- or tissue-specific manner.

As evidenced by micro-CT, global ablation of *Abcc6* with CMV-*Cre* resulted in calcification of the fibrous capsule surrounding the muzzle vibrissae at 20 weeks of age, fully recapitulating the phenotype of *Abcc6*$^{-/-}$ mice (Fig. 20A, B; one-way analysis of variance: P=2.2x10^{-16}). Contrary to the proposed liver-centric model, however, efficient liver-specific deletion of *Abcc6* using Albumin-*Cre* (*Abcc6*$^{flox/flox}$; Alb-*Cre*) failed to induce any calcification at 20 weeks (Fig. 20A, B). We verified efficient deletion of *Abcc6* in hepatocytes by breeding the Alb-*Cre* mice to a *Rosa*^{mTmG} mouse line; all cells that recombine change expression from membrane Tomato (mT; red fluorescence) to green fluorescent protein (mG; green fluorescence). All hepatocytes in the *Rosa*^{mTmG}; Alb-*Cre* mice showed green fluorescence (Fig. 20C).

Cell-type or tissue-specific ablation of *Abcc6* using *Cre* drivers specific for vascular smooth muscle (SM22α-*Cre*), vascular endothelium (VE-Cadherin-*Cre*), skeletal muscle (Pax7-*Cre*), renal tubular cells (Cdh16-*Cre*), pericytes (Pdgfrβ-*Cre*), adipocytes (Fabp4-*Cre*), and bone marrow (CD45-*Cre*), also failed to induce calcification at 20 weeks of age (Table 3). Curiously, one of 22 mice with Wnt1-*Cre* mediated ablation of *Abcc6* in the neural crest, including local cells surrounding the vibrissae, showed mild calcification of

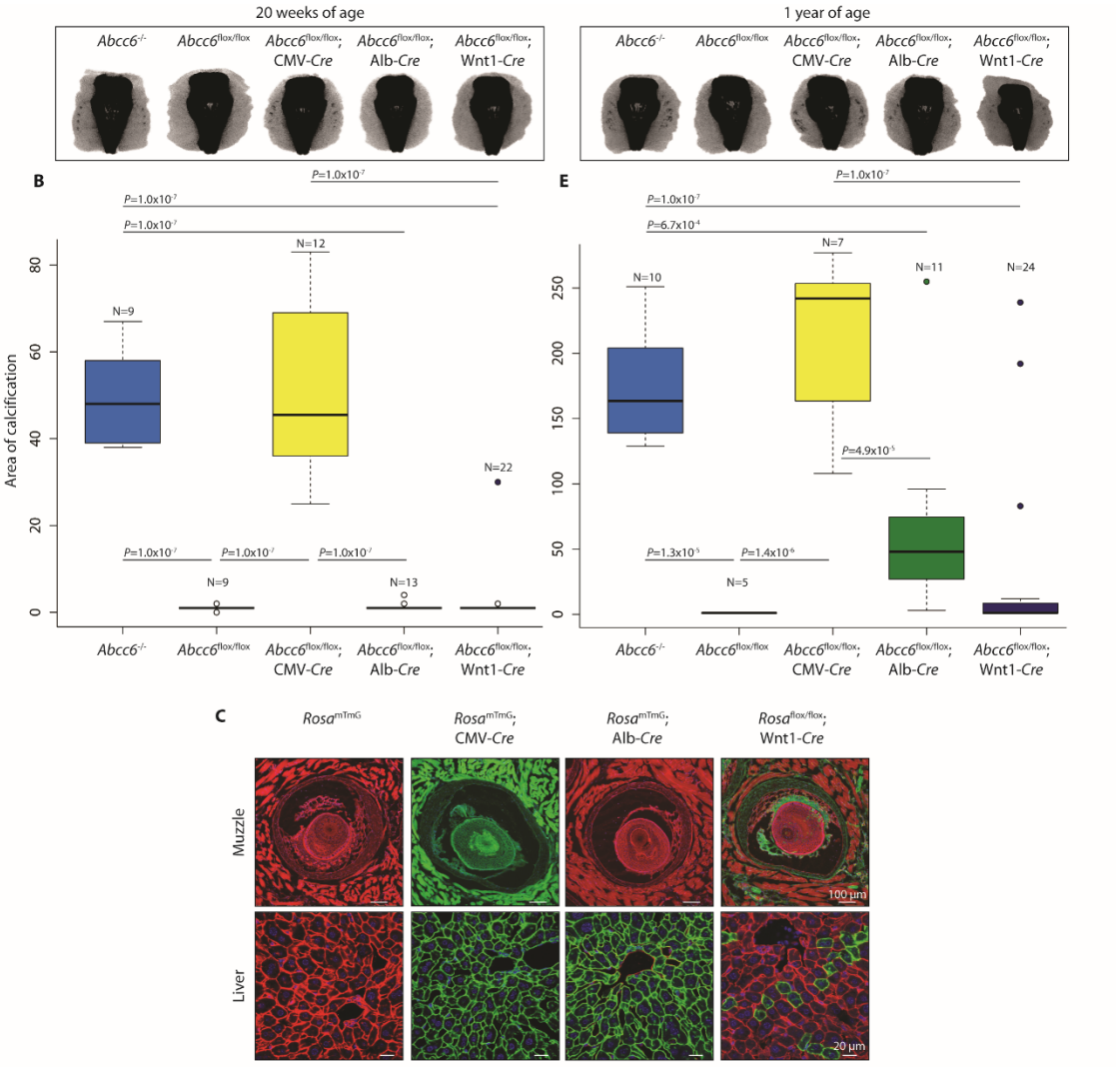

Fig. 20. Liver-specific deletion of *Abcc6* does not phenocopy constitutive ablation of *Abcc6*. Micro-CT scans of the muzzle to evaluate the extent of vibrissae fibrous capsule calcification were obtained at 20 weeks of age (**A**) and 1 year (**D**). (**B, E**) Quantification of ectopic calcification from micro-CT images. A one-way analysis of variance with a Tukey's honest significance difference post-hoc analysis was performed; *P*-values indicated. (**C**) Visualization and confirmation of *Cre*-targeted tissues and cell types utilizing the *Rosa*^{mTmG} reporter mouse line. All cells which are successfully recombined transition from expression of membrane Tomato (mT; red fluorescence) to green fluorescent protein (mG; green fluorescence). Representative images shown.

the fibrous capsule at 20 weeks of age (Fig. 20A, B; Table 3). Upon breeding the Wnt1-*Cre* mouse line to a *Rosa*^{mTmG} reporter, we discovered mosaic recombination within the liver; at 20 weeks of age, green fluorescence (indicating recombination) was observed in approximately 12% of hepatocytes (Fig. 20C).

When aged to one year, *Abcc6*$^{flox/flox}$; Alb-*Cre* and *Abcc6*$^{flox/flox}$; Wnt1-*Cre* mice showed reduced penetrance and variable expressivity of calcification of the vibrissae fibrous capsule compared to *Abcc6*$^{flox/flox}$; CMV-*Cre* mice (Fig. 20D, E; table S2; one-way analysis of variance: P=4.68x10^{-11}). Deleting *Abcc6* in all other cell types and tissues tested did not result in calcification at one year of age (Table 3). These data suggest that the loss of *Abcc6* expression in the liver sensitizes to calcification, but that this event in isolation is insufficient to achieve the threshold loss-of-function needed for highly penetrant and severe phenotypic expression. The efficiency of the tissue-specific *Abcc6* ablation was confirmed by measuring *Abcc6* expression at one year of age. Like *Abcc6*$^{-/-}$ mice, *Abcc6*$^{flox/flox}$; CMV-*Cre* mice had no measureable expression of *Abcc6* in the liver or kidney when compared to normal levels in control mice (Fig. 21A; one-way analysis of variance: P=2.2x10^{-16}, Fig. 21B; one-way analysis of variance: P=2.2x10^{-16}). *Abcc6*$^{flox/flox}$; Alb-*Cre* mice had no *Abcc6* expression in the liver (Fig. 21A), though normal expression in the kidney (Fig. 21B). *Abcc6*$^{flox/flox}$; Wnt1-*Cre* mice had a substantial (five-fold), yet incomplete, reduction of *Abcc6* expression in the liver (Fig. 21A), but not in the kidney (Fig. 21B).

	Abcc6$^{flox/flox}$; CMV-*Cre*	*Abcc6*$^{flox/flox}$; Alb-*Cre*	*Abcc6*$^{flox/flox}$; SM22α-*Cre*	*Abcc6*$^{flox/flox}$; VE-Cad-*Cre*	*Abcc6*$^{flox/flox}$; Pax7-*Cre*	*Abcc6*$^{flox/flox}$; Cdh16-*Cre*	*Abcc6*$^{flox/flox}$; Pdgfrβ-*Cre*	*Abcc6*$^{flox/flox}$; Fabp4-*Cre*	*Abcc6*$^{flox/flox}$; CD45-*Cre*	*Abcc6*$^{flox/flox}$; Wnt1-*Cre*
	Constitutive	Liver	Vascular smooth muscle	Vascular endothelium	Skeletal muscle	Renal tubular cells	Pericytes	Adipocytes	Bone marrow cells	Fibrous capsule cells
20 weeks										
Penetrance	12/12	0/13	0/10	0/9	0/16	0/23	0/10	0/11	0/10	1/22
Percent	100%	0%	0%	0%	0%	0%	0%	0%	0%	4.5%
1 year										
Penetrance	7/7	11/11	0/8	0/8	0/6	0/23	0/10	0/9	0/9	8/24
Percent	100%	100%	0%	0%	0%	0%	0%	0%	0%	33.3%

Table 3. Number of calcified mice at 20 weeks and one year of age.

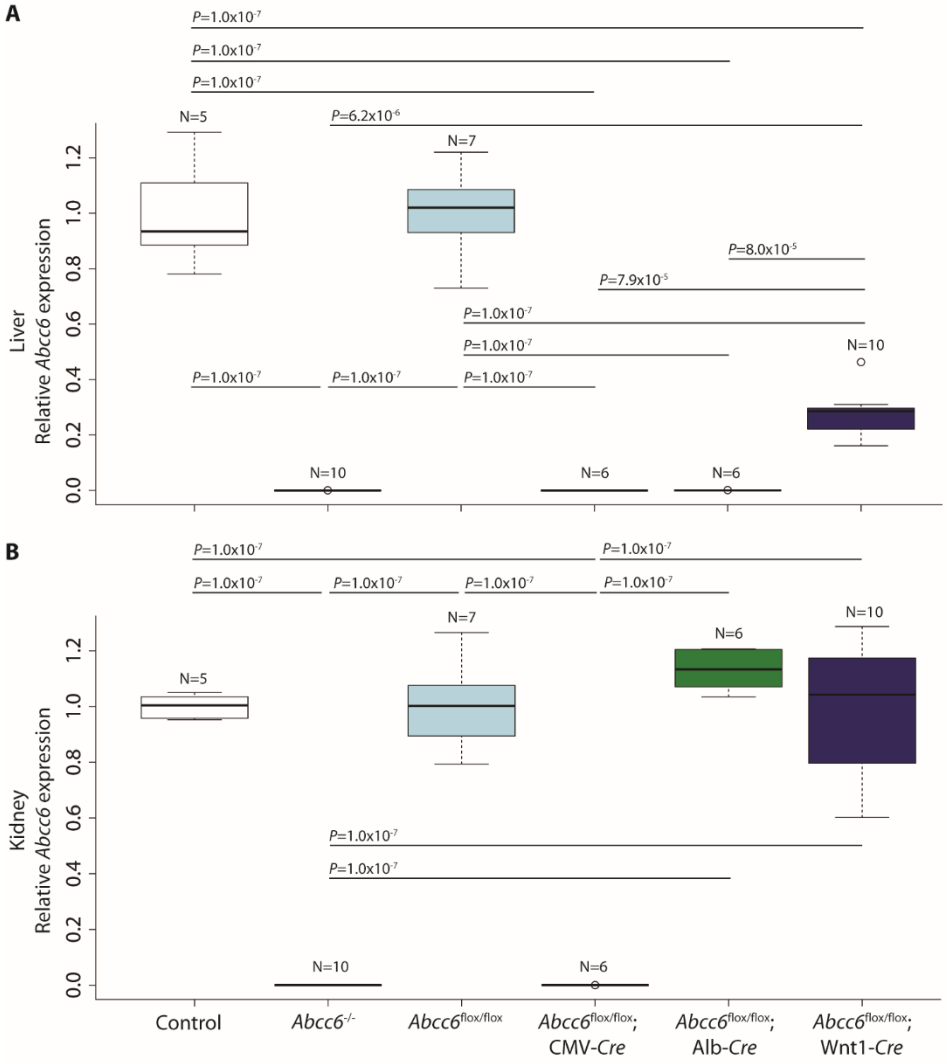

Fig. 21. Demonstration of efficient liver-specific deletion of *Abcc6* in mice.

Expression of *Abcc6* in the liver (**A**) and kidney (**B**) of control, *Abcc6*$^{-/-}$, and *Cre*-targeted *Abcc6*$^{flox/flox}$ mice. A one-way analysis of variance with a Tukey's honest significance difference post-hoc analysis was performed; *P*-values indicated.

Next, we deleted *Abcc6* in a combinatorial manner in an attempt to recapitulate the robust calcification seen at 20 weeks in *Abcc6*$^{-/-}$ and *Abcc6*$^{flox/flox}$; CMV-*Cre* mice. Deleting *Abcc6* in all organs caudal to the heart and lungs (*Abcc6*$^{flox/flox}$; Alb-*Cre*; Cdx1-*Cre*), including the liver and kidney, did not result in calcification at 20 weeks of age, providing strong evidence against a pathogenic hypothesis that singularly invokes an endocrine mechanism (Fig. 22A, B). Knocking out *Abcc6* in the liver and all skeletal muscle cells, including those resident in the muzzle (*Abcc6*$^{flox/flox}$; Alb-*Cre*; Pax7-*Cre*), also did not induce calcification. Interestingly, targeting *Abcc6* in the liver and in Wnt1-positive cells, including local cells in the fibrous capsule surrounding the vibrissae (*Abcc6*$^{flox/flox}$; Alb-*Cre*; Wnt1-*Cre*), induced calcification at 20 weeks, albeit with reduced penetrance (5 of 13 mice calcified). All *Cre*-line combinations were also bred to a *Rosa*^{mTmG} mouse line to confirm efficient targeting of the cell and/or tissue type (Fig. 22C).

Although circulating PPi levels appear decreased in *Abcc6*$^{-/-}$ mice and PXE patients[252], it remains uncertain whether decreased plasma PPi is the primary determinant of disease. To explore if deleting *Abcc6* in a combinatorial method was further decreasing circulating PPi levels in an additive manner that correlated with the severity of ectopic calcification, we measured plasma PPi levels in different cell- and tissue-specific *Abcc6* knockout mouse models at one year of age and simultaneously quantified vibrissae fibrous capsule calcification via micro-CT (Fig. 23). As expected, constitutive deletion of *Abcc6* (*Abcc6*$^{flox/flox}$; CMV-*Cre*) resulted in a robust calcification phenotype (Fig. 23A, B; one-way analysis of variance: P=1.09x10^{-5}), along with plasma PPi levels that were

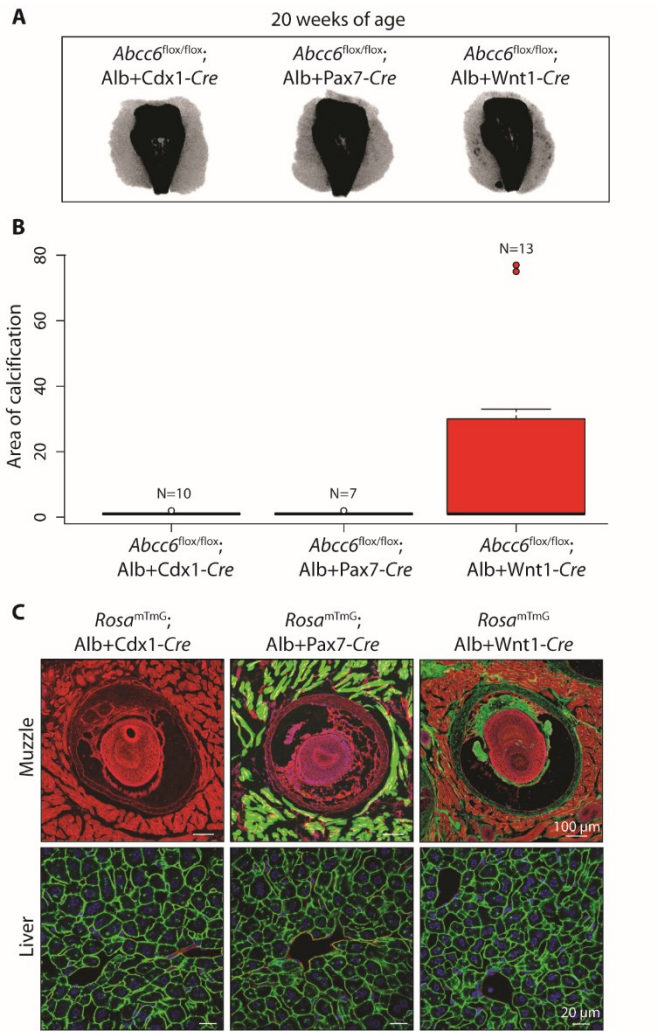

Fig. 22. Evidence that both local and systemic defects in ATP metabolism are needed to promote PXE-associated ectopic calcification. (**A**) Micro-CT scans of the muzzle demonstrating ectopic calcification at 20 weeks of age upon deletion of *Abcc6* in both the liver and local Wnt1-positive cells in the fibrous capsule, albeit with reduced penetrance compared to constitutive targeting (Fig. 3A, B). (**B**) Quantification of ectopic calcification from micro-CT images. A one-way analysis of variance with a Tukey's honest significance difference post-hoc analysis was performed; *P*-values indicated. (**C**) Visualization and confirmation of *Cre*-targeted tissues and cell types utilizing the *Rosa*^{mTmG} reporter mouse line. Representative images shown.

significantly below those observed in control animals (*Abcc6*$^{flox/flox}$) (Fig. 23C; one-way analysis of variance: P=0.0087). However, two knockout combinations (*Abcc6*$^{flox/flox}$; Alb-*Cre* and *Abcc6*$^{flox/flox}$; Alb-*Cre*; Cdx1-*Cre*) exhibited much milder vibrissae calcification compared with the *Abcc6*$^{flox/flox}$; CMV-*Cre* mice (Fig. 23A, B), and yet showed comparably reduced levels of circulating PPi (Fig. 23C). The same knockout combinations showed calcification equivalent to that observed in *Abcc6*$^{flox/flox}$; Wnt1-*Cre* mice despite normal circulating PPi levels in the latter. These data document poor correlation between the severity of calcification and the level of circulating PPi.

Of all the cell-type or tissue-specific *Cre* drivers utilized in this study, only use of Wnt1-*Cre* was associated with recombination within the fibrous capsule of the vibrissae (Fig. 20C). Furthermore, the increase in disease penetrance in *Abcc6*$^{flox/flox}$; Alb-*Cre*; Wnt1-*Cre* mice compared to *Abcc6*$^{flox/flox}$; Alb-*Cre* animals cannot plausibly relate to enhanced liver recombination. Taken together, these data suggest cooperation between local and systemic events in the initiation of calcification in PXE.

TNAP inhibition prevents in vitro calcification in cell lines with biallelic *ABCC6* mutations under osteogenic conditions.

With evidence that local cells contribute to PXE pathogenesis, *ABCC6*$^{Mut/Mut}$ patient fibroblasts emerged as a viable model for investigating potential therapies. We explored whether the calcification was related to increased TNAP levels, since it is known that TNAP is a major regulator of in vitro[305] and in vivo calcification[160,306,307]. When stimulated with osteogenic media for five days, *ABCC6*$^{Mut/Mut}$ cells had increased TNAP

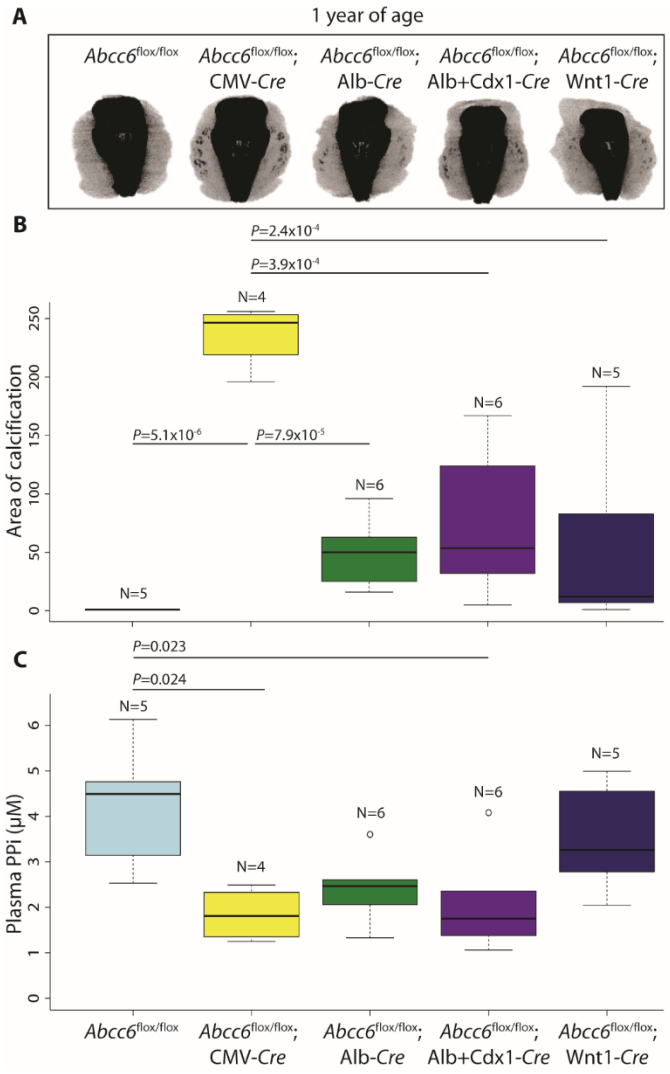

Fig. 23. Circulating PPi levels do not correlate with severity of calcification phenotype. (**A**) Micro-CT scans of the muzzle to evaluate the extent of vibrissae fibrous capsule calcification were obtained at one year of age. (**B**) Quantification of ectopic calcification from micro-CT images. (**C**) Quantification of plasma PPi levels. (**B, C**) A one-way analysis of variance with a Tukey's honest significance difference post-hoc analysis was performed; *P*-values indicated.

enzymatic activity compared to controls (Fig. 24A; two-way analysis of variance, genotype effect: P=0.010, treatment effect: P=0.0029, interaction effect: P=0.039). Expression of *ALPL*, the gene encoding TNAP, was concordantly increased (Fig. 24B; two-way analysis of variance, genotype effect: P=0.012, treatment effect: P=0.048, interaction effect: P=0.18).

Arylsulfonamides are potent and selective inhibitors of TNAP[313]. SBI-425, an arylsulfonamide derivative with optimized pharmacokinetic properties, effectively inhibits TNAP in vivo[160]. Treatment of *ABCC6*$^{Mut/Mut}$ cells under osteogenic conditions with SBI-425 prevented in vitro calcification, whereas mutant cells treated with vehicle proceeded to calcify (Fig. 24C, D; two-way analysis of variance, genotype effect: P=0.029, treatment effect: P=0.028, interaction effect: P=0.029). These data demonstrate that in vitro calcification of *ABCC6*$^{Mut/Mut}$ cells is TNAP-dependent, suggesting a potential therapeutic target for PXE.

TNAP inhibition attenuates both the development and progression of calcification in a PXE mouse model.

Our demonstration of excessive TNAP levels and activity in *ABCC6*$^{Mut/Mut}$ cells prompted a treatment trial in six week old *Abcc6*$^{-/-}$ mice with the TNAP inhibitor SBI-425 (30 mg/kg/day), etidronate (240 mg/kg/day), or control food for 14 weeks. Micro-CT scans at 20 weeks of age revealed significant and equivalent attenuation of the calcification phenotype in both SBI-425 and etidronate-treated *Abcc6*$^{-/-}$ mice (Fig. 25A, B; two-way analysis of variance, genotype effect: P=1.2x10^{-12}, treatment effect: P=3.7x10^{-5},

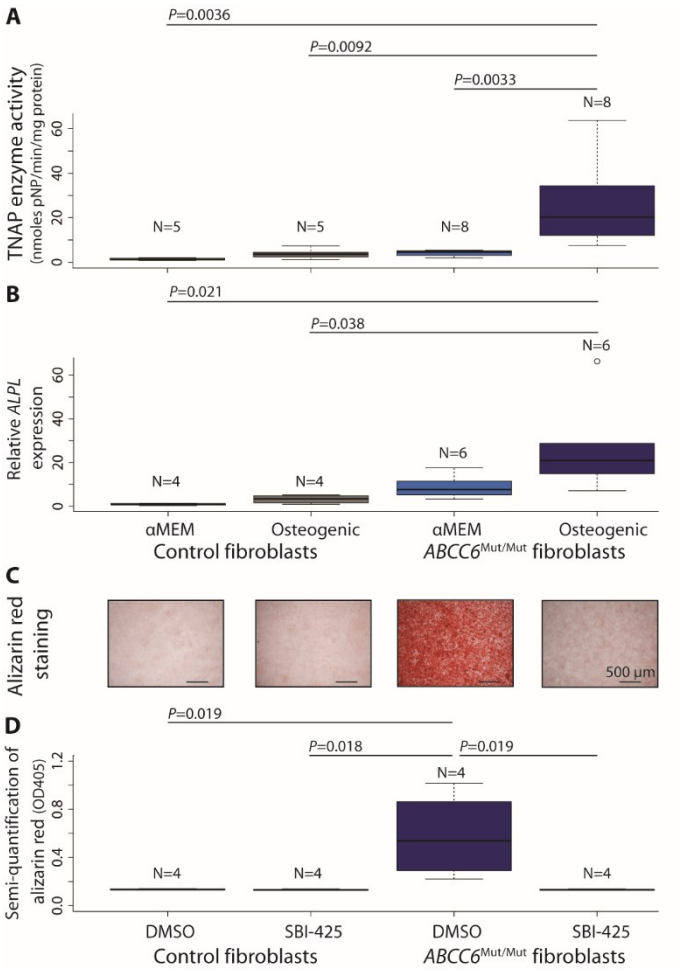

Fig. 24. Primary dermal fibroblasts derived from patients with biallelic mutations in *ABCC6* show TNAP-dependent in vitro calcification. (**A, B**) TNAP enzyme activity and gene (*ALPL*) expression in control and *ABCC6*$^{Mut/Mut}$ fibroblasts with and without osteogenic stimulation. (**C, D**) Calcification of *ABCC6*$^{Mut/Mut}$ fibroblasts is abrogated upon treatment with the TNAP inhibitor, SBI-425. (**A, B, D**) A two-way analysis of variance with a Tukey's honest significance difference post-hoc analysis was performed; *P*-values indicated.

interaction effect: P=2.1x10^{-5}). Mice were treated before the onset of any sign of calcification, as evidenced by micro-CT at six weeks of age, although microscopic nidi of calcification cannot be excluded. The therapeutic effect of both SBI-425 and etidronate was substantiated by measuring the calcium phosphate precipitate in muzzle tissue (Fig. 25C; one-way analysis of variance: P=8.4x10^{-4}). Serum samples taken from treated mice demonstrated that SBI-425 robustly inhibited plasma TNAP activity, whereas etidronate and control treatments did not, as expected (Fig. 25D). Since there was no effect of genotype (two-way analysis of variance, genotype effect: P=0.64, treatment effect: P=8.7x10^{-12}, interaction effect: P=0.92), genotype was collapsed to evaluate for differences across treatment groups (one-way analysis of variance: P=1.5x10^{-13}). While *Abcc6*$^{-/-}$ mice had decreased circulating PPi levels compared to control mice, SBI-425 did not significantly increase PPi levels, potentially highlighting the contribution of local events to the pathogenesis of PXE (Fig. 26; two-way analysis of variance, genotype effect: P=0.0017, treatment effect: P=0.24, interaction effect: P=0.72).

Femora were evaluated for bone microarchitecture, mineralization, and mechanical properties at the conclusion of the treatment trial. Imaging of the femora showed significant effects of sex and treatment, but not genotype, across all trabecular bone parameters. It has been well-established that trabecular architecture differs between male and female C57BL/6 mice, in an age-related manner, starting between two and six months of age[308]. SBI-425 treatment did not result in any changes to bone microarchitecture. In contrast, etidronate treatment resulted in increased trabecular bone volume (Fig. 27A, E; three-way analysis of variance, gender effect: P=4.16x10^{-12},

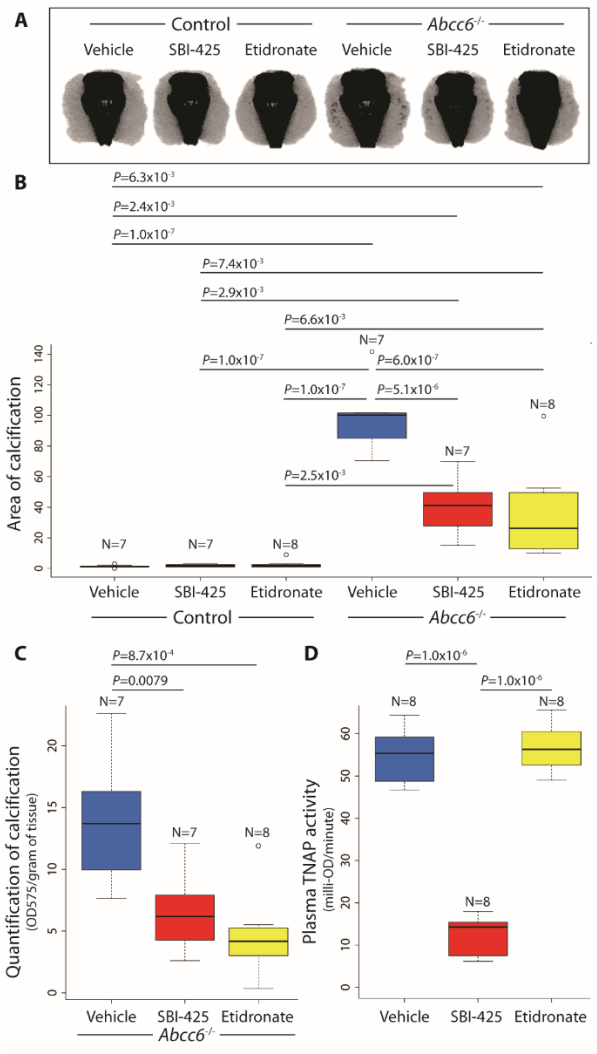

Fig. 25. TNAP inhibition attenuates calcification in a PXE mouse model. (**A, B**) Micro-CT scans revealed significant attenuation of the calcification phenotype in both SBI-425 and etidronate-treated *Abcc6*$^{-/-}$ mice. Control mice did not calcify. A two-way analysis of variance with a Tukey's honest significance difference post-hoc analysis was performed; *P*-values indicated. **(C)** Micro-CT results were validated by dissolving the muzzle tissue and quantifying the calcium phosphate precipitate. (**D**) Plasma obtained from mice at the conclusion of the treatment trial showed that SBI-425 strongly inhibited residual TNAP activity levels. (**C, D**) A one-way analysis of variance with a Tukey's honest significance difference post-hoc analysis was performed; *P*-values indicated.

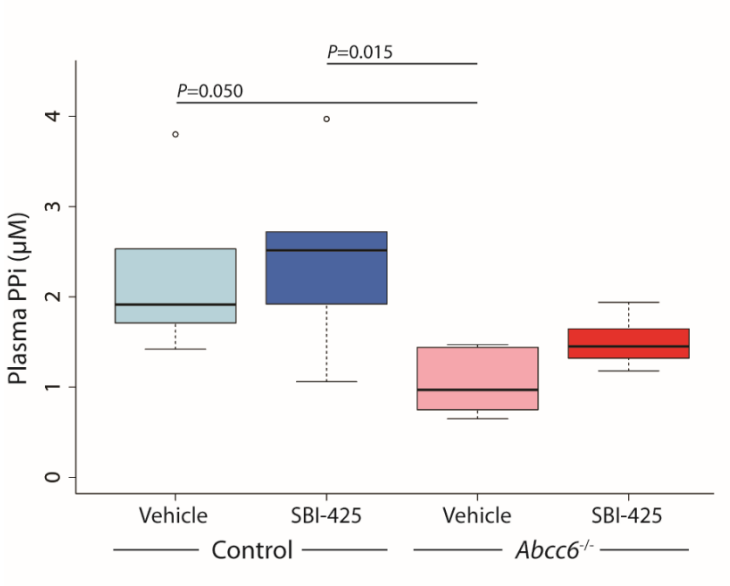

Fig. 26. TNAP inhibition does not alter circulating PPi levels in mice. Quantification of PPi levels in control and *Abcc6*$^{-/-}$ mice treated with vehicle or the TNAP inhibitor SBI-425. A two-way analysis of variance with a Tukey's honest significance difference post-hoc analysis was performed; *P*-values indicated.

treatment effect: P=8.06x10^{-8}, genotype effect: P=0.49) and increased number of trabeculae (Fig. 27B, E; three-way analysis of variance, gender effect: P=1.08x10^{-13}, treatment effect: P=4.7x10^{-10}, genotype effect: P=0.48), with decreased intertrabecular space (Fig. 27C, E; three-way analysis of variance, gender effect: P=2.52x10^{-12}, treatment effect: P=5.59x10^{-5}, genotype effect: P=0.77) in the distal femur in both male and female mice. Etidronate-treated male, but not female, mice also had significantly increased trabecular thickness compared to vehicle-treated mice (Fig. 27D, E; three-way analysis of variance, gender effect: P=7.2x10^{-9}, treatment effect: P=0.0050, genotype effect: P=0.62). Trichrome staining of the undecalcified distal femora showed no abnormalities of bone mineralization in SBI-425 mice, but increased accumulation of osteoid was apparent in etidronate-treated animals, as previously reported (Fig. 27F)[309,310]. Neither of the treatment arms altered the cortical bone of the femoral diaphysis, as quantified by micro-CT (Table 4) and mechanical testing (Table 5).

To assess for therapeutic potential of SBI-425 in mice with established calcification, *Abcc6*$^{-/-}$animals were aged to 20 weeks and then treated with either vehicle or SBI-425 (30 mg/kg/day) for 16 weeks. While vehicle-treated *Abcc6*$^{-/-}$ mice showed progressive muzzle calcification, SBI-425-treated animals did not (Fig. 28; one-way analysis of variance: P=0.050). These data suggest that while TNAP inhibition does not reverse existing calcification in this experimental context, it can prevent progression of the phenotype. The potential for chronic treatment to achieve therapeutic tissue remodeling in patients remains to be determined.

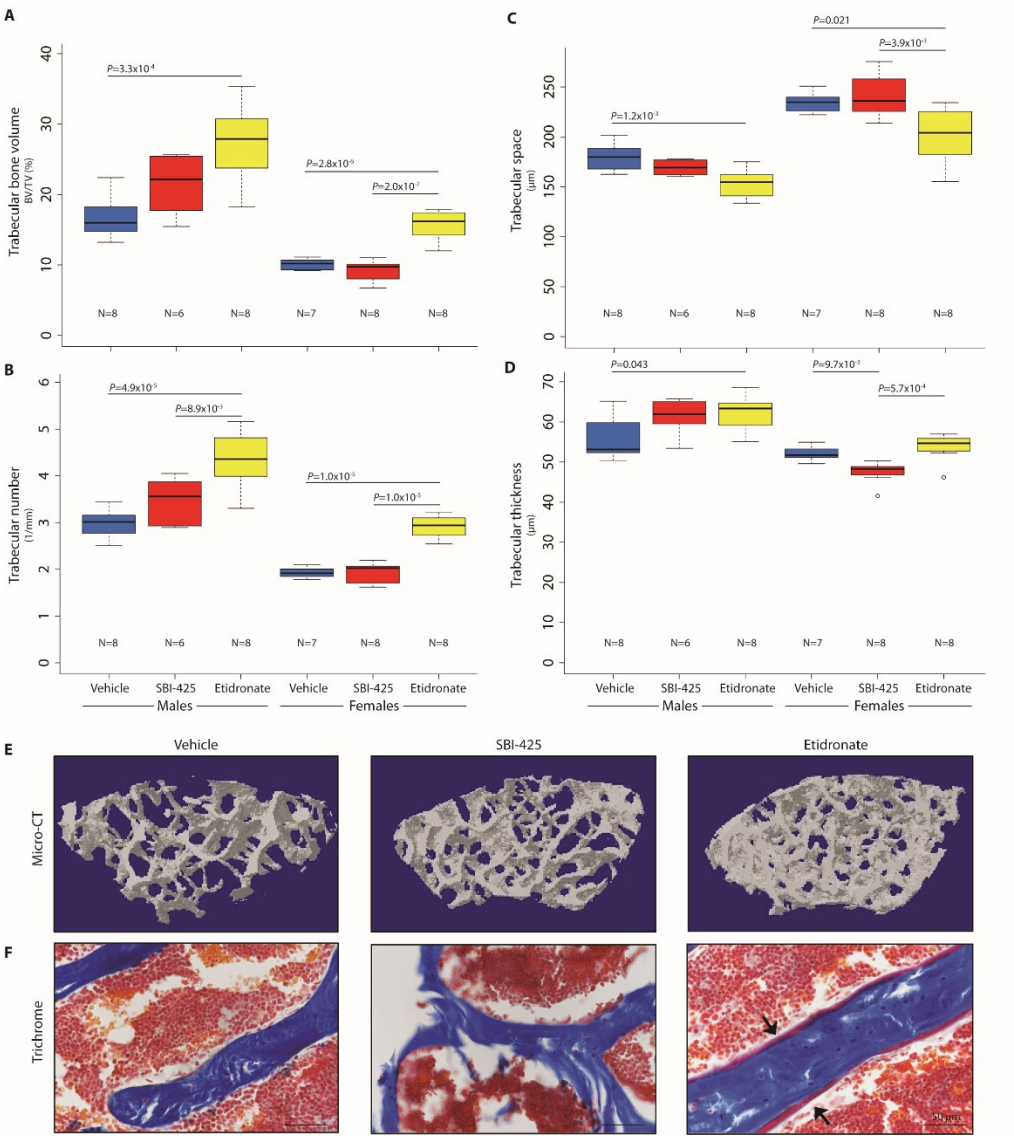

Fig. 27. TNAP inhibition had no negative effects on bone microarchitecture or mineralization in a PXE mouse model. Quantification of trabecular bone volume (**A**), number (**B**), space (**C**), and thickness (**D**) in vehicle-, SBI-425-, and etidronate- treated mice. Since there was no effect of genotype in any of the trabecular bone parameters, genotype was collapsed to evaluate for differences across treatment groups within each sex with a one-way analysis of variance and a Tukey's honest significance difference post-hoc test; *P*-values indicated. Representative images from micro-CT scans (**E**) and trichrome staining of the distal femur (**F**). Arrows point to osteoid.

	TMD (g/cm^3)	Tissue area (mm^2)	Bone area (mm^2)	BA/TA (%)	Marrow area (mm^2)	Cortical thickness (μm)	pMOI (mm^4)
Males							
Vehicle	1.22±0.02	1.61±0.13	0.84±0.06	52.21±1.29	0.77±0.07	184.87±11.00	0.34±0.05
SBI-425	1.22±0.02	1.82±0.23	0.94±0.12	51.49±1.58	0.88±0.12	178.10±13.00	0.43±0.10
Etidronate	1.22±0.02	1.81±0.26	0.95±0.14	52.50±1.83	0.86±0.13	178.69±8.64	0.43±0.12
Females							
Vehicle	1.24±0.04	1.52±0.07	0.81±0.03	53.05±1.73	0.71±0.05	195.15±8.18	0.30±0.03
SBI-425	1.21±0.04	1.51±0.07	0.79±0.05	51.99±2.34	0.73±0.06	185.42±6.43	0.29±0.03
Etidronate	1.21±0.03	1.52±0.09	0.81±0.07	53.27±2.57	0.71±0.04	185.61±15.17	0.30±0.05

Table 4. Cortical bone microarchitecture. Treatment with SBI-425 or etidronate did not affect cortical bone microarchitecture. TMD = total mineral density; BA/TA = bone area/total area; pMOI = polar moment of inertia. Data presented as mean ± standard deviation.

	Ultimate Moment (Nmm)	Bending rigidity (Nmm^2)	Ultimate stress (MPa)	Young's modulus (MPa)	Ultimate displacement (mm)	Toughness (J/mm^3)
Males						
Vehicle	24.31±4.21	556.14±83.37	64.10±4.61	2649.59±584.13	0.49±0.11	4.47±1.18
SBI-425	27.32±4.62	636.96±210.14	59.88±7.13	2285.95±662.57	0.43±0.14	4.45±2.03
Etidronate	26.34±4.65	670.84±113.70	60.18±5.24	2624.95±294.17	0.53±0.16	5.03±2.01
Females						
Vehicle	24.40±1.56	637.74±43.43	74.74±9.58	3419.77±595.07	0.53±0.28	5.76±2.93
SBI-425	23.80±1.25	590.60±86.27	74.71±5.89	3256.18±464.60	0.47±0.10	5.19±1.12
Etidronate	24.43±3.34	532.41±126.29	73.98±5.60	2863.08±890.42	0.50±0.14	5.74±1.43

Table 5. Cortical bone strength. Treatment with SBI-425 or etidronate did not affect cortical bone strength as evidenced by mechanical testing. Data presented as mean ± standard deviation.

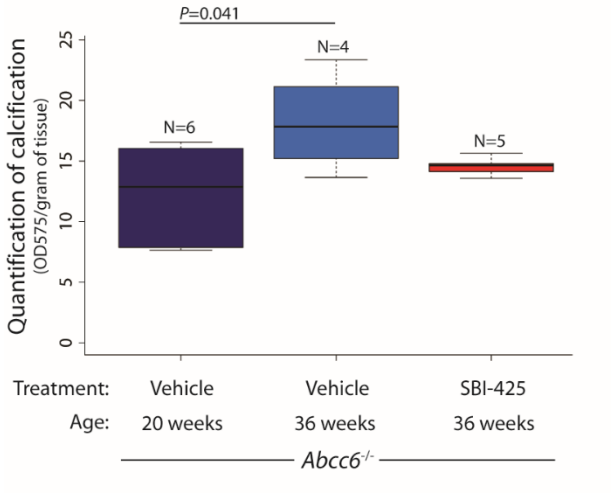

Fig. 28. TNAP inhibition prevents progression of established calcification in a PXE mouse model. *Abcc6*$^{-/-}$ mice were aged to 20 weeks and then treated with either vehicle or SBI-425 for 16 weeks. The calcium phosphate precipitate was quantified at the specified time point. A one-way analysis of variance with a Tukey's honest significance difference post-hoc analysis was performed; *P*-value indicated.

IV. DISCUSSION

In this study, both genetic and metabolic analyses provide compelling evidence that ABCC6 acts in concert with ENPP1 and CD73 to regulate extracellular PPi, a major physiologic inhibitor of calcification. This work suggests that ENPP1 is required for generation of PPi while ABCC6 and CD73 cooperate downstream to inhibit TNAP expression and activity and maintain normal PPi levels (Fig. 29). This interactive network reconciles the pronounced clinical severity of GACI and may provide insight into the phenotypic diversity associated with *ABCC6* deficiency, ranging from early-onset GACI to late-onset PXE. Perturbation of this pathway limits the bioavailability of PPi, implying the potential for broad therapeutic relevance of TNAP inhibitors.

We demonstrate that *ABCC6*$^{Mut/Mut}$ cells have the intrinsic capacity to calcify in vitro and have altered activity of enzymes involved in ATP catabolism, specifically, increased ENPP1 and TNAP and decreased CD73 enzymatic activities. Consistent with our findings, *ABCC6*$^{Mut/Mut}$ dermal fibroblasts were previously shown to be morphologically and biochemically distinct from controls[246–248] and to have a tendency for matrix mineralization[249]. Although our data concur with prior studies demonstrating that *ABCC6*$^{Mut/Mut}$ cells have higher gene expression and activity of TNAP[249,311], we showed that *ABCC6*$^{Mut/Mut}$ cells had increased (rather than decreased) ENPP1 enzymatic activity and mRNA levels. These discrepancies might arise from differences in experimental design — we measured ENPP1 enzymatic activity and mRNA after five days in culture whereas previous reports assayed after 21 days in culture; compensatory mechanisms might be at play[249].

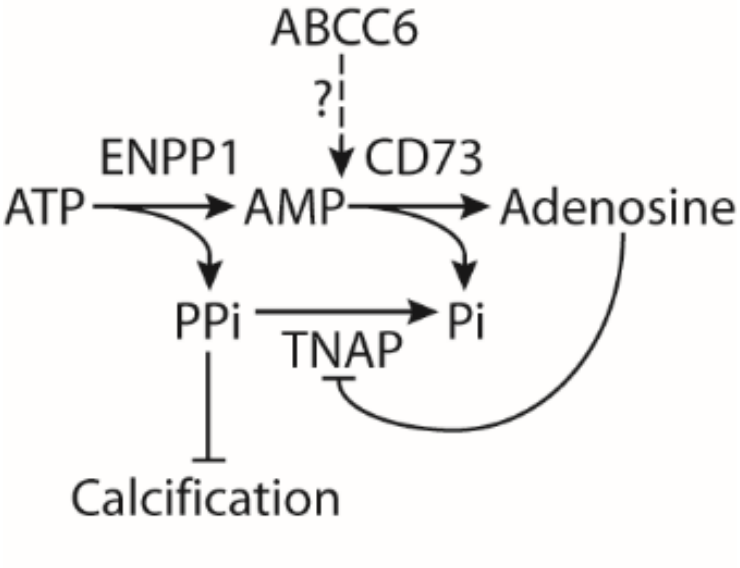

Fig. 29. Proposed involvement of ABCC6 in extracellular ATP metabolism and the suppression of ectopic calcification. ENPP1 metabolizes ATP into AMP and PPi while CD73 further degrades AMP into adenosine and Pi. Adenosine can bind to its cell surface receptor to repress *ALPL*, the gene encoding TNAP. TNAP degrades PPi into Pi and is a primary distal regulator of PPi, a major negative inhibitor of calcification. Our data suggest that ABCC6 is integral to the extracellular ATP metabolism pathway and likely works downstream of ENPP1 and in tandem with CD73 to maintain low TNAP levels and prevent pathological calcification.

It has been proposed that the altered behavior of PXE fibroblasts in culture manifest memory for an in vivo imbalance of a circulating factor[250]. However, there exists additional evidence that inherent, cell-autonomous defects are operative in PXE. For example, *Abcc6*-deficient zebrafish show ectopic calcification in the vicinity of osteoblasts that normally express *Abcc6*[251]. A reconciling view might invoke a role for ABCC6 in determining the level of a circulating factor that regulates calcification and a local sensitization to its perturbation.

Prior work had shown that fibroblasts from GACI patients deficient for ENPP1 activity can also calcify in vitro, yet overexpression of ENPP1 in some, but not all locations in *enpp1*-deficient zebrafish could attenuate calcification at distant target sites[312]. Taken together, these data are consistent with the concept that while necessary, systemic perturbations may not be sufficient to elicit disease in ectopic calcification disorders. Such considerations highlight the relative importance of in vivo models to interrogate disease pathogenesis.

Uitto and colleagues have postulated that PXE is specifically caused by a defect in liver secretion of an endocrine inhibitor of calcification at distant target sites[243,244]. Indeed, parabiosis between *Abcc6*$^{-/-}$ and control mice showed attenuation of the calcification phenotype in the mutant animals, when compared to parabiosis between knockouts[245]. However, if PXE is solely driven by a deficiency of a systemic factor that equilibrates in the circulation, the wildtype partner in a wildtype-to-*Abcc6*$^{-/-}$ pairing (established prior to the onset of calcification) should show the same phenotype as the knockout mouse; this

was not observed. Hence, isolated deficiency of a circulating metabolite appears insufficient to initiate PXE-associated calcification indicating that another factor, perhaps imposed by a local cell, contributes to PXE pathogenesis. Consistent with this, we found that deletion of *Abcc6* in both the liver and local cells in the fibrous capsule surrounding the vibrissae was required to phenocopy the early onset calcification seen upon constitutive gene ablation; the ongoing observation of reduced penetrance heralds additional complexity regarding the critical threshold level and spatial distribution of ABCC6 function.

The observation of decreased circulating PPi in PXE mice and patients[252] has led to the suggestion that PPi is the protective endocrine factor that is missing in PXE; its deficiency in the extracellular space could result from impaired transport of ATP out of cells, with consequent reduction in AMP and PPi production from ATP catabolism[252]. In fact, overexpression of *ABCC6* in HEK293 cells resulted in increased extracellular monophosphates, including AMP, a finding thought most consistent with enhanced ATP secretion. However, while increased extracellular ATP was observed after concomitant treatment with an ENPP1 inhibitor, there was also a generalized increase in triphosphates, diphosphates, and monophosphates suggesting promiscuous effects in this experimental system[252]. In our studies, there was poor correlation between plasma PPi levels and the extent of muzzle calcification in mouse models. While these data do not exclude a contribution of low circulating PPi, they suggest other determinants of disease pathogenesis.

Though our data have not revealed the precise function of ABCC6, they provide evidence that ABCC6 acts downstream of ENPP1, a view inconsistent with the hypothesis that ABCC6 is primarily involved in ATP transport. In addition, the fact that the classical GACI phenotype is more severe than later-onset PXE also suggests that ENPP1 functions upstream of ABCC6. Indeed, if ABCC6 were needed to export ATP for extracellular processing by ENPP1, then it would be expected that PXE would routinely have a phenotype as severe as, or more severe than, GACI; this is not observed. Our data are consistent with a model in which ATP is degraded, at least in part, by intracellular ENPP1 to AMP and PPi, with ABCC6 potentially serving to secrete AMP for subsequent extracellular processing by CD73 to adenosine, which is then presumed to act through cell-surface adenosine receptors to inhibit TNAP expression (Fig. 29)[20]. While this remains to be formally tested, it is notable that prior reports have described intracellular ENPP1 activity and there is no described AMP exporter[172–174]. In theory, ABCC6 could also contribute to secretion of PPi, although this is not directly inferred from the data, and there is already an established plasma membrane PPi transporter, ANK[169]. Finally, the model proposed by Jansen and colleagues that ABCC6 acts upstream of ENPP1 and transports ATP could be partially consistent with our genetic data if there is an alternative but limited source of extracellular ATP[252]. It remains notable, however, that such a model would not reconcile our findings suggesting that ABCC6 and CD73 do not act sequentially, but rather show cooperative function.

Because of the elusive pathological mechanism underlying PXE, therapeutic targets have been limited. Oral bisphosphonates, which directly disrupt calcium and phosphate

precipitation and hence deposition, have been proposed as a treatment strategy for PXE[155]. Although the first generation bisphosphonate etidronate (100 μg/kg administered twice a week intraperitoneally) failed to prevent calcification in *Enpp1*$^{-/-}$ mice[156], it effectively attenuated calcification in *Abcc6*$^{-/-}$ mice when used at a high dose (240 mg/kg/day orally)[157]. Nevertheless, etidronate is currently being tested in the treatment of patients with GACI[156] and CALJA[3] (ClinicalTrials.gov ID NCT01585402). One drawback is that etidronate results in detrimental changes to bone microarchitecture in mice[157] and in acquired hypophosphatemia with severe skeletal mineralization defects in GACI patients[18]. Our findings suggest that the TNAP inhibitor SBI-425 does not have these side effects.

Demonstration that TNAP inhibition attenuates both the development and progression of calcification in both in vitro and in vivo models of PXE helps further establish TNAP as a disease mediator and an attractive therapeutic target in calcification disorders including PXE, GACI, and CALJA. This finding might also shed light on disease mechanism. The prevailing view that PXE relates to the liver's inability to secrete ATP predicts that there is a profound impairment in the generation of extracellular PPi. In this scenario, TNAP inhibition and consequent prevention of PPi degradation would not be effective. Here we provide both genetic and biochemical studies suggesting a role for ABCC6 distal to the degradation of ATP to AMP and PPi by ENPP1. This offers the first rationale that TNAP inhibition would be effective. Given lack of apparent toxicity, TNAP inhibition might also be considered for other disorders of ectopic calcification including common

conditions such as aortic valve calcification[313,314] and chronic kidney disease-associated vascular calcification[17,234], in which decreased PPi has also been documented.

Despite this progress, a number of limitations should be considered. First, while our study draws attention to the potential importance of local events in PXE pathogenesis, the precise nature of microenvironmental alterations remains speculative and the ability to robustly monitor relevant metabolites is subject to both practical and technical limitations in the absence of specific information regarding the physiologic ABCC6 cargo. Second, this study uses the early onset and highly penetrant vibrissae fibrous capsule calcification phenotype as a surrogate for tissue calcification events with relevance to patients with PXE such as those in the eye and vasculature. While there has been no documentation that vibrissae fibrous capsule calcification is somehow specialized in this regard, the broader relevance of findings made in this context remains assumed and will need to be documented. Finally, as always, observations made using model systems allow the generation of hypotheses that will require validation in patients with PXE.

V. MATERIALS AND METHODS

Study design

The purpose of this study was to elucidate the pathophysiological mechanisms underlying PXE and the function of ABCC6 in an effort to rationally design treatment strategies for this rare disease patient population. In order to explore the functional relationships among *Abcc6*, *Enpp1*, and *Nt5e*, we generated double-mutant mice and evaluated fibrous capsule vibrissae calcification via micro-CT. Since we saw strong evidence for genetic

interaction, we further explored the role of extracellular ATP metabolism in primary fibroblasts derived from PXE, GACI, and CALJA patients. We found evidence for a provoked cell-autonomous defect and tested the relevance of these findings in vivo by generating a conditional *Abcc6* knockout mouse model. The ability to recapitulate pathogenic events in vitro also allowed us to utilize *ABCC6*$^{Mut/Mut}$ cell lines to explore possible therapeutic targets. When provoked under osteogenic conditions, *ABCC6*$^{Mut/Mut}$ demonstrated TNAP-dependent in vitro calcification. To extend these findings in vivo, we treated our *Abcc6*$^{-/-}$ mice with a TNAP inhibitor. Efficacy and potential negative effects of therapy were evaluated using micro-CT, quantification of calcium phosphate deposition, serum collection, and studies of bone microarchitecture, histology, and mechanical strength.

Sample sizes were determined on the basis of statistical considerations and on pilot experiments that indicated the number of mice per group needed to generate statistical significance. For human cell lines experiments, our sample size was limited by the number of skin biopsy samples we were able to collect from patients with these very rare conditions. Both male and female mice and cell lines obtained from males and females were evaluated in this study. Mice were randomly assigned to treatment groups; sex was equally distributed among the groups. All experiments were performed blind to genotype and/or treatment. No outliers were excluded. Number of biological replicates in each group is specified in the figures.

Subjects

Patients were enrolled in clinical protocol 76-HG-0238, "Natural History of Patients with Inborn Errors of Metabolism" (clinicaltrials.gov identifier NCT00369421), approved by the NHGRI Institutional Review Board. Written, informed consent was obtained.

Mice

Abcc6 knockout mice (*Abcc6*^{tm1Jfk}/J; termed *Abcc6*$^{-/-}$) were generously provided by Jouni Uitto at Thomas Jefferson University. *Enpp1*-ablated mice (*Enpp1*^{asj}/GrsrJ, stock number: 012810; termed *Enpp1*$^{-/-}$) and *Nt5e* knockout mice (*Nt5e* ^{tm1Lft}/J, stock number: 018986; termed *Nt5e*$^{-/-}$) were obtained from The Jackson Laboratory. The first sign of calcification in *Abcc6*$^{-/-}$ mice is in the fibrous capsule surrounding their vibrissae or whiskers on the muzzle[145]. While there is no human equivalent for this fibrous structure, its calcification has been well-established as an early biomarker for vascular calcification and can be monitored in vivo with micro-CT[315]. Therefore, all studies analyzed the vibrissae fibrous capsule calcification phenotype at 15 or 20 weeks of age since *Abcc6*$^{-/-}$ do not develop other signs of calcification without provocation until many months later, extending beyond the lifespan of *Enpp1*$^{-/-}$ mice. We found that *Nt5e*$^{-/-}$ mice did not develop fibrous capsule vibrissae calcification until one year of age. Therefore, *Abcc6* bred to *Nt5e* mice were analyzed at both 15 weeks and one year.

Abcc6$^{tm1a(EUCOMM)}$ embryonic stem cell lines with conditional potential were purchased from the European Conditional Mouse Mutagenesis Program. Embryonic stem cells were injected into an albino C57BL/6 blastocyst (B6N-*Tyr*$^{c-Brd}$/BrdCrCrl; Charles River) and chimeras were generated. After germline transmission was confirmed,

Abcc6$^{tm1a(EUCOMM)}$ mice were bred to B6.Cg-Tg(ACTFLPe)9205Dym/J (stock number: 005703) mice to generate *Abcc6*$^{tm1c(EUCOMM)}$ (termed *Abcc6*$^{flox/flox}$) mice. To knockout *Abcc6* in a cell-type and/or tissue-specific matter, these mice were bred to the following *Cre* expressing mouse lines, which were obtained from The Jackson Laboratory unless otherwise indicated: B6.C-Tg(CMV-cre)1Cgn/J (stock number: 006054; termed CMV-*Cre*), B6.Cg-Tg(Alb-cre)21Mgn/J (stock number: 003574; termed Alb-*Cre*), B6.Cg-Tg(Tagln-cre)1Her/J (stock number: 017491; termed SM22α-*Cre*), B6.FVB-Tg(Cdh5-cre)7Mlia/J (stock number: 006137; termed VE-Cadherin-*Cre*), *Pax7*$^{tm1(cre)Mrc}$/J (stock number: 010530; termed Pax7-*Cre*), B6.Cg-Tg(Cdh16-cre)91Igr/J (stock number: 012237; termed Cdh16-*Cre*), Tg(Pdgfrb-Cre)^{35Vli} (a generous donation from Volkhard Lindner at Maine Medical Center; termed Pdgfrβ-*Cre*), B6.Cg-Tg(Fabp4-cre)1Rev/J (stock number: 005069; termed Fabp4-*Cre*), Ptprc$^{tm1(cre)Medv}$ (a generous donation from Joseph Mee at the University of Edinburgh; termed CD45-*Cre*), 129S4.Cg-Tg(Wnt1-cre)2Sor/J (stock number: 022137; termed Wnt1-*Cre*), and Tg(Cdx1-cre)23Kem (a generous donation from Jeremy Nathans at Johns Hopkins University School of Medicine; termed Cdx1-*Cre*). The B6.129(Cg)-*Gt(ROSA)26Sor*$^{tm4(ACTB-tdTomato,-EGFP)Luo}$/J (stock number: 007676, termed *Rosa*^{mTmG}) mouse line was employed to mark recombined cells.

For all crosses, litter size was normal, gender distribution of the progeny was balanced, and pups appeared healthy with the expected Mendelian patterns of gene transmission. Littermates were used as controls for analysis. All mice were maintained on a C57BL/6J background; mice derived from other strains or substrains were backcrossed onto

C57BL/6J for at least five generations before proceeding with experimental crosses. Mice derived from other strains were also checked for the SNP at position rs32756904 in exon 14 of *Abcc6* which has previously been shown to confound results when studying PXE in mice[316]. All mice carried the non-disease associated allele in the homozygous state (G/G). Sequencing methods described below.

Mice were housed in a clean, specific pathogen-free facility with ventilated racks supplied with HEPA filtered, tempered, and humidified air and exhausted direct to the outside through the interstitial space above. Mice were given ad libitum access to standard global 19% protein extruded rodent diet (Envigo) unless otherwise indicated; see Drug treatments section below. Cages were supplied with reverse osmosis filtered hyperchlorinated water via an in-cage automatic watering system. Light was controlled by central timer providing 14 hours light/10 hours dark. The welfare of the mice was monitored daily by trained staff. All animal experiments were approved by the Johns Hopkins Animal Care and Use Committee and performed with strict adherence to their guidelines (protocol number MO15M88).

Mutation analysis

For human subjects, genomic DNA was isolated from leukocytes. For mice, genomic DNA was isolated from a piece of tail. All exon and intron-exon boundaries of *ABCC6*, *ENPP1*, or *NT5E* were amplified by polymerase chain reaction (PCR) using genomic DNA as a template. PCR was performed in a final volume of 10 µl containing 50 ng of genomic DNA, 1 µM of forward and reserve primers, and 5 µl of HotStart Master Mix

(Qiagen). The PCR products were purified using ExoSap-IT for 45 minutes at 37 °C and sequenced in both directions using the same primers and the Big Dye terminator kit v3.1 (Applied Biosystems). Reactions were purified over G-50 Sephadex beads (Sigma-Aldrich). Linear amplification products were separated in an automated capillary sequencer (ABI PRISM 3130xl Genetic Analyzer, Applied Biosystems). Sequences were analyzed with Sequencher software 4.8. Primer sequences available upon request.

Mouse genotyping

DNA was extracted from a piece of tail using an NaOH extraction[317]. PCR was performed in a final volume of 20 µl containing 2 µl of genomic DNA, 1 µM of each primer, and 10µl of REDTaq ReadyMix PCR Reaction Mix (Sigma-Aldrich). PCR products were then run on a 1.5% ethidium bromide-containing agarose gel and visualized under UV light. Primer sequences available upon request.

Cell culture

Primary dermal fibroblasts were cultured from a 3 or 4 mm forearm punch-biopsy specimen of skin, obtained from each patient, and grown in Dulbecco's modified Eagle's medium (Gibco) containing 10% fetal bovine serum (Sigma-Aldrich, Lot 15C177), 1 mM L-glutamine (Life Technologies), and 1% penicillin-streptomycin (Gibco), as previously described. Cells were fed twice a week and split 1:2 at confluence.

Osteogenic assay

A modified protocol for in vitro calcification was used for fibroblasts. Cells were grown until confluent and were treated with 0.1 μM dexamethasone (Sigma-Aldrich), 50 μM ascorbic acid-2-phosphate (Sigma-Aldrich), and 10 mM β-glycerophosphate (Sigma-Aldrich) in α-Minimal Essential Medium (Corning; termed αMEM) supplemented with 10% fetal bovine serum (Sigma-Aldrich, Lot 15C177) and 1% penicillin-streptomycin (termed osteogenic media) for 21 days, with replenishment of the medium every four or five days. On day 21, cells were washed with phosphate-buffered saline (Gibco) and fixed in 10% formalin (Fisher Scientific) for 10 minutes. After washing with water, a solution of 2% alizarin red S (Sigma-Aldrich), pH 4.2, was used to stain calcium phosphate crystals. Bright field images of cells were obtained using a Nikon 80i with a color camera and a 10x objective and the NIS Elements software (Nikon). After imaging, to semi-quantify the staining, cells were incubated with 10% warm acetic acid for 30 minutes at room temperature. Cells were then scrapped down and spun at 16,000 g for 15 minutes. Supernatant was quantified at 405 nm on a spectrophotometer.

ENPP1, TNAP, and CD73 enzyme assays

Cells were seeded in 6-well plates and grown until confluent for five days. To measure ENPP1 enzyme activity, cells were lysed in 100 mM Tris-HCl (pH 9.0), 500 mM NaCl, 5 mM $MgCl_2$, and 0.05% Triton X-100 and scraped into microcentrifuge tubes and kept on ice. Cell suspensions were spun at 12,000 g for 5 minutes. A 50 μl aliquot of the supernatant was added to a clear-bottom 96-well plate and the reaction with initiated upon adding 50 μl of 1mM para-nitrophenol-thymidine monophosphate (pNP-TMP; Sigma-Aldrich).

For TNAP enzyme activity assays, cells were first stimulated with osteogenic media for five days. Measurement of TNAP was performed with the use of the StemTAG Alkaline Phosphatase Activity Assay kit (Cell BioLabs). Briefly, cells were washed with phosphate-buffered saline (Gibco) and then lysed and scraped down in Cell Lysis Buffer (Cell BioLabs). Cell suspensions were spun at 12,000 g for 5 minutes. A 50 µl aliquot of supernatant was added to a clear-bottom 96-well plate and the reaction was initiated by adding 50 µl of StemTAG AP Activity Assay Substrate (Cell BioLabs).

Both ENPP1 and TNAP assays relied on the production of p-nitrophenol (pNP) to quantify enzymatic activity, as determined by absorption at 405 nm, and normalized to micrograms of protein (as quantified by a bicinchoninic acid assay; Pierce) over time (measured in minutes).

To measure CD73 enzyme activity, cells were washed with 2 mM magnesium chloride, 120 mM sodium chloride, 5 mM potassium chloride, 10 mM glucose, and 20 mM HEPES. Incubation buffer, consisting of the wash solution supplemented with 2 mM AMP, was added, and cells were incubated at 37 °C for 10 min. An aliquot of the supernatant was removed and inorganic phosphate was measured with the SensoLyte MG Phosphate Assay Kit (AnaSpec) according to the manufacturer's instructions. Inorganic phosphate measurements were normalized to micrograms of protein (as quantified by a bicinchoninic acid assay; Pierce).

Expression studies

RNA was isolated from cultured fibroblasts or solid organs with Trizol (Life Technologies) and the RNeasy kit (Qiagen). Solid organs were first homogenized with the MP shaker. RNA concentration and purity were measured on a Nanodrop ND-1000. First strand cDNA was synthesized using the high capacity RNA-to-cDNA kit (Life Technologies). Quantitative PCR was performed utilizing 1 μg cDNA, TaqMan gene expression master mix reagents, and probes specific for human *ENPP1, NT5E, ALPL,* and *ACTB* and mouse *Abcc6* and *Gapdh* (Life Technologies) on a QuantStudio 7 (Life Technologies) using the $2^{-\Delta\Delta CT}$ method for relative gene expression.

Histology and immunofluorescence

Adult mice were humanely sacrificed via inhalation overdose of 2-Bromo-2-chloro-1,1,1-trifluoroethane (Sigma-Aldrich). Mice underwent immediate laparotomy, inferior vena cava transection, and phosphate-buffered saline was infused through the left ventricle to flush out the blood. Organs of interest were then excised. Organs were fixed in 4% PFA overnight at 4 °C before being subjected to dehydration with sequentially increasing concentrations of sucrose (10%, 20%, and 30% sucrose in phosphate-buffered saline) for 12 hours at 4 °C. Organs were then immersed in optimal cutting temperature compound (VWR Scientific) and slowly frozen over a liquid nitrogen bath. Ten μm sections were cut on a cryostat and placed on SuperFrost slides.

To visualize the location of calcification in the fibrous capsule of the vibrissae, 10 μm muzzle sections were stained with 2% alizarin red S (Sigma-Aldrich). Histological slides

were then dehydrated in acetone and cleared in xylene before mounting with a synthetic mounting medium and imaged on a Nikon 80i with a color camera and a 10x objective with NIS Elements software (Nikon).

Immunofluorescent slides were washed with phosphate-buffered saline before being sealed with Hardset VectaShield containing DAPI (H-1500) and imaged on a Zeiss LSM 780 confocal microscope. To test for tissue and cell specificity of *Cre*-mediated recombination, all *Cre* mouse lines were bred to a *Rosa*^{mTmG} reporter; expression of membrane green florescent protein indicates recombination. Endogenous expression of tdTomato and green florescent protein were imaged. To quantify the extent of mosaic recombination in the liver, the number of green hepatocytes was counted in three separate fields of view across three different *Rosa*^{mTmG};Wnt1-*Cre* adult mice.

Drug treatments

The development and characterization of the uncompetitive TNAP-specific inhibitor compound SBI-425 (PCT WO 2013126608; Preparation of pyridinylsulfonamide derivatives for use as TNAP inhibitors) was published previously[160,318]. SBI-425 only binds to the enzyme in the presence of the substrate to form a three-way complex (inhibitor-enzyme-substrate) that effectively inhibits the enzyme. The inhibition is reversible upon dilution of the complex. Unlike bisphosphonates, SBI-425 does not bind to mineral where it could concentrate and provoke crystal toxicity. For the in vitro experiments, 10 μM SBI-425 (dissolved in 100% DMSO) or DMSO-control was added

to the culture every time the medium was changed during the duration of the 21 day experiment.

Mouse chow was formulated with SBI-425 (30 mg/kg/day) or etidronate (240 mg/kg/day; TCI America), assuming a 20 g mouse who consumes 2 to 5 g of food/day. For SBI-425, the drug was crushed with mortar and pestle and added to powdered feed and vigorously mixed (300 mg of SBI-425 in 1 kg of powdered feed; LabDiet). For etidronate, custom-dyed food pellets were made after incorporation of etidronate into the feed (960 mg of etidronate in 1 kg of feed; LabDiet). Control diet had the same standard base formulation as the drug-supplemented diets (LabDiet 5001).

Micro-CT imaging and analysis

All mice were imaged on a SPECT/CT (Gamma Medica X-SPECT) small animal machine. For the *Abcc6* and *Enpp1* genetic crosses, mice were analyzed at 15 weeks of age; for the *Abcc6* and *Nt5e* genetic crosses, mice were analyzed at 15 weeks and one year. For the $Abcc6^{flox/flox}$ mouse crosses, mice were analyzed at 20 weeks of age and one year. For the treatment trial, mice were scanned at six weeks of age (baseline analysis before initiation of treatment) and at 20 weeks of age (final analysis after 14 weeks on treatment).

Mice were anesthetized with continuous isoflurane during the acquisition of the micro-CT scans. Images were reconstructed and analyzed with ImageJ (NIH). Briefly, a Z-stack was created to encompass the entire region of pathological calcification (rostrally,

from the tip of the nose to caudally, the zygomatic arch). To quantify this calcification, a threshold was manually determined to calculate the total area of ectopic calcification, excluding the radiodense nasal bones and sinuses. For the treatment trial, data are an average of micro-CT analysis by six masked observers.

Mouse plasma PPi assay

Adult mice were humanely sacrificed with inhalation overdose of 2-Bromo-2-chloro-1,1,1-trifluoroethane (Sigma-Aldrich). Mice underwent immediate laparotomy and blood was obtained from the inferior vena cava and collected directly into EDTA-coated microcontainers (BD). Samples were placed on ice and spun at 20,000 g for 5 minutes at 4 °C within 5 minutes after sample collection. Plasma was placed onto a centrifugal filter (Ultrafree-MC UFC30VV00, Millipore) and spun again at 20,000 g for 5 minutes at 4 °C. Filtrate was collected and stored at -80 °C until further processing.

Detection of PPi relied on an enzymatic method to detect an ATP sulfurylase-catalyzed reaction and was modified from a previously published method[252]. Briefly, 10 µl of plasma sample or known PPi standard (ranging from 0.05 µM to 10 µM; Sigma-Aldrich) was added to 40 µl of assay mixture containing 20 µM adenosine 5' phosphosulfate sodium salt (Sigma-Aldrich), 25 µM $MgCl_2$, 12.5 mM HEPES with or without 1 U/ml ATP sulfurylase (New England BioLabs). The mixture was incubated at 37 °C for 30 minutes and heat-inactivated at 90 °C for 10 minutes. After centrifugation at 20,000 g for 5 minutes at 4 °C, 10 µl of supernatant was transferred in duplicate to a 96-well white-bottom plate. One-hundred µl of CellTiter-Glo 2.0 (diluted 1:5, Promega) was added to

every well. Luminescence was measured after a 10-minute room temperature incubation in the dark. To generate a calibration curve, the luminescent signals were calculated by subtracting the blank signals (reaction without ATP sulfurylase) from the assay signals (reaction with ATP sulfurylase); the subtracted values were plotted against the PPi standards by a weighed least-squares linear regression method. Samples with noticeable hemolysis were excluded from analysis because of red blood cell contamination.

Calcium phosphate quantification

Adult mice were humanely sacrificed with inhalation overdose of 2-Bromo-2-chloro-1,1,1-trifluoroethane (Sigma-Aldrich). Mice underwent immediate laparotomy, inferior vena cava transection, and phosphate-buffered saline was infused through the left ventricle to flush out the blood. The muzzle was dissected from the underlying nasal bones and bisected. Half of the muzzle was fixed in 10% formalin (Fisher Scientific) and frozen at -80 °C. The muzzle was then freeze-dried with a lyophilizer and weighed. The tissue was physically macerated before homogenizing with a bead homogenizer (MP) for 15 minutes at 4 °C. Tissue was then soaked overnight in 10% formic acid (Sigma-Aldrich). Samples were spun at 16,000 g for 5 minutes before 10 µl of the supernatant was used in a Calcium Quantification Assay (BioVision), as per manufacturer's instructions. Absorbance readings at 575 nm were normalized to tissue weight in grams.

Mouse plasma alkaline phosphatase analysis

At the conclusion of the treatment trial, mice were euthanized with inhalation overdose of 2-Bromo-2-chloro-1,1,1-trifluoroethane before collecting blood by cardiac puncture with

a 21 gauge needle. Blood was collected in lithium-heparin-coated microcontainers (BD) for alkaline phosphatase analysis. Blood was spun at 150 g for 15 minutes at 4 °C and supernatant was collected and stored at -80 °C until assays were performed. Residual alkaline phosphatase levels were assayed as previously described[319]. Briefly, plasma samples were thawed on ice and spun at 2,400 g for 10 minutes. The plasma samples were mixed with substrates in buffer in 3:1 volume ratio to initiate the reaction in a 1536-well clear-bottom assay plate, with 1 mM $MgCl_2$, 50 μM $ZnCl_2$, 1 mM pNPP, and 100 mM diethanolamine buffer at pH 9.8. Ten μM of SBI-425 was spiked in control treatment plasma samples to determine non-TNAP phosphatase activity levels. Samples were read kinetically for an hour on the PHERAstar FS plate reader at 380 nm, to detect amount of pNP produced.

Bone microarchitecture and integrity studies

At the same time of sacrifice, the femur and tibia were dissected out en bloc and muscles and tendons were carefully removed. The bones were fixed in 4% PFA or stored at -20 °C until ex vivo analyses were performed. High resolution images of the mouse femur were acquired using a desktop micro-tomographic imaging system (Skyscan 1172, Bruker) in accordance with the recommendations of the American Society for Bone and Mineral Research (ASBMR)[320]. Bones were scanned at 65 keV and 200 mA using a 0.5 mm aluminum filter with an isotropic voxel size of 10 μm. In the femur, trabecular bone parameters were assessed in the 500 μm proximal to the growth plate and extending for 2 mm (200 CT slices). Cortical bone structure was assessed 5 mm proximal to the growth plate and extending for 500 μm. Following this, fixed bones were embedded in resin and

cut with on a macrotome; slides were stained with trichrome solutions. Images of slides were captured on a Nikon 80i with a color camera and a 40x objection using NIS Elements software (Nikon). Frozen femora were subjected to three point bending on a Bose Electroforce 3100. Force-displacement data were analyzed using a custom MATLAB script.

Statistical analysis

All statistical analyses and graphs were generated in R Studio. One-way, two-way, or three-way analyses of variance with a Tukey's honest significance difference post-hoc analysis were used to assess for major effects and determine if there were differences between multiple groups. A one-tailed Student's t-test was used to analyze between two groups. All significant pairwise comparisons are shown and *P*-values indicated in the figures. No outliers were excluded. An alpha ≤ 0.05 was considered statistically significant. Data obtained from the intercrossing of *Enpp1-, Nt5e-,* and *Abcc6*-deficient mice were log-transformed before analysis to normalize the data. For all graphs, the lower and upper margins of each box define the 25^{th} and 75^{th} centiles, respectively; the internal line defines the median, and the whiskers define the range. Values outside 1.5 times the interquartile distance are shown as open circles whereas values outside 2 times the interquartile distance are shown as filled circles. Number of biological replicates in each group is specified.

REFERENCES

1. Durante, G. Athérome congénital de l'aorte et de l'artère pulmonaire. *Bull Soc Anat Paris* **74,** 97–101 (1899).
2. Bryant, J. H. & Hale-White, W. A case of calcification of the arteries and obliterative endarteritis, associated with hydronephrosis, in a child aged six months. *Guys Hosp. Rep.* **55,** 17–28 (1901).
3. Ferreira, C., Ziegler, S. & Gahl, W. in *GeneReviews(®)* (eds. Pagon, R. A. et al.) (University of Washington, Seattle, 2014).
4. Rutsch, F. *et al.* Mutations in ENPP1 are associated with 'idiopathic' infantile arterial calcification. *Nat. Genet.* **34,** 379–381 (2003).
5. Chong, C. R. & Hutchins, G. M. Idiopathic infantile arterial calcification: the spectrum of clinical presentations. *Pediatr. Dev. Pathol. Off. J. Soc. Pediatr. Pathol. Paediatr. Pathol. Soc.* **11,** 405–415 (2008).
6. Rutsch, F. *et al.* Hypophosphatemia, hyperphosphaturia, and bisphosphonate treatment are associated with survival beyond infancy in generalized arterial calcification of infancy. *Circ. Cardiovasc. Genet.* **1,** 133–140 (2008).
7. Vera, J., Lucaya, J., Garcia Conesa, J. A., Aso, C. & Balaguer, A. Idiopathic infantile arterial calcification: unusual features. *Pediatr. Radiol.* **20,** 585–587 (1990).
8. Nitschke, Y. *et al.* Generalized arterial calcification of infancy and pseudoxanthoma elasticum can be caused by mutations in either ENPP1 or ABCC6. *Am. J. Hum. Genet.* **90,** 25–39 (2012).

9. Brachet, C., Mansbach, A. L., Clerckx, A., Deltenre, P. & Heinrichs, C. Hearing loss is part of the clinical picture of ENPP1 loss of function mutation. *Horm. Res. Pædiatrics* **81,** 63–66 (2014).

10. Moran, J. J. Idiopathic arterial calcification of infancy: a clinicopathologic study. *Pathol. Annu.* **10,** 393–417 (1975).

11. Thomas, P. *et al.* Idiopathic arterial calcification of infancy: a case with prolonged survival. *Pediatr. Nephrol. Berl. Ger.* **4,** 233–235 (1990).

12. Hault, K., Sebire, N. J., Ho, S. Y. & Sheppard, M. N. The difficulty in diagnosing idiopathic arterial calcification of infancy, its variation in presentation, and the importance of autopsy. *Cardiol. Young* **18,** 624–627 (2008).

13. Freychet, C. *et al.* [GACI syndrome: a case report with a neonatal beginning]. *Arch. Pédiatrie Organe Off. Sociéte Fr. Pédiatrie* **21,** 632–636 (2014).

14. Sakata, S., Su, J. C., Robertson, S., Yin, M. & Chow, C. Varied presentations of pseudoxanthoma elasticum in a family. *J. Paediatr. Child Health* **42,** 817–820 (2006).

15. Le Boulanger, G. *et al.* An unusual severe vascular case of pseudoxanthoma elasticum presenting as generalized arterial calcification of infancy. *Am. J. Med. Genet. A.* **152A,** 118–123 (2010).

16. Li, Q., Schumacher, W., Jablonski, D., Siegel, D. & Uitto, J. Cutaneous features of pseudoxanthoma elasticum in a patient with generalized arterial calcification of infancy due to a homozygous missense mutation in the ENPP1 gene. *Br. J. Dermatol.* **166,** 1107–1111 (2012).

17. Lomashvili, K. A., Monier-Faugere, M.-C., Wang, X., Malluche, H. H. & O'Neill, W. C. Effect of bisphosphonates on vascular calcification and bone metabolism in experimental renal failure. *Kidney Int.* **75,** 617–625 (2009).

18. Otero, J. E. *et al.* Severe skeletal toxicity from protracted etidronate therapy for generalized arterial calcification of infancy. *J. Bone Miner. Res. Off. J. Am. Soc. Bone Miner. Res.* **28,** 419–430 (2013).

19. Ferreira, C. R. *et al.* Treatment of hypophosphatemic rickets in generalized arterial calcification of infancy (GACI) without worsening of vascular calcification. *Am. J. Med. Genet. A.* **170,** 1308–1311 (2016).

20. St Hilaire, C. *et al.* NT5E mutations and arterial calcifications. *N. Engl. J. Med.* **364,** 432–442 (2011).

21. Ichikawa, N. *et al.* Arterial Calcification Due to Deficiency of CD73 (ACDC) As One of Rheumatic Diseases Associated With Periarticular Calcification. *J. Clin. Rheumatol. Pract. Rep. Rheum. Musculoskelet. Dis.* **21,** 216–220 (2015).

22. Zhang, Z., He, J.-W., Fu, W.-Z., Zhang, C.-Q. & Zhang, Z.-L. Calcification of joints and arteries: second report with novel NT5E mutations and expansion of the phenotype. *J. Hum. Genet.* **60,** 561–564 (2015).

23. de Nijs, T. *et al.* Isolated arterial calcifications of the lower extremities: A clue for NT5E mutation. *Int. J. Cardiol.* **212,** 248–250 (2016).

24. Markello, T. C. *et al.* Vascular pathology of medial arterial calcifications in NT5E deficiency: implications for the role of adenosine in pseudoxanthoma elasticum. *Mol. Genet. Metab.* **103,** 44–50 (2011).

25. Fausther, M., Lavoie, E. G., Goree, J. R., Baldini, G. & Dranoff, J. A. NT5E mutations that cause human disease are associated with intracellular mistrafficking of NT5E protein. *PloS One* **9,** e98568 (2014).

26. Rigal, D. Observation pour servir a l'histoire de la cheloide diffuse xanthelasmique. *Ann. Dermatol. Syphilgraphie* **2,** 491–501 (1881).

27. Darier, J. Pseudoxanthoma elasticum. *Monatshefte Für Prakt. Dermatol.* **23,** 609–617 (1896).

28. Grönblad, E. Angioid streaks—pseudoxanthoma elasticum. *Acta Ophthalmol. (Copenh.)* **7,** 329–329 (1929).

29. Strandberg, J. Pseudoxanthoma elasticum. *Z. Für Haut- Geschlechtskrankh.* **31,** 689 (1929).

30. Chassaing, N., Martin, L., Calvas, P., Le Bert, M. & Hovnanian, A. Pseudoxanthoma elasticum: a clinical, pathophysiological and genetic update including 11 novel ABCC6 mutations. *J. Med. Genet.* **42,** 881–892 (2005).

31. Trip, M. D. *et al.* Frequent mutation in the ABCC6 gene (R1141X) is associated with a strong increase in the prevalence of coronary artery disease. *Circulation* **106,** 773–775 (2002).

32. Le Saux, O. *et al.* Evidence for a founder effect for pseudoxanthoma elasticum in the Afrikaner population of South Africa. *Hum. Genet.* **111,** 331–338 (2002).

33. Neldner, K. H. Pseudoxanthoma elasticum. *Clin. Dermatol.* **6,** 1–159 (1988).

34. Goodman, R. M. *et al.* Pseudoxanthoma elasticum: A clinical and histopathological study. *Medicine (Baltimore)* **42,** 297–334 (1963).

35. Bercovitch, R. S. *et al.* Testicular microlithiasis in association with pseudoxanthoma elasticum. *Radiology* **237,** 550–554 (2005).

36. Goede, J., Hack, W. W. M., Sijstermans, K. & Pierik, F. H. Testicular microlithiasis in a 2-year-old boy with pseudoxanthoma elasticum. *J. Ultrasound Med. Off. J. Am. Inst. Ultrasound Med.* **27,** 1503–1505 (2008).

37. Tanioka, M. *et al.* Calcification of the placenta in a woman with pseudoxanthoma elasticum with a mutation of the ABCC6 gene. *J. Dermatol.* **41,** 189–191 (2014).

38. Terry, S. F. & Bercovitch, L. in *GeneReviews(®)* (eds. Pagon, R. A. et al.) (University of Washington, Seattle, 2012).

39. Hosen, M. J., Lamoen, A., De Paepe, A. & Vanakker, O. M. Histopathology of pseudoxanthoma elasticum and related disorders: histological hallmarks and diagnostic clues. *Scientifica* **2012,** 598262 (2012).

40. Nagpal, K. C., Asdourian, G., Goldbaum, M., Apple, D. & Goldberg, M. F. Angioid streaks and sickle haemoglobinopathies. *Br. J. Ophthalmol.* **60,** 31–34 (1976).

41. Condon, P. I. & Serjeant, G. R. Ocular findings of elderly cases of homozygous sickle-cell disease in Jamaica. *Br. J. Ophthalmol.* **60,** 361–364 (1976).

42. Aessopos, A. *et al.* Angioid streaks in homozygous beta thalassemia. *Am. J. Ophthalmol.* **108,** 356–359 (1989).

43. Aessopos, A. *et al.* Angioid streaks in sickle-thalassemia. *Am. J. Ophthalmol.* **117,** 589–592 (1994).

44. Aessopos, A. *et al.* Arterial calcifications in beta-thalassemia. *Angiology* **49,** 137–143 (1998).

45. Baccarani-Contri, M. *et al.* Characterization of pseudoxanthoma elasticum-like lesions in the skin of patients with beta-thalassemia. *J. Am. Acad. Dermatol.* **44,** 33–39 (2001).

46. Christensen, O. B. An exogenous variety of pseudoxanthoma elasticum in old farmers. *Acta Derm. Venereol.* **58,** 319–321 (1978).

47. Nielsen, A. O., Christensen, O. B., Hentzer, B., Johnson, E. & Kobayasi, T. Salpeter-induced dermal changes electron-microscopically indistinguishable from pseudoxanthoma elasticum. *Acta Derm. Venereol.* **58,** 323–327 (1978).

48. Burge, S. & Ryan, T. Penicillamine-induced pseudo-pseudoxanthoma elasticum in a patient with rheumatoid arthritis. *Clin. Exp. Dermatol.* **13,** 255–258 (1988).

49. Bolognia, J. L. & Braverman, I. Pseudoxanthoma-elasticum-like skin changes induced by penicillamine. *Dermatol. Basel Switz.* **184,** 12–18 (1992).

50. Coatesworth, A. P., Darnton, S. J., Green, R. M., Cayton, R. M. & Antonakopoulos, G. N. A case of systemic pseudo-pseudoxanthoma elasticum with diverse symptomatology caused by long-term penicillamine use. *J. Clin. Pathol.* **51,** 169–171 (1998).

51. Rayatt, S., Pandey, U. & Khanna, A. Familial pseudo pseudoxanthoma elasticum. *J. Plast. Reconstr. Aesthetic Surg. JPRAS* **59,** 1127–1129 (2006).

52. Bercovitch, L. *et al.* Acquired pseudoxanthoma elasticum presenting after liver transplantation. *J. Am. Acad. Dermatol.* **64,** 873–878 (2011).

53. Mitsudo, S. M. Chronic idiopathic hyperphosphatasia associated with pseudoxanthoma elasticum. *J. Bone Joint Surg. Am.* **53,** 303–314 (1971).

54. Fretzin, D. F. Pseudoxanthoma elasticum in hyperphosphatasia. *Arch. Dermatol.* **111,** 271–272 (1975).

55. Eng, A. M. & Bryant, J. Clinical pathologic observations in pseudoxanthoma elasticum. *Int. J. Dermatol.* **14,** 586–605 (1975).

56. Saxe, N. & Beighton, P. Cutaneous manifestations of osteoectasia. *Clin. Exp. Dermatol.* **7,** 605–609 (1982).

57. Sharif, K. W., Doig, W. M. & Kinsella, F. P. Visual impairment in a case of juvenile Paget's disease with pseudoxanthoma elasticum: an eleven year follow up. *J. Pediatr. Ophthalmol. Strabismus* **26,** 299–302 (1989).

58. Whyte, M. P. *et al.* Juvenile Paget's disease: the second reported, oldest patient is homozygous for the TNFRSF11B 'Balkan' mutation (966_969delTGACinsCTT), which elevates circulating immunoreactive osteoprotegerin levels. *J. Bone Miner. Res. Off. J. Am. Soc. Bone Miner. Res.* **22,** 938–946 (2007).

59. Kerr, N. M. *et al.* Ocular manifestations of juvenile Paget disease. *Arch. Ophthalmol. Chic. Ill 1960* **128,** 698–703 (2010).

60. Mallette, L. E. & Mechanick, J. I. Heritable syndrome of pseudoxanthoma elasticum with abnormal phosphorus and vitamin D metabolism. *Am. J. Med.* **83,** 1157–1162 (1987).

61. Jin, L. *et al.* Genetic Heterogeneity of Pseudoxanthoma Elasticum: The Chinese Signature Profile of ABCC6 and ENPP1 Mutations. *J. Invest. Dermatol.* **135,** 2338 (2015).

62. Pfendner, E. G. *et al.* Mutation detection in the ABCC6 gene and genotype-phenotype analysis in a large international case series affected by pseudoxanthoma elasticum. *J. Med. Genet.* **44,** 621–628 (2007).

63. Ringpfeil, F. *et al.* Pseudoxanthoma elasticum is a recessive disease characterized by compound heterozygosity. *J. Invest. Dermatol.* **126,** 782–786 (2006).

64. Bergen, A. A. B. Pseudoxanthoma elasticum: the end of the autosomal dominant segregation myth. *J. Invest. Dermatol.* **126,** 704–705 (2006).

65. Schön, S. *et al.* Polymorphisms in the xylosyltransferase genes cause higher serum XT-I activity in patients with pseudoxanthoma elasticum (PXE) and are involved in a severe disease course. *J. Med. Genet.* **43,** 745–749 (2006).

66. Vanakker, O. M. *et al.* Pseudoxanthoma elasticum-like phenotype with cutis laxa and multiple coagulation factor deficiency represents a separate genetic entity. *J. Invest. Dermatol.* **127,** 581–587 (2007).

67. Marconi, B. *et al.* Pseudoxanthoma elasticum and skin: Clinical manifestations, histopathology, pathomechanism, perspectives of treatment. *Intractable Rare Dis. Res.* **4,** 113–122 (2015).

68. Zitnan, D. & Sitaj, S. Calcification multiple du cartilage articulaire (étude clinique et radiologique). *IX E Congrès Int. Mal. Rhum. II* **291,** (1957).

69. Andrew, L. J. *et al.* Refinement of the chromosome 5p locus for familial calcium pyrophosphate dihydrate deposition disease. *Am. J. Hum. Genet.* **64,** 136–145 (1999).

70. Hughes, A. E., McGibbon, D., Woodward, E., Dixey, J. & Doherty, M. Localisation of a gene for chondrocalcinosis to chromosome 5p. *Hum. Mol. Genet.* **4,** 1225–1228 (1995).

71. Hirsch, J. H., Killien, F. C. & Troupin, R. H. The arthropathy of hemochromatosis. *Radiology* **118,** 591–596 (1976).

72. Punzi, L. *et al.* Chondrocalcinosis is a feature of Gitelman's variant of Bartter's syndrome. A new look at the hypomagnesemia associated with calcium pyrophosphate dihydrate crystal deposition disease. *Rev. Rhum. Engl. Ed* **65,** 571–574 (1998).

73. O'Duffy, J. D. Hypophosphatasia associated with calcium pyrophosphate dihydrate deposits in cartilage. Report of a case. *Arthritis Rheum.* **13,** 381–388 (1970).

74. Eade, A. W., Swannell, A. J. & Williamson, N. Pyrophosphate arthropathy in hypophosphatasia. *Ann. Rheum. Dis.* **40,** 164–170 (1981).

75. Chuck, A. J., Pattrick, M. G., Hamilton, E., Wilson, R. & Doherty, M. Crystal deposition in hypophosphatasia: a reappraisal. *Ann. Rheum. Dis.* **48,** 571–576 (1989).

76. McClure, J. & Smith, P. S. Calcium pyrophosphate dihydrate deposition in the intervertebral discs in a case of Wilson's disease. *J. Clin. Pathol.* **36,** 764–768 (1983).

77. Reginato, A. J., Ralph Schumacher, H. & Martinez, V. A. Ochronotic arthropathy with calcium pyrophosphate crystal deposition a light and electron microscopic study. *Arthritis Rheum.* **16,** 705–714 (1973).

78. Rynes, R. I., Sosman, J. L. & Holdsworth, D. E. Pseudogout in ochronosis. Report of a case. *Arthritis Rheum.* **18,** 21–25 (1975).

79. McClure, J., Smith, P. S. & Gramp, A. A. Calcium pyrophosphate dihydrate (CPPD) deposition in ochronotic arthropathy. *J. Clin. Pathol.* **36,** 894–902 (1983).

80. Pendleton, A. *et al.* Mutations in ANKH cause chondrocalcinosis. *Am. J. Hum. Genet.* **71,** 933–940 (2002).

81. Reichenberger, E. *et al.* Autosomal dominant craniometaphyseal dysplasia is caused by mutations in the transmembrane protein ANK. *Am. J. Hum. Genet.* **68,** 1321–1326 (2001).

82. Gurley, K. A., Reimer, R. J. & Kingsley, D. M. Biochemical and genetic analysis of ANK in arthritis and bone disease. *Am. J. Hum. Genet.* **79,** 1017–1029 (2006).

83. Zajac, A. *et al.* Novel ANKH mutation in a patient with sporadic craniometaphyseal dysplasia. *Am. J. Med. Genet. A.* **152A,** 770–776 (2010).

84. Baynam, G., Goldblatt, J. & Schofield, L. Craniometaphyseal dysplasia and chondrocalcinosis cosegregating in a family with an ANKH mutation. *Am. J. Med. Genet. A.* **149A,** 1331–1333 (2009).

85. Morava, E. *et al.* Autosomal recessive mental retardation, deafness, ankylosis, and mild hypophosphatemia associated with a novel ANKH mutation in a consanguineous family. *J. Clin. Endocrinol. Metab.* **96,** E189-198 (2011).

86. Giard, A. Sur la calcification hibernale. *CR Soc Biol* **10,** 1013–1015 (1898).

87. Duret, M. Tumeurs multiples et singulières des bourses séreuses endotheliomas peut être d'origine parasitaire. *Bull Soe Anat Paris* **74,** 725–731 (1899).

88. Teutschlaender. Über Progressive Lipogranulomatose der Muskulatur. *Klin. Wochenschr.* **14,** 451–453 (1935).

89. Inclan, A., Leon, P. & Camejo, M. Tumoral calcinosis. *J. Am. Med. Assoc.* **121,** 490–495 (1943).

90. Frishberg, Y. *et al.* Identification of a recurrent mutation in GALNT3 demonstrates that hyperostosis-hyperphosphatemia syndrome and familial tumoral calcinosis are allelic disorders. *J. Mol. Med. Berl. Ger.* **83,** 33–38 (2005).

91. Joseph, L. *et al.* Familial tumoral calcinosis and hyperostosis-hyperphosphataemia syndrome are different manifestations of the same disease: novel missense mutations in GALNT3. *Skeletal Radiol.* **39,** 63–68 (2010).

92. Rafaelsen, S., Johansson, S., Ræder, H. & Bjerknes, R. Long-term clinical outcome and phenotypic variability in hyperphosphatemic familial tumoral calcinosis and hyperphosphatemic hyperostosis syndrome caused by a novel GALNT3 mutation; case report and review of the literature. *BMC Genet.* **15,** 98 (2014).

93. Foster, B. L. *et al.* Rare bone diseases and their dental, oral, and craniofacial manifestations. *J. Dent. Res.* **93,** 7S–19S (2014).

94. Pomerleau, D. *et al.* Angioid streaks and optic nerve head drusen in hyperphosphatemic familial tumoral calcinosis. *Retin. Cases Brief Rep.* **3,** 54–56 (2009).

95. McGrath, E., Harney, F. & Kinsella, F. An ocular presentation of familial tumoral calcinosis. *BMJ Case Rep.* **2010,** (2010).

96. Campagnoli, M. F. *et al.* Familial tumoral calcinosis and testicular microlithiasis associated with a new mutation of GALNT3 in a white family. *J. Clin. Pathol.* **59,** 440–442 (2006).

97. Ramnitz, M. S. *et al.* Phenotypic and Genotypic Characterization and Treatment of a Cohort with Familial Tumoral Calcinosis/Hyperostosis-Hyperphosphatemia Syndrome. *J. Bone Miner. Res. Off. J. Am. Soc. Bone Miner. Res.* (2016). doi:10.1002/jbmr.2870

98. Topaz, O. *et al.* A deleterious mutation in SAMD9 causes normophosphatemic familial tumoral calcinosis. *Am. J. Hum. Genet.* **79,** 759–764 (2006).

99. Narumi, S. *et al.* SAMD9 mutations cause a novel multisystem disorder, MIRAGE syndrome, and are associated with loss of chromosome 7. *Nat. Genet.* (2016). doi:10.1038/ng.3569

100. Farrow, E. G., Imel, E. A. & White, K. E. Miscellaneous non-inflammatory musculoskeletal conditions. Hyperphosphatemic familial tumoral calcinosis (FGF23, GALNT3 and αKlotho). *Best Pract. Res. Clin. Rheumatol.* **25,** 735–747 (2011).

101. Delacour, A. Ossification des capillaires du cerveau. *Ann Med Psychol* **2,** 458–61 (1850).

102. Klein, C. & Vieregge, P. The confusion history of 'Fahr's disease'. *Neurology* **50,** A59 (1998).

103. Manyam, B. V. What is and what is not 'Fahr's disease'. *Parkinsonism Relat. Disord.* **11,** 73–80 (2005).

104. Manyam, B. V., Walters, A. S. & Narla, K. R. Bilateral striopallidodentate calcinosis: clinical characteristics of patients seen in a registry. *Mov. Disord. Off. J. Mov. Disord. Soc.* **16,** 258–264 (2001).

105. Nicolas, G. *et al.* Phenotypic spectrum of probable and genetically-confirmed idiopathic basal ganglia calcification. *Brain J. Neurol.* **136,** 3395–3407 (2013).

106. Nicolas, G. *et al.* Brain calcification process and phenotypes according to age and sex: Lessons from SLC20A2, PDGFB, and PDGFRB mutation carriers. *Am. J. Med. Genet. Part B Neuropsychiatr. Genet. Off. Publ. Int. Soc. Psychiatr. Genet.* **168,** 586–594 (2015).

107. Takashima, S. & Becker, L. E. Basal ganglia calcification in Down's syndrome. *J. Neurol. Neurosurg. Psychiatry* **48,** 61–64 (1985).

108. Koob, M. *et al.* Neuroimaging in Cockayne syndrome. *AJNR Am. J. Neuroradiol.* **31,** 1623–1630 (2010).

109. Finsterer, J. & Kopsa, W. Basal Ganglia calcification in mitochondrial disorders. *Metab. Brain Dis.* **20,** 219–226 (2005).

110. Schmidt, H., Ullrich, K., Korinthenberg, R. & Peters, P. E. Basal ganglion calcification in hyperphenylalaninemia due to deficiency of dihydropteridine reductase. *Pediatr. Radiol.* **19,** 54–56 (1988).

111. Saillour, Y. *et al.* Mutations in the AP1S2 gene encoding the sigma 2 subunit of the adaptor protein 1 complex are associated with syndromic X-linked mental retardation with hydrocephalus and calcifications in basal ganglia. *J. Med. Genet.* **44,** 739–744 (2007).

112. Briggs, T. A. *et al.* Cerebroretinal microangiopathy with calcifications and cysts (CRMCC). *Am. J. Med. Genet. A.* **146A,** 182–190 (2008).

113. Al Mane, K. A., Coates, R. K. & McDonald, P. Intracranial calcification in Raine syndrome. *Pediatr. Radiol.* **26,** 55–58 (1996).

114. Uggetti, C. *et al.* Aicardi-Goutieres syndrome: neuroradiologic findings and follow-up. *AJNR Am. J. Neuroradiol.* **30,** 1971–1976 (2009).

115. Manabe, Y., Araki, M., Takeda, K., Yokota, S. & Kimura, T. Pseudohypoparathyroidism with striopallidodentate calcification--a case report and review of the literature. *Jpn. J. Med.* **28,** 391–395 (1989).

116. Livingston, J. H. *et al.* Intracranial calcification in early infantile Krabbe disease: nothing new under the sun. *Dev. Med. Child Neurol.* **54,** 376–379 (2012).

117. Bosley, T. M. *et al.* The neurology of carbonic anhydrase type II deficiency syndrome. *Brain J. Neurol.* **134,** 3502–3515 (2011).

118. Zhang, X. *et al.* Human intracellular ISG15 prevents interferon-α/β over-amplification and auto-inflammation. *Nature* **517,** 89–93 (2015).

119. Wang, H., Das, L., Tan Hung Tiong, J., Vasanwala, R. F. & Arkachaisri, T. CANDLE syndrome: an extended clinical spectrum. *Rheumatol. Oxf. Engl.* **53,** 2119–2120 (2014).

120. Isojima, T. *et al.* A recurrent de novo FAM111A mutation causes kenny–caffey syndrome type 2. *J. Bone Miner. Res.* **29,** 992–998 (2014).

121. Mankad, K. & Davagnanam, I. Teaching NeuroImages: Nasu Hakola syndrome. *Neurology* **74,** e102 (2010).

122. Gonçalves, F. G., de Melo, M. B., de L Matos, V., Barra, F. R. & Figueroa, R. E. Amygdalae and striatum calcification in lipoid proteinosis. *AJNR Am. J. Neuroradiol.* **31,** 88–90 (2010).

123. Hsu, S. C. *et al.* Mutations in SLC20A2 are a major cause of familial idiopathic basal ganglia calcification. *Neurogenetics* **14,** 11–22 (2013).

124. Yamada, M. *et al.* Evaluation of SLC20A2 mutations that cause idiopathic basal ganglia calcification in Japan. *Neurology* **82,** 705–712 (2014).

125. Nicolas, G. *et al.* Overall mutational spectrum of SLC20A2, PDGFB and PDGFRB in idiopathic basal ganglia calcification. *neurogenetics* **15,** 215–216 (2014).

126. Anheim, M. *et al.* XPR1 mutations are a rare cause of primary familial brain calcification. *J. Neurol.* (2016). doi:10.1007/s00415-016-8166-4

127. Loeb, J. A. Functional improvement in a patient with cerebral calcinosis using a bisphosphonate. *Mov. Disord. Off. J. Mov. Disord. Soc.* **13,** 345–349 (1998).

128. Oliveira, J. R. M. & Oliveira, M. F. Primary brain calcification in patients undergoing treatment with the biphosphanate alendronate. *Sci. Rep.* **6,** 22961 (2016).

129. Keutel, J., Jorgensen, G. & Gabriel, P. A new autosomal recessive syndrome: peripheral pulmonary stenoses, brachytelephalangism, neural hearing loss and abnormal cartilage calcifications-ossification. *Birth Defects* **8,** 60–68 (1972).

130. Sun, L. *et al.* [Keutel syndrome with tracheal stenosis as the major symptom: case report and literature review]. *Zhonghua Er Ke Za Zhi Chin. J. Pediatr.* **51,** 527–530 (2013).

131. Demirel, G. *et al.* A case of Keutel syndrome diagnosed in the neonatal period: associated with Binder phenotype. *Genet. Couns. Geneva Switz.* **23,** 25–30 (2012).

132. Miller, S. F. Brachytelephalangy with sparing of the fifth distal phalanx: a feature highly suggestive of Keutel syndrome. *Pediatr. Radiol.* **33,** 186–189 (2003).

133. Meier, M., Weng, L. P., Alexandrakis, E., Rüschoff, J. & Goeckenjan, G. Tracheobronchial stenosis in Keutel syndrome. *Eur. Respir. J.* **17,** 566–569 (2001).

134. Khosroshahi, H. E., Sahin, S. C., Akyuz, Y. & Ede, H. Long term follow-up of four patients with Keutel syndrome. *Am. J. Med. Genet. A.* **164A,** 2849–2856 (2014).

135. Weaver, K. N. *et al.* Keutel syndrome: report of two novel MGP mutations and discussion of clinical overlap with arylsulfatase E deficiency and relapsing polychondritis. *Am. J. Med. Genet. A.* **164A,** 1062–1068 (2014).

136. Pauli, R. M., Lian, J. B., Mosher, D. F. & Suttie, J. W. Association of congenital deficiency of multiple vitamin K-dependent coagulation factors and the phenotype of the warfarin embryopathy: clues to the mechanism of teratogenicity of coumarin derivatives. *Am. J. Hum. Genet.* **41,** 566–583 (1987).

137. Cordeddu, V. *et al.* Mutations in ZBTB20 cause Primrose syndrome. *Nat. Genet.* **46,** 815–817 (2014).

138. Gottesman, G. S. *et al.* Auricular ossification: A newly recognized feature of osteoprotegerin-deficiency juvenile Paget disease. *Am. J. Med. Genet. A.* **170,** 978–985 (2016).

139. Munroe, P. B. *et al.* Mutations in the gene encoding the human matrix Gla protein cause Keutel syndrome. *Nat. Genet.* **21,** 142–144 (1999).

140. Cranenburg, E. C. M. *et al.* Circulating matrix γ-carboxyglutamate protein (MGP) species are refractory to vitamin K treatment in a new case of Keutel syndrome. *J. Thromb. Haemost. JTH* **9,** 1225–1235 (2011).

141. Feigenbaum, A. *et al.* Singleton-Merten syndrome: an autosomal dominant disorder with variable expression. *Am. J. Med. Genet. A.* **161A,** 360–370 (2013).

142. Rutsch, F. *et al.* A specific IFIH1 gain-of-function mutation causes Singleton-Merten syndrome. *Am. J. Hum. Genet.* **96,** 275–282 (2015).

143. Jang, M.-A. *et al.* Mutations in DDX58, which encodes RIG-I, cause atypical Singleton-Merten syndrome. *Am. J. Hum. Genet.* **96,** 266–274 (2015).

144. Mackenzie, N. C. W. *et al.* Altered bone development and an increase in FGF-23 expression in Enpp1(-/-) mice. *PloS One* **7,** e32177 (2012).

145. Klement, J. F. *et al.* Targeted ablation of the abcc6 gene results in ectopic mineralization of connective tissues. *Mol. Cell. Biol.* **25,** 8299–8310 (2005).

146. Jiang, Q. & Uitto, J. Restricting dietary magnesium accelerates ectopic connective tissue mineralization in a mouse model of pseudoxanthoma elasticum (Abcc6(-/-)). *Exp. Dermatol.* **21,** 694–699 (2012).

147. Li, Q. *et al.* Warfarin accelerates ectopic mineralization in Abcc6(-/-) mice: clinical relevance to pseudoxanthoma elasticum. *Am. J. Pathol.* **182,** 1139–1150 (2013).

148. Li, Q. *et al.* Mutant Enpp1asj mice as a model for generalized arterial calcification of infancy. *Dis. Model. Mech.* **6,** 1227–1235 (2013).

149. Li, Q., Price, T. P., Sundberg, J. P. & Uitto, J. Juxta-articular joint-capsule mineralization in CD73 deficient mice: similarities to patients with NT5E mutations. *Cell Cycle Georget. Tex* **13,** 2609–2615 (2014).

150. Gorgels, T. G. M. F. *et al.* Dietary magnesium, not calcium, prevents vascular calcification in a mouse model for pseudoxanthoma elasticum. *J. Mol. Med. Berl. Ger.* **88,** 467–475 (2010).

151. LaRusso, J., Li, Q., Jiang, Q. & Uitto, J. Elevated dietary magnesium prevents connective tissue mineralization in a mouse model of pseudoxanthoma elasticum (Abcc6(-/-)). *J. Invest. Dermatol.* **129,** 1388–1394 (2009).

152. Li, Q., Larusso, J., Grand-Pierre, A. E. & Uitto, J. Magnesium carbonate-containing phosphate binder prevents connective tissue mineralization in Abcc6(-/-) mice-potential for treatment of pseudoxanthoma elasticum. *Clin. Transl. Sci.* **2,** 398–404 (2009).

153. Blumenthal, N. C. Mechanisms of inhibition of calcification. *Clin. Orthop.* 279–289 (1989).

154. Gorgels, T. G. M. F. *et al.* Disruption of Abcc6 in the mouse: novel insight in the pathogenesis of pseudoxanthoma elasticum. *Hum. Mol. Genet.* **14,** 1763–1773 (2005).

155. Drake, M. T., Clarke, B. L. & Khosla, S. Bisphosphonates: mechanism of action and role in clinical practice. *Mayo Clin. Proc.* **83,** 1032–1045 (2008).

156. Huesa, C., Staines, K. A., Millán, J. L. & MacRae, V. E. Effects of etidronate on the Enpp1$^{-/-}$ mouse model of generalized arterial calcification of infancy. *Int. J. Mol. Med.* **36,** 159–165 (2015).

157. Li, Q., Sundberg, J. P., Levine, M. A., Terry, S. F. & Uitto, J. The effects of bisphosphonates on ectopic soft tissue mineralization caused by mutations in the ABCC6 gene. *Cell Cycle Georget. Tex* **14,** 1082–1089 (2015).

158. Albright, R. A. *et al.* ENPP1-Fc prevents mortality and vascular calcifications in rodent model of generalized arterial calcification of infancy. *Nat. Commun.* **6,** 10006 (2015).

159. Ziegler, S. G. *et al.* Toward identification of the pathogenic cell type driving calcification in pseudoxanthoma elasticum (Abstract 2266). in (2015).

160. Sheen, C. R. *et al.* Pathophysiological role of vascular smooth muscle alkaline phosphatase in medial artery calcification. *J. Bone Miner. Res. Off. J. Am. Soc. Bone Miner. Res.* **30,** 824–836 (2015).

161. Hessle, L. *et al.* Tissue-nonspecific alkaline phosphatase and plasma cell membrane glycoprotein-1 are central antagonistic regulators of bone mineralization. *Proc. Natl. Acad. Sci. U. S. A.* **99,** 9445–9449 (2002).

162. Sweet, H. O. & Green, M. C. Progressive ankylosis, a new skeletal mutation in the mouse. *J. Hered.* **72,** 87–93 (1981).

163. Ho, A. M., Johnson, M. D. & Kingsley, D. M. Role of the mouse ank gene in control of tissue calcification and arthritis. *Science* **289,** 265–270 (2000).

164. Gurley, K. A. *et al.* Mineral formation in joints caused by complete or joint-specific loss of ANK function. *J. Bone Miner. Res. Off. J. Am. Soc. Bone Miner. Res.* **21,** 1238–1247 (2006).

165. Chen, I.-P. *et al.* Introduction of a Phe377del mutation in ANK creates a mouse model for craniometaphyseal dysplasia. *J. Bone Miner. Res. Off. J. Am. Soc. Bone Miner. Res.* **24,** 1206–1215 (2009).

166. Chen, I.-P., Wang, L., Jiang, X., Aguila, H. L. & Reichenberger, E. J. A Phe377del mutation in ANK leads to impaired osteoblastogenesis and osteoclastogenesis in a

mouse model for craniometaphyseal dysplasia (CMD). *Hum. Mol. Genet.* **20,** 948–961 (2011).

167. Tew, W. P., Mahle, C., Benavides, J., Howard, J. E. & Lehninger, A. L. Synthesis and characterization of phosphocitric acid, a potent inhibitor of hydroxylapatite crystal growth. *Biochemistry (Mosc.)* **19,** 1983–1988 (1980).
168. Krug, H. E., Mahowald, M. L., Halverson, P. B., Sallis, J. D. & Cheung, H. S. Phosphocitrate prevents disease progression in murine progressive ankylosis. *Arthritis Rheum.* **36,** 1603–1611 (1993).
169. Harmey, D. *et al.* Concerted regulation of inorganic pyrophosphate and osteopontin by akp2, enpp1, and ank: an integrated model of the pathogenesis of mineralization disorders. *Am. J. Pathol.* **164,** 1199–1209 (2004).
170. Foster, B. L. *et al.* Central role of pyrophosphate in acellular cementum formation. *PloS One* **7,** e38393 (2012).
171. Nociti, F. H. *et al.* Cementum: a phosphate-sensitive tissue. *J. Dent. Res.* **81,** 817–821 (2002).
172. Johnson, K. *et al.* Differential mechanisms of inorganic pyrophosphate production by plasma cell membrane glycoprotein-1 and B10 in chondrocytes. *Arthritis Rheum.* **42,** 1986–1997 (1999).
173. Johnson, K. *et al.* Mitochondrial oxidative phosphorylation is a downstream regulator of nitric oxide effects on chondrocyte matrix synthesis and mineralization. *Arthritis Rheum.* **43,** 1560–1570 (2000).
174. Terkeltaub, R. A. Inorganic pyrophosphate generation and disposition in pathophysiology. *Am. J. Physiol. Cell Physiol.* **281,** C1–C11 (2001).

175. Warraich, S. *et al.* Loss of equilibrative nucleoside transporter 1 in mice leads to progressive ectopic mineralization of spinal tissues resembling diffuse idiopathic skeletal hyperostosis in humans. *J. Bone Miner. Res. Off. J. Am. Soc. Bone Miner. Res.* **28,** 1135–1149 (2013).

176. Shimada, T. *et al.* Targeted ablation of Fgf23 demonstrates an essential physiological role of FGF23 in phosphate and vitamin D metabolism. *J. Clin. Invest.* **113,** 561–568 (2004).

177. Esapa, C. T. *et al.* A mouse with an N-Ethyl-N-nitrosourea (ENU) Induced Trp589Arg Galnt3 mutation represents a model for hyperphosphataemic familial tumoural calcinosis. *PloS One* **7,** e43205 (2012).

178. Esapa, C. T. *et al.* N-ethyl-N-Nitrosourea (ENU) induced mutations within the klotho gene lead to ectopic calcification and reduced lifespan in mouse models. *PloS One* **10,** e0122650 (2015).

179. Ichikawa, S. *et al.* Ablation of the Galnt3 gene leads to low-circulating intact fibroblast growth factor 23 (Fgf23) concentrations and hyperphosphatemia despite increased Fgf23 expression. *Endocrinology* **150,** 2543–2550 (2009).

180. Ichikawa, S., Austin, A. M., Gray, A. K., Allen, M. R. & Econs, M. J. Dietary phosphate restriction normalizes biochemical and skeletal abnormalities in a murine model of tumoral calcinosis. *Endocrinology* **152,** 4504–4513 (2011).

181. Katai, K. *et al.* Nicotinamide inhibits sodium-dependent phosphate cotransport activity in rat small intestine. *Nephrol. Dial. Transplant. Off. Publ. Eur. Dial. Transpl. Assoc. - Eur. Ren. Assoc.* **14,** 1195–1201 (1999).

182. Wu, K. I., Bacon, R. A., Al-Mahrouq, H. A. & Kempson, S. A. Nicotinamide as a rapid-acting inhibitor of renal brush-border phosphate transport. *Am. J. Physiol.* **255,** F15-21 (1988).

183. Reilly, A. M., Gray, A. K., Moe, S. M. & Ichikawa, S. Nicotinamide treatment in a murine model of familial tumoral calcinosis reduces serum Fgf23 and raises heart calcium. *Bone* **67,** 139–144 (2014).

184. Kuro-o, M. *et al.* Mutation of the mouse klotho gene leads to a syndrome resembling ageing. *Nature* **390,** 45–51 (1997).

185. Sitara, D. *et al.* Homozygous ablation of fibroblast growth factor-23 results in hyperphosphatemia and impaired skeletogenesis, and reverses hypophosphatemia in Phex-deficient mice. *Matrix Biol. J. Int. Soc. Matrix Biol.* **23,** 421–432 (2004).

186. Stubbs, J. R. *et al.* Role of hyperphosphatemia and 1,25-dihydroxyvitamin D in vascular calcification and mortality in fibroblastic growth factor 23 null mice. *J. Am. Soc. Nephrol. JASN* **18,** 2116–2124 (2007).

187. Razzaque, M. S., Sitara, D., Taguchi, T., St-Arnaud, R. & Lanske, B. Premature aging-like phenotype in fibroblast growth factor 23 null mice is a vitamin D-mediated process. *FASEB J. Off. Publ. Fed. Am. Soc. Exp. Biol.* **20,** 720–722 (2006).

188. Sitara, D. *et al.* Genetic ablation of vitamin D activation pathway reverses biochemical and skeletal anomalies in Fgf-23-null animals. *Am. J. Pathol.* **169,** 2161–2170 (2006).

189. Hesse, M., Fröhlich, L. F., Zeitz, U., Lanske, B. & Erben, R. G. Ablation of vitamin D signaling rescues bone, mineral, and glucose homeostasis in Fgf-23 deficient mice. *Matrix Biol. J. Int. Soc. Matrix Biol.* **26,** 75–84 (2007).

190. Tsujikawa, H., Kurotaki, Y., Fujimori, T., Fukuda, K. & Nabeshima, Y.-I. Klotho, a gene related to a syndrome resembling human premature aging, functions in a negative regulatory circuit of vitamin D endocrine system. *Mol. Endocrinol. Baltim. Md* **17,** 2393–2403 (2003).

191. Voelkl, J. *et al.* Spironolactone ameliorates PIT1-dependent vascular osteoinduction in klotho-hypomorphic mice. *J. Clin. Invest.* **123,** 812–822 (2013).

192. Fischer, S. S. *et al.* Hyperaldosteronism in Klotho-deficient mice. *Am. J. Physiol. Renal Physiol.* **299,** F1171-1177 (2010).

193. Leibrock, C. B. *et al.* NH4Cl Treatment Prevents Tissue Calcification in Klotho Deficiency. *J. Am. Soc. Nephrol. JASN* **26,** 2423–2433 (2015).

194. Leibrock, C. B. *et al.* Bicarbonate-sensitive calcification and lifespan of klotho-deficient mice. *Am. J. Physiol. Renal Physiol.* **310,** F102-108 (2016).

195. Li, C. F. *et al.* Human sterile alpha motif domain 9, a novel gene identified as down-regulated in aggressive fibromatosis, is absent in the mouse. *BMC Genomics* **8,** 92 (2007).

196. Jensen, N. *et al.* Loss of function of Slc20a2 associated with familial idiopathic Basal Ganglia calcification in humans causes brain calcifications in mice. *J. Mol. Neurosci. MN* **51,** 994–999 (2013).

197. Wallingford, M. C. *et al.* SLC20A2 deficiency in mice leads to elevated phosphate levels in cerbrospinal fluid and glymphatic pathway-associated arteriolar

calcification, and recapitulates human idiopathic basal ganglia calcification. *Brain Pathol. Zurich Switz.* (2016). doi:10.1111/bpa.12362

198. Hellström, M., Kalén, M., Lindahl, P., Abramsson, A. & Betsholtz, C. Role of PDGF-B and PDGFR-beta in recruitment of vascular smooth muscle cells and pericytes during embryonic blood vessel formation in the mouse. *Dev. Camb. Engl.* **126,** 3047–3055 (1999).
199. Nakamura, T. *et al.* Relationships among parvalbumin-immunoreactive neuron density, phase-locked gamma oscillations, and autistic/schizophrenic symptoms in PDGFR-β knock-out and control mice. *PloS One* **10,** e0119258 (2015).
200. Keller, A. *et al.* Mutations in the gene encoding PDGF-B cause brain calcifications in humans and mice. *Nat. Genet.* **45,** 1077–1082 (2013).
201. Miklossy, J. *et al.* Severe vascular disturbance in a case of familial brain calcinosis. *Acta Neuropathol. (Berl.)* **109,** 643–653 (2005).
202. Saitou, M. *et al.* Complex phenotype of mice lacking occludin, a component of tight junction strands. *Mol. Biol. Cell* **11,** 4131–4142 (2000).
203. Wang, C. *et al.* Mutations in SLC20A2 link familial idiopathic basal ganglia calcification with phosphate homeostasis. *Nat. Genet.* **44,** 254–256 (2012).
204. Arts, F. A. *et al.* Idiopathic basal ganglia calcification-associated PDGFRB mutations impair the receptor signalling. *J. Cell. Mol. Med.* **19,** 239–248 (2015).
205. Demoulin, J.-B. *et al.* Platelet-derived growth factor stimulates membrane lipid synthesis through activation of phosphatidylinositol 3-kinase and sterol regulatory element-binding proteins. *J. Biol. Chem.* **279,** 35392–35402 (2004).

206. Luo, G. *et al.* Spontaneous calcification of arteries and cartilage in mice lacking matrix GLA protein. *Nature* **386,** 78–81 (1997).

207. Howe, A. M. & Webster, W. S. Warfarin exposure and calcification of the arterial system in the rat. *Int. J. Exp. Pathol.* **81,** 51–56 (2000).

208. Price, P. A. & Williamson, M. K. Effects of warfarin on bone. Studies on the vitamin K-dependent protein of rat bone. *J. Biol. Chem.* **256,** 12754–12759 (1981).

209. Schurgers, L. J. *et al.* Regression of warfarin-induced medial elastocalcinosis by high intake of vitamin K in rats. *Blood* **109,** 2823–2831 (2007).

210. Azuma, K. *et al.* Osteoblast-Specific γ-Glutamyl Carboxylase-Deficient Mice Display Enhanced Bone Formation With Aberrant Mineralization. *J. Bone Miner. Res. Off. J. Am. Soc. Bone Miner. Res.* **30,** 1245–1254 (2015).

211. Funabiki, M. *et al.* Autoimmune disorders associated with gain of function of the intracellular sensor MDA5. *Immunity* **40,** 199–212 (2014).

212. El-Abbadi, M. M. *et al.* Phosphate feeding induces arterial medial calcification in uremic mice: role of serum phosphorus, fibroblast growth factor-23, and osteopontin. *Kidney Int.* **75,** 1297–1307 (2009).

213. Shobeiri, N., Adams, M. A. & Holden, R. M. Vascular calcification in animal models of CKD: A review. *Am. J. Nephrol.* **31,** 471–481 (2010).

214. Neven, E. & D'Haese, P. C. Vascular calcification in chronic renal failure: what have we learned from animal studies? *Circ. Res.* **108,** 249–264 (2011).

215. Eto, N., Miyata, Y., Ohno, H. & Yamashita, T. Nicotinamide prevents the development of hyperphosphataemia by suppressing intestinal sodium-dependent phosphate transporter in rats with adenine-induced renal failure. *Nephrol. Dial.*

Transplant. Off. Publ. Eur. Dial. Transpl. Assoc. - Eur. Ren. Assoc. **20,** 1378–1384 (2005).

216. Fleisch, H., Schibler, D., Maerki, J. & Frossard, I. Inhibition of aortic calcification by means of pyrophosphate and polyphosphates. *Nature* **207,** 1300–1301 (1965).
217. Schibler, D., Russell, R. G. & Fleisch, H. Inhibition by pyrophosphate and polyphosphate of aortic calcification induced by vitamin D3 in rats. *Clin. Sci.* **35,** 363–372 (1968).
218. O'Neill, W. C., Lomashvili, K. A., Malluche, H. H., Faugere, M.-C. & Riser, B. L. Treatment with pyrophosphate inhibits uremic vascular calcification. *Kidney Int.* **79,** 512–517 (2011).
219. Towler, D. A., Bidder, M., Latifi, T., Coleman, T. & Semenkovich, C. F. Diet-induced diabetes activates an osteogenic gene regulatory program in the aortas of low density lipoprotein receptor-deficient mice. *J. Biol. Chem.* **273,** 30427–30434 (1998).
220. Nguyen, N., Naik, V. & Speer, M. Y. Diabetes mellitus accelerates cartilaginous metaplasia and calcification in atherosclerotic vessels of LDLr mutant mice. *Cardiovasc. Pathol. Off. J. Soc. Cardiovasc. Pathol.* **22,** 167–175 (2013).
221. Villa-Bellosta, R. *et al.* Defective extracellular pyrophosphate metabolism promotes vascular calcification in a mouse model of Hutchinson-Gilford progeria syndrome that is ameliorated on pyrophosphate treatment. *Circulation* **127,** 2442–2451 (2013).
222. Persy, V. P. & McKee, M. D. Prevention of vascular calcification: is pyrophosphate therapy a solution? *Kidney Int.* **79,** 490–493 (2011).

223. Abedin, M., Tintut, Y. & Demer, L. L. Vascular calcification: mechanisms and clinical ramifications. *Arterioscler. Thromb. Vasc. Biol.* **24,** 1161–1170 (2004).

224. Johnsson, M. S. & Nancollas, G. H. The role of brushite and octacalcium phosphate in apatite formation. *Crit. Rev. Oral Biol. Med. Off. Publ. Am. Assoc. Oral Biol.* **3,** 61–82 (1992).

225. Villa-Bellosta, R. & Egido, J. Phosphate, pyrophosphate, and vascular calcification: a question of balance. *Eur. Heart J.* (2015). doi:10.1093/eurheartj/ehv605

226. Shanahan, C. M., Crouthamel, M. H., Kapustin, A. & Giachelli, C. M. Arterial calcification in chronic kidney disease: key roles for calcium and phosphate. *Circ. Res.* **109,** 697–711 (2011).

227. Giovannini, D., Touhami, J., Charnet, P., Sitbon, M. & Battini, J.-L. Inorganic phosphate export by the retrovirus receptor XPR1 in metazoans. *Cell Rep.* **3,** 1866–1873 (2013).

228. Legati, A. *et al.* Mutations in XPR1 cause primary familial brain calcification associated with altered phosphate export. *Nat. Genet.* **47,** 579–581 (2015).

229. Terkeltaub, R. Physiologic and pathologic functions of the NPP nucleotide pyrophosphatase/phosphodiesterase family focusing on NPP1 in calcification. *Purinergic Signal.* **2,** 371–377 (2006).

230. Villa-Bellosta, R. & Sorribas, V. Prevention of vascular calcification by polyphosphates and nucleotides- role of ATP. *Circ. J. Off. J. Jpn. Circ. Soc.* **77,** 2145–2151 (2013).

231. Stuart, A. G. Idiopathic arterial calcification of infancy and pyrophosphate deficiency. *J. Pediatr.* **123,** 170–171 (1993).

232. Rutsch, F. *et al.* Low levels of urinary inorganic pyrophosphate indicating systemic pyrophosphate deficiency in a boy with idiopathic infantile arterial calcification. *Acta Paediatr. Oslo Nor. 1992* **89,** 1265–1269 (2000).

233. Lomashvili, K. A., Khawandi, W. & O'Neill, W. C. Reduced plasma pyrophosphate levels in hemodialysis patients. *J. Am. Soc. Nephrol. JASN* **16,** 2495–2500 (2005).

234. O'Neill, W. C., Sigrist, M. K. & McIntyre, C. W. Plasma pyrophosphate and vascular calcification in chronic kidney disease. *Nephrol. Dial. Transplant. Off. Publ. Eur. Dial. Transpl. Assoc. - Eur. Ren. Assoc.* **25,** 187–191 (2010).

235. Lomashvili, K. A., Garg, P., Narisawa, S., Millan, J. L. & O'Neill, W. C. Upregulation of alkaline phosphatase and pyrophosphate hydrolysis: potential mechanism for uremic vascular calcification. *Kidney Int.* **73,** 1024–1030 (2008).

236. Price, P. A., Urist, M. R. & Otawara, Y. Matrix Gla protein, a new gamma-carboxyglutamic acid-containing protein which is associated with the organic matrix of bone. *Biochem. Biophys. Res. Commun.* **117,** 765–771 (1983).

237. Murshed, M., Schinke, T., McKee, M. D. & Karsenty, G. Extracellular matrix mineralization is regulated locally; different roles of two gla-containing proteins. *J. Cell Biol.* **165,** 625–630 (2004).

238. Spronk, H. M. *et al.* Matrix Gla protein accumulates at the border of regions of calcification and normal tissue in the media of the arterial vessel wall. *Biochem. Biophys. Res. Commun.* **289,** 485–490 (2001).

239. Zebboudj, A. F., Imura, M. & Boström, K. Matrix GLA protein, a regulatory protein for bone morphogenetic protein-2. *J. Biol. Chem.* **277,** 4388–4394 (2002).

240. Iliás, A. *et al.* Loss of ATP-dependent transport activity in pseudoxanthoma elasticum-associated mutants of human ABCC6 (MRP6). *J. Biol. Chem.* **277,** 16860–16867 (2002).

241. Matsuzaki, Y., Nakano, A., Jiang, Q.-J., Pulkkinen, L. & Uitto, J. Tissue-specific expression of the ABCC6 gene. *J. Invest. Dermatol.* **125,** 900–905 (2005).

242. Pomozi, V. *et al.* ABCC6 is a basolateral plasma membrane protein. *Circ. Res.* **112,** e148-151 (2013).

243. Jiang, Q. & Uitto, J. Pseudoxanthoma elasticum: a metabolic disease? *J. Invest. Dermatol.* **126,** 1440–1441 (2006).

244. Jiang, Q., Endo, M., Dibra, F., Wang, K. & Uitto, J. Pseudoxanthoma elasticum is a metabolic disease. *J. Invest. Dermatol.* **129,** 348–354 (2009).

245. Jiang, Q. *et al.* Parabiotic heterogenetic pairing of Abcc6-/-/Rag1-/- mice and their wild-type counterparts halts ectopic mineralization in a murine model of pseudoxanthoma elasticum. *Am. J. Pathol.* **176,** 1855–1862 (2010).

246. Tiozzo Costa, R. *et al.* Pseudoxanthoma elasticum (PXE): ultrastructural and biochemical study on proteoglycan and proteoglycan-associated material produced by skin fibroblasts in vitro. *Coll. Relat. Res.* **8,** 49–64 (1988).

247. Quaglino, D. *et al.* Abnormal phenotype of in vitro dermal fibroblasts from patients with Pseudoxanthoma elasticum (PXE). *Biochim. Biophys. Acta* **1501,** 51–62 (2000).

248. Gheduzzi, D. *et al.* Matrix Gla protein is involved in elastic fiber calcification in the dermis of pseudoxanthoma elasticum patients. *Lab. Investig. J. Tech. Methods Pathol.* **87,** 998–1008 (2007).

249. Dabisch-Ruthe, M., Kuzaj, P., Götting, C., Knabbe, C. & Hendig, D. Pyrophosphates as a major inhibitor of matrix calcification in Pseudoxanthoma elasticum. *J. Dermatol. Sci.* **75,** 109–120 (2014).

250. Le Saux, O. *et al.* Serum factors from pseudoxanthoma elasticum patients alter elastic fiber formation in vitro. *J. Invest. Dermatol.* **126,** 1497–1505 (2006).

251. Mackay, E. W., Apschner, A. & Schulte-Merker, S. Vitamin K reduces hypermineralisation in zebrafish models of PXE and GACI. *Dev. Camb. Engl.* **142,** 1095–1101 (2015).

252. Jansen, R. S. *et al.* ABCC6 prevents ectopic mineralization seen in pseudoxanthoma elasticum by inducing cellular nucleotide release. *Proc. Natl. Acad. Sci. U. S. A.* **110,** 20206–20211 (2013).

253. Shanahan, C. M. *et al.* Medial localization of mineralization-regulating proteins in association with Mönckeberg's sclerosis: evidence for smooth muscle cell-mediated vascular calcification. *Circulation* **100,** 2168–2176 (1999).

254. Moe, S. M., Duan, D., Doehle, B. P., O'Neill, K. D. & Chen, N. X. Uremia induces the osteoblast differentiation factor Cbfa1 in human blood vessels. *Kidney Int.* **63,** 1003–1011 (2003).

255. Neven, E. *et al.* Chondrocyte rather than osteoblast conversion of vascular cells underlies medial calcification in uremic rats. *Arterioscler. Thromb. Vasc. Biol.* **30,** 1741–1750 (2010).

256. Schlieper, G., Schurgers, L., Brandenburg, V., Reutelingsperger, C. & Floege, J. Vascular calcification in chronic kidney disease: an update. *Nephrol. Dial.*

Transplant. Off. Publ. Eur. Dial. Transpl. Assoc. - Eur. Ren. Assoc. **31,** 31–39 (2016).

257. Tanimura, A., McGregor, D. H. & Anderson, H. C. Matrix vesicles in atherosclerotic calcification. *Proc. Soc. Exp. Biol. Med. Soc. Exp. Biol. Med. N. Y. N* **172,** 173–177 (1983).

258. Steitz, S. A. *et al.* Smooth muscle cell phenotypic transition associated with calcification: upregulation of Cbfa1 and downregulation of smooth muscle lineage markers. *Circ. Res.* **89,** 1147–1154 (2001).

259. Li, X., Yang, H.-Y. & Giachelli, C. M. Role of the sodium-dependent phosphate cotransporter, Pit-1, in vascular smooth muscle cell calcification. *Circ. Res.* **98,** 905–912 (2006).

260. Jono, S. *et al.* Phosphate regulation of vascular smooth muscle cell calcification. *Circ. Res.* **87,** E10-17 (2000).

261. Li, X., Yang, H.-Y. & Giachelli, C. M. BMP-2 promotes phosphate uptake, phenotypic modulation, and calcification of human vascular smooth muscle cells. *Atherosclerosis* **199,** 271–277 (2008).

262. Ng, F. *et al.* PDGF, TGF-beta, and FGF signaling is important for differentiation and growth of mesenchymal stem cells (MSCs): transcriptional profiling can identify markers and signaling pathways important in differentiation of MSCs into adipogenic, chondrogenic, and osteogenic lineages. *Blood* **112,** 295–307 (2008).

263. Reynolds, J. L. *et al.* Human vascular smooth muscle cells undergo vesicle-mediated calcification in response to changes in extracellular calcium and phosphate

concentrations: a potential mechanism for accelerated vascular calcification in ESRD. *J. Am. Soc. Nephrol. JASN* **15,** 2857–2867 (2004).

264. Speer, M. Y. *et al.* Smooth muscle cells give rise to osteochondrogenic precursors and chondrocytes in calcifying arteries. *Circ. Res.* **104,** 733–741 (2009).
265. Khavandgar, Z. *et al.* Elastin haploinsufficiency impedes the progression of arterial calcification in MGP-deficient mice. *J. Bone Miner. Res. Off. J. Am. Soc. Bone Miner. Res.* **29,** 327–337 (2014).
266. Beazley, K. E., Reckard, S., Nurminsky, D., Lima, F. & Nurminskaya, M. Two sides of MGP null arterial disease: chondrogenic lesions dependent on transglutaminase 2 and elastin fragmentation associated with induction of adipsin. *J. Biol. Chem.* **288,** 31400–31408 (2013).
267. Qiao, J.-H., Mertens, R. B., Fishbein, M. C. & Geller, S. A. Cartilaginous metaplasia in calcified diabetic peripheral vascular disease: morphologic evidence of enchondral ossification. *Hum. Pathol.* **34,** 402–407 (2003).
268. Neven, E., Dauwe, S., De Broe, M. E., D'Haese, P. C. & Persy, V. Endochondral bone formation is involved in media calcification in rats and in men. *Kidney Int.* **72,** 574–581 (2007).
269. Demer, L. L. & Tintut, Y. Vascular calcification: pathobiology of a multifaceted disease. *Circulation* **117,** 2938–2948 (2008).
270. Kawai, T. & Akira, S. The roles of TLRs, RLRs and NLRs in pathogen recognition. *Int. Immunol.* **21,** 317–337 (2009).

271. Shaw, L. J., Raggi, P., Schisterman, E., Berman, D. S. & Callister, T. Q. Prognostic Value of Cardiac Risk Factors and Coronary Artery Calcium Screening for All-Cause Mortality. *Radiology* **228,** 826–833 (2003).

272. Lehto, S., Niskanen, L., Suhonen, M., Rönnemaa, T. & Laakso, M. Medial Artery Calcification: A Neglected Harbinger of Cardiovascular Complications in Non–Insulin-Dependent Diabetes Mellitus. *Arterioscler. Thromb. Vasc. Biol.* **16,** 978–983 (1996).

273. Collin-Osdoby, P. Regulation of Vascular Calcification by Osteoclast Regulatory Factors RANKL and Osteoprotegerin. *Circ. Res.* **95,** 1046–1057 (2004).

274. Boström, K. *et al.* Bone morphogenetic protein expression in human atherosclerotic lesions. *J. Clin. Invest.* **91,** 1800–1809 (1993).

275. Colgan, S. P., Eltzschig, H. K., Eckle, T. & Thompson, L. F. Physiological roles for ecto-5'-nucleotidase (CD73). *Purinergic Signal.* **2,** 351–360 (2006).

276. Magnus-Levy, A. Ueber ungewöhnliche Verkalkung der Arterien. *DMW - Dtsch. Med. Wochenschr.* **40,** 1305–1309 (1914).

277. Levitin, J. A Case of Arterial and Periarticular Calcinosis of Unknown Etiology. *Radiology* **44,** 489–494 (1945).

278. Sharp, J. Heredo-familial vascular and articular calcification. *Ann. Rheum. Dis.* **13,** 15–27 (1954).

279. Mori, H. *et al.* Extensive arterial calcification of unknown etiology in a 29-year-old male. *Heart Vessels* **7,** 211–214 (1992).

280. Henthorn, P. S., Raducha, M., Fedde, K. N., Lafferty, M. A. & Whyte, M. P. Different missense mutations at the tissue-nonspecific alkaline phosphatase gene

locus in autosomal recessively inherited forms of mild and severe hypophosphatasia. *Proc. Natl. Acad. Sci. U. S. A.* **89,** 9924–9928 (1992).

281. Yang, D. *et al.* The A2B adenosine receptor protects against inflammation and excessive vascular adhesion. *J. Clin. Invest.* **116,** 1913–1923 (2006).
282. Ramjan, K. A., Roscioli, T., Rutsch, F., Sillence, D. & Munns, C. F. J. Generalized arterial calcification of infancy: treatment with bisphosphonates. *Nat. Clin. Pract. Endocrinol. Metab.* **5,** 167–172 (2009).
283. Hayashi, E., Maeda, T. & Shinozuka, K. Adenosine and dipyridamole: actions and interactions on the contractile response of guinea-pig ileum to high frequency electrical field stimulation. *Br. J. Pharmacol.* **84,** 765–771 (1985).
284. Roberts, S., Narisawa, S., Harmey, D., Millán, J. L. & Farquharson, C. Functional involvement of PHOSPHO1 in matrix vesicle-mediated skeletal mineralization. *J. Bone Miner. Res. Off. J. Am. Soc. Bone Miner. Res.* **22,** 617–627 (2007).
285. Delomenède, M., Buchet, R. & Mebarek, S. Lansoprazole is an uncompetitive inhibitor of tissue-nonspecific alkaline phosphatase. *Acta Biochim. Pol.* **56,** 301–305 (2009).
286. Koszalka, P. *et al.* Targeted disruption of cd73/ecto-5'-nucleotidase alters thromboregulation and augments vascular inflammatory response. *Circ. Res.* **95,** 814–821 (2004).
287. Castrop, H. *et al.* Impairment of tubuloglomerular feedback regulation of GFR in ecto-5'-nucleotidase/CD73-deficient mice. *J. Clin. Invest.* **114,** 634–642 (2004).

288. Normand, J. & Karasek, M. A. A method for the isolation and serial propagation of keratinocytes, endothelial cells, and fibroblasts from a single punch biopsy of human skin. *Vitro Cell. Dev. Biol. - Anim.* **31,** 447–455 (1995).

289. Bockenhauer, D. *et al.* Epilepsy, Ataxia, Sensorineural Deafness, Tubulopathy, and *KCNJ10* Mutations. *N. Engl. J. Med.* **360,** 1960–1970 (2009).

290. Livak, K. J. Allelic discrimination using fluorogenic probes and the 5' nuclease assay. *Genet. Anal. Biomol. Eng.* **14,** 143–149 (1999).

291. Deaglio, S. *et al.* Adenosine generation catalyzed by CD39 and CD73 expressed on regulatory T cells mediates immune suppression. *J. Exp. Med.* **204,** 1257–1265 (2007).

292. Ding, H.-T., Wang, C.-G., Zhang, T.-L. & Wang, K. Fibronectin enhances in vitro vascular calcification by promoting osteoblastic differentiation of vascular smooth muscle cells via ERK pathway. *J. Cell. Biochem.* **99,** 1343–1352 (2006).

293. Hoemann, C. D., El-Gabalawy, H. & McKee, M. D. In vitro osteogenesis assays: influence of the primary cell source on alkaline phosphatase activity and mineralization. *Pathol. Biol. (Paris)* **57,** 318–323 (2009).

294. Proudfoot, D. *et al.* Apoptosis regulates human vascular calcification in vitro: evidence for initiation of vascular calcification by apoptotic bodies. *Circ. Res.* **87,** 1055–1062 (2000).

295. Levy-Litan, V. *et al.* Autosomal-recessive hypophosphatemic rickets is associated with an inactivation mutation in the ENPP1 gene. *Am. J. Hum. Genet.* **86,** 273–278 (2010).

296. Lorenz-Depiereux, B., Schnabel, D., Tiosano, D., Häusler, G. & Strom, T. M. Loss-of-function ENPP1 mutations cause both generalized arterial calcification of infancy and autosomal-recessive hypophosphatemic rickets. *Am. J. Hum. Genet.* **86,** 267–272 (2010).

297. Sholler, G. F. *et al.* Generalized arterial calcification of infancy: Three case reports, including spontaneous regression with long-term survival. *J. Pediatr.* **105,** 257–260 (1984).

298. Ciana, G. *et al.* Generalized arterial calcification of infancy: two siblings with prolonged survival. *Eur. J. Pediatr.* **165,** 258–263 (2006).

299. Meradji, M., de Villeneuve, V. H., Huber, J., de Bruijn, W. C. & Pearse, R. G. Idiopathic infantile arterial calcification in siblings: radiologic diagnosis and successful treatment. *J. Pediatr.* **92,** 401–405 (1978).

300. van der Sluis, I. M., Boot, A. M., Vernooij, M., Meradji, M. & Kroon, A. A. Idiopathic infantile arterial calcification: clinical presentation, therapy and long-term follow-up. *Eur. J. Pediatr.* **165,** 590–593 (2006).

301. Westerhof, N., Stergiopulos, N. & Noble, M. I. M. *Snapshots of hemodynamics: an aid for clinical research and graduate education*. (Springer, 2005).

302. Lomashvili, K. A., Cobbs, S., Hennigar, R. A., Hardcastle, K. I. & O'Neill, W. C. Phosphate-induced vascular calcification: role of pyrophosphate and osteopontin. *J. Am. Soc. Nephrol. JASN* **15,** 1392–1401 (2004).

303. Bergen, A. A. *et al.* Mutations in ABCC6 cause pseudoxanthoma elasticum. *Nat. Genet.* **25,** 228–231 (2000).

304. Le Saux, O. *et al.* Mutations in a gene encoding an ABC transporter cause pseudoxanthoma elasticum. *Nat. Genet.* **25,** 223–227 (2000).

305. Narisawa, S. *et al.* Novel inhibitors of alkaline phosphatase suppress vascular smooth muscle cell calcification. *J. Bone Miner. Res. Off. J. Am. Soc. Bone Miner. Res.* **22,** 1700–1710 (2007).

306. Millán, J. L. & Whyte, M. P. Alkaline Phosphatase and Hypophosphatasia. *Calcif. Tissue Int.* **98,** 398–416 (2016).

307. Savinov, A. Y. *et al.* Transgenic Overexpression of Tissue-Nonspecific Alkaline Phosphatase (TNAP) in Vascular Endothelium Results in Generalized Arterial Calcification. *J. Am. Heart Assoc.* **4,** (2015).

308. Glatt, V., Canalis, E., Stadmeyer, L. & Bouxsein, M. L. Age-related changes in trabecular architecture differ in female and male C57BL/6J mice. *J. Bone Miner. Res. Off. J. Am. Soc. Bone Miner. Res.* **22,** 1197–1207 (2007).

309. Schenk, R., Merz, W. A., Mühlbauer, R., Russell, R. G. & Fleisch, H. Effect of ethane-1-hydroxy-1,1-diphosphonate (EHDP) and dichloromethylene diphosphonate (Cl 2 MDP) on the calcification and resorption of cartilage and bone in the tibial epiphysis and metaphysis of rats. *Calcif. Tissue Res.* **11,** 196–214 (1973).

310. Price, P. A., Faus, S. A. & Williamson, M. K. Bisphosphonates alendronate and ibandronate inhibit artery calcification at doses comparable to those that inhibit bone resorption. *Arterioscler. Thromb. Vasc. Biol.* **21,** 817–824 (2001).

311. Boraldi, F. *et al.* Matrix Gla Protein and Alkaline Phosphatase Are Differently Modulated in Human Dermal Fibroblasts from PXE Patients and Controls. *J. Invest. Dermatol.* **133,** 946–954 (2013).

312. Apschner, A., Huitema, L. F. A., Ponsioen, B., Peterson-Maduro, J. & Schulte-Merker, S. Zebrafish enpp1 mutants exhibit pathological mineralization, mimicking features of generalized arterial calcification of infancy (GACI) and pseudoxanthoma elasticum (PXE). *Dis. Model. Mech.* **7,** 811–822 (2014).

313. Rattazzi, M. *et al.* Extracellular pyrophosphate is reduced in aortic interstitial valve cells acquiring a calcifying profile: implications for aortic valve calcification. *Atherosclerosis* **237,** 568–576 (2014).

314. Rathan, S., Yoganathan, A. P. & O'Neill, C. W. The role of inorganic pyrophosphate in aortic valve calcification. *J. Heart Valve Dis.* **23,** 387–394 (2014).

315. Le Corre, Y. *et al.* Quantification of the calcification phenotype of Abcc6-deficient mice with microcomputed tomography. *Am. J. Pathol.* **180,** 2208–2213 (2012).

316. Berndt, A. *et al.* A single-nucleotide polymorphism in the Abcc6 gene associates with connective tissue mineralization in mice similar to targeted models for pseudoxanthoma elasticum. *J. Invest. Dermatol.* **133,** 833–836 (2013).

317. Truett, G. E. *et al.* Preparation of PCR-quality mouse genomic DNA with hot sodium hydroxide and tris (HotSHOT). *BioTechniques* **29,** 52, 54 (2000).

318. Dahl, R. *et al.* Discovery and validation of a series of aryl sulfonamides as selective inhibitors of tissue-nonspecific alkaline phosphatase (TNAP). *J. Med. Chem.* **52,** 6919–6925 (2009).

319. Sergienko, E. A., Sun, Q. & Ma, C.-T. A method for direct assessment of tissue-nonspecific alkaline phosphatase (TNAP) inhibitors in blood samples. *Methods Mol. Biol. Clifton NJ* **1053,** 103–113 (2013).

320. Bouxsein, M. L. *et al.* Guidelines for assessment of bone microstructure in rodents using micro-computed tomography. *J. Bone Miner. Res. Off. J. Am. Soc. Bone Miner. Res.* **25,** 1468–1486 (2010).

CURRICULUM VITAE

CONTACT INFORMATION
1305 Dock Street
Apt. 720
Baltimore, MD 21231
Phone: (301) 351-5586
Email: sgziegler@jhmi.edu

EDUCATION

Johns Hopkins University School of Medicine, Baltimore, Maryland M.D./Ph.D., 2018
Medical Scientist Training Program, MSIII/GSIV
Thesis: Delineating the mechanisms underlying rare disorders of ectopic calcification to reveal novel therapeutic strategies
Mentors: Drs. Hal Dietz and William Gahl

Oberlin College, Oberlin, Ohio B.A. May, 2008
Highest Honors in Neuroscience with a Minor in Jewish Studies
Cumulative GPA: 3.96/4.00

Hebrew University Rothberg International School, Jerusalem, Israel Spring, 2007

WORK EXPERIENCE

National Institutes of Health, Post-Baccalaureate Intramural Research Training Award (2008-2010)
National Human Genome Research Institute, Undiagnosed Diseases Program
Explored possible causes at the biochemical, molecular, and cellular levels for patients with undiagnosed diseases; delineated the disease-causing mechanism for a new disorder of arterial and joint calcification; investigated the potential of gene therapy for disorders of lysosome-related organelle biogenesis; molecular screening/analysis for known rare genetic disorders

Oberlin College (2007-2008)
Neuroscience Department
Examined the effects of decreased luteinizing hormone on hippocampal-dependent spatial learning and memory in female rats as a model for the treatment of Alzheimer's disease

The Johns Hopkins Medical Institutions (summer, 2007)
Department of Neurosurgery
Investigated toxicity and efficacy of drug treatments on malignant glioma in vitro and in vivo

National Institutes of Health, Intramural Research Training Award (summers, 2003-2006)
National Human Genome Research Institute / National Institute of Mental Health
Analyzed roles of conserved regulatory elements in the glucocerebrosidase gene locus; explored genetic associations between Gaucher disease and Parkinsons; compared genetic, biochemical, clinical characteristics of patients with Congenital Disorders of Glycosylation-Ia

Environmental Defense Fund, intern in Environmental Health Program (January, 2005)
Environmental Defense is a nonprofit organization that links science, economics, and law to create innovative solutions to urgent environmental problems.
Analyzed industry reports on toxicity of high-production-volume chemicals
Compiled research on nanotechnology related to public health

EXTRACURRICULAR ACTIVITIES AND LEADERSHIP

Johns Hopkins MSTP Advisory Committee (2012-present)
Committee Chair (2013-2016)
Peer Advising and Mentorship Sub-Committee, peer mentor (2012-present)

Ethics and Professionalism Sub-Committee, co-chair (2012-2013)

JHUSOM Genetic Medicine Interest Group (2011-present)
Co-founded interest group focused on clinical genetics and genetic medicine.
Co-chair (2011-2012)

JHUSOM Jewish Student Association (2010-present)
President (2011-2016)

HONORS AND AWARDS

Stanley L. Blumenthal Cardiology Research Award – First Place Basic Science Oral Presentation (2016)
American Society for Human Genetics Reviewers' Choice Abstract Award (2015, 2016)
Barry M. Goldwater Scholarship (2008)
Faculty of Undergraduate Neuroscience Travel Award (2008)
The Nancy Robell Memorial Prize in Neuroscience (2008)
USA Today All-Academic College Team Honorable Mention (2008)
Hillel Award for Leadership in the Oberlin Jewish Community (2008)
Hebrew University Rothberg International School Undergraduate Merit Scholarship (2007)
John F. Oberlin Scholarship (2004-2008)

PUBLICATIONS

1. MacFarlane EG, Shin J, **Ziegler SG**, Parker S, Creamer T, Bagirzadeh R, Bedja D, Chen Y, Calderon JF, Lindsay ME, Habashi J, Dietz HC. Lineage-specific sensitivity to TGF-β signaling perturbation drives aneurysm development. Nature 2017, in revision.

2. **Ziegler SG**, Ferreira CR, Gallo MacFarlane E, Riddle RC, Tomlinson R, Martin L, Ma C, Sergienko E, Pinkerton AB, Millan JL, Gahl WA, Dietz HC. The ectopic calcification disorder PXE integrates local and systemic alterations in ATP metabolism and responds to TNAP inhibition. Science Translational Medicine 2017, in press.

3. Introne WJ, Westbroek W, Cullinane AR, Groden CA, Bhambhani V, Golas GA, Baker EH, Lehky TJ, Snow J, **Ziegler SG**, Adams DR, Dorward HM, Hess RA, Huizing M, Gahl WA, Toro C. Neurological involvement in patients with mild Chediak-Higashi disease. Neurology 2016; 86(14):1320-8. PMID: 26944273.

4. Ferreira CR, **Ziegler SG**, Gupta A, Groden C, Hsu K, Gahl WA. Treatment of hypophosphatemic rickets in generalized arterial calcification of infancy (GACI) without worsening of vascular calcification. American Journal of Medical Genetics 2016; 170(5):1308-11. PMID: 26857895.

5. Janecke AR, Li B, Boehm M, Krabichler B, Rohrbach M, Muller T, Fuchs I, Golas G, Katagiri Y, **Ziegler SG**, Gahl WA, Wilnai Y, Zoppi N, Geller HM, Ciunta C, Slavotinek A, Steinmann B. The phenotype of the musculocontractural type of Ehlers-Danlos syndrome due to CHST14. American Journal of Human Genetics 2016; 170A(1):103-15 . PMID: 26373698.

6. Westbroek W, Klar A, Cullinane AR, **Ziegler SG**, Hurvitz H, Ganem A, Wilson K, Dorward H, Huizing M, Tamimi H, Vainshtein I, Berkun Y, Lavie M, Gahl WA, Anikster Y. Cellular and clinical report of new Griscelli syndrome type III cases. Pigment Cell and Melanoma Research 2012; 25(1):47-56. PMID: 21883982.

7. Markello TC, Pak LK, St. Hilaire C, Dorward H, **Ziegler SG**, Chen MY, Chaganti K, Nussbaum RL, Boehm M, Gahl WA. Vascular pathology of medial arterial calcifications in *NT5E* deficiency: Implications for the role of adenosine in pseudoxanthoma elasticum. Molecular Genetics and Metabolism 2011; 103(1):44-50. PMID: 21371928.

8. St. Hilaire C*, **Ziegler SG***, Markello T*, Brusco A, Groden C, Gill F, Carlson-Donohoe H, Lederman RJ, Chen MY, Yang D, Siegenthaler MP, Arduino C, Mancini C, Freudenthal B, Stanescu HC, Zdebik AA, Chaganti RK, Nussbaum R, Kleta R*, Gahl WA*, Boehm M*. *NT5E* mutations and

arterial calcifications. New England Journal of Medicine 2011; 364(5):432-42. PMID: 21288095. *contributed equally

9. El-Chemaly S, **Ziegler SG**, Calado RT, Wilson K, Wu HP, Haughey M, Peterson NR, Young NS, Gahl WA, Moss J, Gochuico BR. Natural history of pulmonary fibrosis in two subjects with the same telomerase mutation. Chest 2011; 139(5):1203-9. PMID: 20966039.

10. **Ziegler SG**, Thornton JE. Low luteinizing hormone enhances spatial memory and has protective effects on memory loss in rats. Hormones and Behavior 2010; 58(5):705-13.8. PMID: 20691694.

11. Blech-Hermoni YN*, **Ziegler SG***, Hruska KS*, Stubblefield B, LaMarca ME, Portnoy ME, NISC Comparative Sequencing Program, Green ED, Sidransky E. *In silico* and functional studies of the regulation of the glucocerebrosidase gene. Molecular Genetics and Metabolism 2010; 99(3):275-82. PMID: 20004604. *contributed equally

12. Gunay-Aygun M, Tuchman M, Font-Montgomery E, Lukose L, Edwards H, Garcia A, Ausawarat S, **Ziegler SG**, Piwnica-Worms K, Bryant J, Bernardini I, Fischer R, Huizing M, Guay-Woodford L, Gahl WA. *PKHD1* sequence variations in 78 children and adults with Autosomal Recessive Polycystic Kidney Disease and Congenital Hepatic Fibrosis. Molecular Genetics and Metabolism 2010; 99(2):160-73. PMID: 19914852.

13. Recinos VR, Bekelis K, **Ziegler SG**, Vick D, Hertig S, Tyler BM, Li KW, Kosztowski T, Legnani FG, Brem H, Olivi A. Epirubicin exhibits potent anti-tumor activity in an animal model of malignant glioma when administered via controlled-release polymers. Journal of Neurooncology 2010; 97(1):1-10. PMID: 19693439.

14. Sidransky E, Nalls MA, Aasly JO, Aharon-Peretz J, Annesi G, Barbosa ER, Bar-Shira A, Berg D, Bras J, Brice A, Chen C, Clark L, Condroyer C, De Marco EV, Dürr A, Eblan MJ, Fahn S, Farrer M, Fung H, Gan-Or Z, Gasser T, Gershoni R, Giladi N, Griffith A, Gurevich T, Januario C, Kropp P, Lang AE, Lee-Chen G, Lesage S, Marder K, Mata IF, Mirelman A, Mitsui J, Mizuta I, Nicoletti G, Oliveira C, Ottman R, Orr-Urtreger A, Pereira LV, Quattrone A, Rogaeva E, Rolfs A, Rosenbaum H, Rozenberg R, Samii A, Sammadar T, Schulte C, Sharma M, Singleton A, Spitz M, Tan E, Tayebi N, Toda T, Troiano A, Tsuji S, Wittstock M, Wolfsberg TG, Wu Y, Zabetian CP, Zhao Y, **Ziegler SG**. Multicenter meta-analysis of glucocerebrosidase mutations in Parkinson disease. New England Journal of Medicine 2009; 22;361(17):1651-61. PMID: 19846850.

15. Vincent LM, Adams D, Hess RA, **Ziegler SG**, Tsilou E, Golas G, O'Brien KJ, White JG, Huizing M, Gahl WA. Hermansky-Pudlak Syndrome Type 1 in patients of Indian Descent. Molecular Genetics and Metabolism 2009; 97(3):227-33. PMID: 19398212.

16. Goker-Alpan O, Wiggs EA, Eblan MJ, Benko W, **Ziegler SG**, Sidransky E, Schiffmann R. Cognitive outcome in treated patients with chronic neuropathic Gaucher disease. Journal of Pediatrics 2008; 153(1):89-94. PMID: 18571543.

17. **Ziegler SG**, Eblan MJ, Gutti U, Hruska KS, Stubblefield BK, Goker-Alpan O, LaMarca ME, Sidransky E. Glucocerebrosidase mutations in Chinese subjects from Taiwan with sporadic Parkinson disease. Molecular Genetics and Metabolism 2007; 91(2):195-200. PMID: 17462935.

18. Holleran W, **Ziegler SG**, Goker-Alpan O, Eblan MJ, Elias PM, Schiffmann R, Sidransky E. Skin abnormalities as an early predictor of neurologic outcome in Gaucher disease. Clinical Genetics 2006; 69(4): 355-7. PMID: 16630170.

19. Eblan MJ, Nguyen N, **Ziegler SG**, Lwin A, Hanson M, Gallardo M, Weiser R, De Lucca M, Singleton A, Sidransky E. Glucocerebrosidase mutations are also found in subjects with early-onset parkinsonism from Venezuela. Movement Disorders 2006; 21(2): 282-3. PMID: 16261622.

BOOK CHAPTERS

1. **Ziegler S**, Gahl W, Ferreira C. Extraosseous Calcification. 2017 May 1. In: Thakker RV, Whyte MP, Eisman J, Igarashi T. Genetics of Bone Biology and Skeletal Disease, second edition. Elsevier Academic Press.

2. Ferreira C, **Ziegler S**, Gahl W. Generalized Arterial Calcification of Infancy. 2014 Nov 13. In: Pagon RA, Adam MP, Ardinger HH, et al., editors. GeneReviews® [Internet]. Seattle (WA): University of Washington, Seattle; 1993-2014.

PLATFORM PRESENTATIONS

1. **SG Ziegler**, CR Ferreira, E Gallo MacFarlane, RC Riddle, R Tomlinson, L Martin, C Ma, E Sergienko, AB Pinkerton, JL Millan, WA Gahl, HC Dietz. Pseudoxanthoma elasticum: Dysregulation of local ATP metabolism and treatment with a tissue non-specific alkaline phosphatase inhibitor. Johns Hopkins Cardiovascular Research annual retreat. Baltimore, MD, 2016.

2. **SG Ziegler**, CR Ferreira, TJ Creamer , DS Warren, L Goff, AB Pinkerton, JL Millan, WA Gahl, HC Dietz. Toward identification of the pathogenic cell type driving calcification in pseudoxanthoma elasticum. National American Vascular Biology Organization annual meeting. Cape Cod, MA, 2015.

3. **SG Ziegler**, CR Ferreira, AB Pinkerton, JL Millan, WA Gahl, HC Dietz. Novel insights regarding the pathogenesis and treatment of Pseudoxanthoma elasticum. American Society for Human Genetics annual meeting. San Diego, CA, 2014.

4. **SG Ziegler**, C St. Hilaire, T Markello, C Groden, F Gill, H Carlson-Donohoe, A Brusco, R Nussbaum, R Kleta, M Boehm, WA Gahl. *NT5E* mutations are associated with arterial calcifications. American Society for Human Genetics annual meeting. Washington DC, 2010.

INVITED PRESENTATIONS

1. **SG Ziegler**, CR Ferreira, E Gallo MacFarlane, RC Riddle, R Tomlinson, L Martin, C Ma, E Sergienko, AB Pinkerton, JL Millan, WA Gahl, HC Dietz. Delineating the mechanisms underlying rare disorders of ectopic calcification to reveal novel therapeutic strategies. 215th Interurban Clinical Club Scientific Meeting. Baltimore, MD 2017.

2. **SG Ziegler**, CR Ferreira, E Gallo MacFarlane, RC Riddle, R Tomlinson, L Martin, C Ma, E Sergienko, AB Pinkerton, JL Millan, WA Gahl, HC Dietz. Pseudoxanthoma elasticum: Dysregulation of local ATP metabolism and treatment with a tissue non-specific alkaline phosphatase inhibitor. PXE Research Symposium. Philadelphia, PA 2016.

POSTER PRESENTATIONS

1. **SG Ziegler**, CR Ferreira, E Gallo MacFarlane, RC Riddle, R Tomlinson, L Martin, C Ma, E Sergienko, AB Pinkerton, JL Millan, WA Gahl, HC Dietz. Pseudoxanthoma elasticum: Dysregulation of local ATP metabolism and treatment with a tissue non-specific alkaline phosphatase inhibitor. American Society for Human Genetics annual meeting. Vancouver, BC, Canada 2016.

2. **SG Ziegler**, CR Ferreira, TJ Creamer , DS Warren, L Goff, AB Pinkerton, JL Millan, WA Gahl, HC Dietz. Toward identification of the pathogenic cell type driving calcification in pseudoxanthoma elasticum. American Society for Human Genetics annual meeting. Baltimore, MD, 2015.

3. **SG Ziegler**, Y Yang, D Malhotra, MT Collins, N Bhattacharyya, RI Gafni, WA Gahl, HC Dietz. Delineation of renal-independent disease mechanism underlying Hyperphosphatemic Familial Tumoral Calcinosis caused by GALNT3 mutations. American Society for Human Genetics annual meeting. Boston, MA, 2013.

4. C Toro, **SG Ziegler**, C Groden, CD Blair, K Cao, H Carlson-Donohoe, DR Simeonov, M Erdos, FS Collins, WA Gahl. Expanding the phenotype of Autosomal Dominant Leukodystrophy associated with *LMNB1* duplication. American Society for Human Genetics annual meeting. Washington, DC, 2010.

5. C Toro, **SG Ziegler**, A Vanderver, C Groden, CD Blair, K Cao, H Carlson-Donohoe, DR Simeonov, M Erdos, FS Collins, WA Gahl. Expanding the phenotype of Autosomal Dominant Leukodystrophy associated with *LMNB1* duplication. American Neurological Association annual meeting, San Francisco, CA, 2010.

6. **SG Ziegler**, W Westbroek, W Introne, K Wilson, T Markello, WA Gahl. Molecular and Cellular Analysis of Patients with Classical and Atypical Chediak-Higashi Disease. NHGRI annual retreat. Gettysburg, MD, 2009.

7. **SG Ziegler**, MP Siegenthaler, D Adams, CE Wahl, C Groden, M Anahtar, TC Markello, WA Gahl. A novel SNP genotyping array analysis yields linkage for a rare medial arterial calcification disorder in five siblings. American Society for Human Genetics annual meeting. Honolulu, HI, 2009.

8. **SG Ziegler**, JE Thornton. Decreased luteinizing hormone (LH) enhances spatial memory in ovariectomized female rats: a potential treatment for Alzheimer's disease. Society for Neuroscience annual meeting. Washington, DC, 2008.

9. LM Vincent, **SG Ziegler**, R Hess, W Westbroek, WA Gahl, M Huizing. Using exon skipping to rescue common mutations in Hermansky-Pudlack Syndrome Type 1. NHGRI annual retreat. Gettysburg, MD, 2008.

10. **SG Ziegler**, JE Thornton. Decreased luteinizing hormone enhances spatial memory in ovariectomized female rats. Society for Behavioral Neuroendocrinology annual meeting. Netherlands, 2008.

11. **SG Ziegler**, VM Renard, BM Tyler, H Brem, A Olivi. Combinatorial treatments with epirubicin, temozolmide, and radiation therapy in experimental malignant glioma *in vitro.* American Association of Neurosurgical Surgeons annual meeting. Chicago, IL, 2008.

12. K Hruska, Y Blech-Hermoni, **SG Ziegler**, B Stubblefield, E Sidransky. Functional evaluation of predicted regulatory sequenced at the GBA locus. Lysosomal Disease Network annual symposium. Las Vegas, NV, 2008.

13. Y Blech-Hermoni, **SG Ziegler**, B Stubblefield, K Hruska, E Sidransky. Functional evaluation of predicted regulatory sequenced at the GBA locus. NHGRI annual retreat. Gettysburg, MD, 2007.

14. E Goldin, D Urban, K Hruska, **SG Ziegler**, E Sidransky, CR Kaneski. Use of C8-DCH-β-glucopyranoside for high-throughput screening of modulators of lysosomal β-glucosidase in intact cells. American Society for Human Genetics annual meeting. New Orleans, LA, 2006.

15. KS Hruska, ME LaMarca, **SG Ziegler**, ME Portnoy, NISC Comparative Sequencing Program, ED Green, E Sidransky. Analysis of conserved regulatory elements in the glucocerebrosidase gene locus. American Society for Human Genetics annual meeting. Salt Lake City, UT, 2005.

16. **SG Ziegler**, D Krasnewich, E Sidransky, J Atkins, J Innis, E Orvisky. Biochemical and Molecular Analyses of United States Patients with Congenital Disorders of Glycosylation Ia (CDG-Ia). NIH Summer Student poster session. Bethesda, MD, 2003.

PATENTS

1. Methods of Treating PXE with TNAP Inhibitors. Number 62/058,505, filed October 1, 2014.

2. A_1 and A_3 adenosine receptor agonists and A_{2a} and A_{2b} adenosine receptor antagonists for the treatment and prevention of vascular or joint capsule calcification disorders. Number 61/319,336, filed March 31, 2010.

INVITED REVIEWER
Genetics Home Reference

INVITED SESSIONS
Invited to chair trainee session entitled "Beyond Mendel: Complexities of Simple Mendelian Disorders" at American Society for Human Genetics. San Diego, CA. October 2014.

SOCIETY AND PROFESSIONAL AFFILIATIONS
Phi Beta Kappa
Sigma Xi Associate Member
American Society for Human Genetics